European Journal of Taxonomy 840: 1–93
https://doi.org/10.5852/ejt.2022.840.1941

ISSN 2118-9773
www.europeanjournaloftaxonomy.eu
2022 · Rataj Križanová F. & Vďačný P.

Monograph
urn:lsid:zoobank.org:pub:CE89365D-A3C5-483D-9C80-E5CAECCA740F

A huge undescribed diversity of the subgenus *Hystricochaetonotus* (Gastrotricha, Chaetonotidae, *Chaetonotus*) in Central Europe

Františka RATAJ KRIŽANOVÁ [1] & Peter VĎAČNÝ [2,*]

[1,2] Department of Zoology, Comenius University in Bratislava, 842 15 Bratislava, Slovakia.

[*] Corresponding author: peter.vdacny@uniba.sk
[1] Email: krizanova66@uniba.sk

[1] urn:lsid:zoobank.org:author:80CC56E1-1046-4748-97B6-5FA90E95DFA7
[2] urn:lsid:zoobank.org:author:47A28E80-E04F-40C4-93A3-F7F685C9533A

Abstract. The subgenus *Hystricochaetonotus* Schwank, 1990 is one of the most species-rich subgenera of *Chaetonotus* Ehrenberg, 1830. It has a worldwide distribution and encompasses 37 species predominantly living in the benthos and periphyton of limnetic habitats. We have discovered further nine new species in running and stagnant waters in Slovakia (Central Europe): *Ch.* (*H.*) *arcanus* sp. nov., *Ch.* (*H.*) *avarus* sp. nov., *Ch.* (*H.*) *gulosus* sp. nov., *Ch.* (*H.*) *iratus* sp. nov., *Ch.* (*H.*) *luxus* sp. nov., *Ch.* (*H.*) *mirabilis* sp. nov., *Ch.* (*H.*) *optabilis* sp. nov., *Ch.* (*H.*) *slavicus* sp. nov., and *Ch.* (*H.*) *superbus* sp. nov. Their morphology was studied using differential interference contrast microscopy and subsequent morphometric analyses were carried out. In addition, the primary and secondary structures of their 18S, ITS2, and 28S rRNA molecules as well as their barcoding mitochondrial gene encoding for cytochrome *c* oxidase (COI) were analyzed. Species boundaries were tested also using the compensatory base change analysis. The new species could be well separated both morphologically and molecularly. The present barcoding analyses revealed that the nuclear ITS2 sequences represent a powerful DNA barcode in addition to the mitochondrial COI gene. According to the multi-gene phylogenetic analyses, the lineage leading to the last common ancestor of the '*Hystricochaetonotus*' clade is the longest internal branch within the family Chaetonotidae Gosse, 1864. Since members of the subgenus *Hystricochaetonotus* are morphologically highly heterogeneous, parallel evolution of *Chaetonotus*-like and/or *Hystricochaetonotus*-like characters of scales and spines occurred during its radiation.

Keywords. Compensatory base changes, cytochrome *c* oxidase, meiofauna, rDNA cistron, RNA secondary structure, Slovakia.

Rataj Križanová F. & Vďačný P. 2022. A huge undescribed diversity of the subgenus *Hystricochaetonotus* (Gastrotricha, Chaetonotidae, *Chaetonotus*) in Central Europe. *European Journal of Taxonomy* 840: 1–93. https://doi.org/10.5852/ejt.2022.840.1941

Introduction

Phylum Gastrotricha Mečnikow, 1865 unites vermiform to bottle-shaped meiobenthic metazoans having locomotory ciliation on the ventral body surface and adhesive tubes distributed along the body or situated

at the rear body end (Balsamo *et al.* 2014; Kånneby & Hochberg 2015; Kieneke & Schmidt-Rhaesa 2015; Todaro *et al.* 2019). The research on gastrotrichs is just at the beginning in Slovakia (Križanová & Vďačný 2021). This country is situated at the geographical center of Europe (Fig. 1), representing the transition zone for the West and East Carpathian as well as the Pannonian fauna (Buchar 1983; Holecová & Franc 2001; Astaloš *et al.* 2003). The diversity of gastrotrichs is regrettably unexplored in this zoogeographically interesting region. There are globally approximately 890 validly described gastrotrich species, classified in two orders (Balsamo *et al.* 2015; Kieneke & Schmidt-Rhaesa 2015; Todaro 2022): the Macrodasyida Remane, 1925 (sensu Rao & Clausen 1970) with over 390 species and the Chaetonotida Remane, 1925 (sensu Rao & Clausen 1970) with almost 500 species. About two-thirds of chaetonotids are known from continental freshwaters (Balsamo *et al.* 2008, 2020). However, the gastrotrich diversity is still insufficiently explored (Kolicka 2020) and the described species might represent less than 20% of the total richness (Appeltans *et al.* 2012).

Dispersal abilities have also a significant impact on the diversification rate and alfa diversity detected in individual study plots. Dispersion of meiofaunal organisms is quite limited due to their small size, absence of a larval phase, and low movement capacity (Giere 2009; Cerca *et al.* 2018; Magpali *et al.* 2021). 'Cosmopolitan' species could comprise cryptic, near-cryptic (subtle, easily overlooked differences, or only statistically supported differences; Lücking *et al.* 2021), or pseudo-cryptic species (overlooked or briefly mentioned and not effectively characterized morphological characters; Magpali *et al.* 2021) that could significantly affect the diversity estimates. To properly address the distribution patterns and species identities of gastrotrichs, broad sampling and sound taxonomy are indispensable.

Morphology-based identification of gastrotrichs is, however, hampered by (1) the lack of standardized methods for species descriptions in the past, (2) a great disparity of species descriptions among authors, (3) the briefness and generality of 'old' descriptions, (4) the over-schematization and simplification of illustrations, and (5) the necessity of detailed examination of living specimens (Kisielewski 1991; Balsamo *et al.* 2008; Garraffoni & Melchior 2015; Kieneke & Nikoukar 2017; Magpali *et al.* 2021 and references cited therein). Nowadays, an integrative approach combining detailed morphological observations (e.g., differential interference contrast optics, confocal laser scanning microscopy, SEM) with multi-gene data is the preferred way for the description of new gastrotrich species (e.g., Kånneby 2011; Todaro *et al.* 2012; Garraffoni *et al.* 2017, 2019a; Kolicka *et al.* 2016, 2018; Kolicka 2019a, 2019b; Bosco *et al.* 2020; Magpali *et al.* 2021). Molecular data are, indeed, crucial for the recognition of cryptic and near-cryptic species, as it is the very definition of cryptic species that it is difficult, if not impossible, to find morphological characters that distinguish among them.

Using the integrative morpho-molecular approach, we have noticed a huge undescribed diversity of gastrotrichs belonging to the family Chaetonotidae Gosse, 1864 in stagnant as well as running waters in Slovakia. Besides morphological and phylogenetical analyses, we employed also the information contained in the secondary structure of the nuclear rRNAs and ITS2 molecules to further test species boundaries of morphologically delimited species. Especially, compensatory base changes (CBC), which force pairing in a helix to remain after a mutation occurred, are taxonomically important (Müller *et al.* 2007; Coleman 2009; Wolf *et al.* 2013). Just a single CBC in helix III of the ITS2 molecules is suggestive of the existence of two biological species incapable of mating.

This publication is dedicated to the description of nine new species phylogenetically closely related to *Chaetonotus* (*Hystricochaetonotus*) *hystrix* Mečnikow, 1865, type species of the subgenus *Hystricochaetonotus* Schwank, 1990. *Hystricochaetonotus* is one of the most species-rich subgenera of *Chaetonotus* Ehrenberg, 1830 (Schwank 1990). It encompasses 37 species predominantly living in the benthos and periphyton of limnetic habitats (Schwank 1990; Kisielewski 1997a; Kolicka 2016; Todaro 2022). Rather recently, Kolicka *et al.* (2018) added three further new species from the Svalbard

archipelago and Kolicka (2019a) discovered two new species in the Jubilee Greenhouse of the Botanical Garden in Kraków (Poland).

Material and methods

Sampling and morphological taxonomic methods

Gastrotrichs were sampled from six water bodies in Slovakia, Central Europe (Fig. 1). Descriptions of the studied sites are provided in the 'Type locality' sections of individual species and their location is shown in Figure 2A–B. Maps were prepared using the Python packages Cartopy ver. 0.20.0 (http://scitools.org.uk/cartopy) (Cartopy 2014) and Matplotlib ver. 3.5.0 (Hunter 2007) as well as the Natural Earth land vector shapefiles at a 1:10-million scale (https://www.naturalearthdata.com/). Map tiles by ©Stamen Design, under a Creative Commons Attribution (CC BY 3.0) license. Data by OpenStreetMap, under ODbL.

Samples consisted of the upper detritus layer (1–2 cm) and about 0.5 liters of water above the sediment. After transportation to the laboratory, they were kept in dark at room temperature for one month. Examination of the detritus was carried out under a Zeiss Axio Imager A2 microscope. Gastrotrichs were collected with an adjusted Pasteur's micropipette and placed in a drop of 0.5% $MgCl_2$ solution to decrease their motility (Todaro *et al.* 2019). Cleaned and narcotized gastrotrichs were observed at

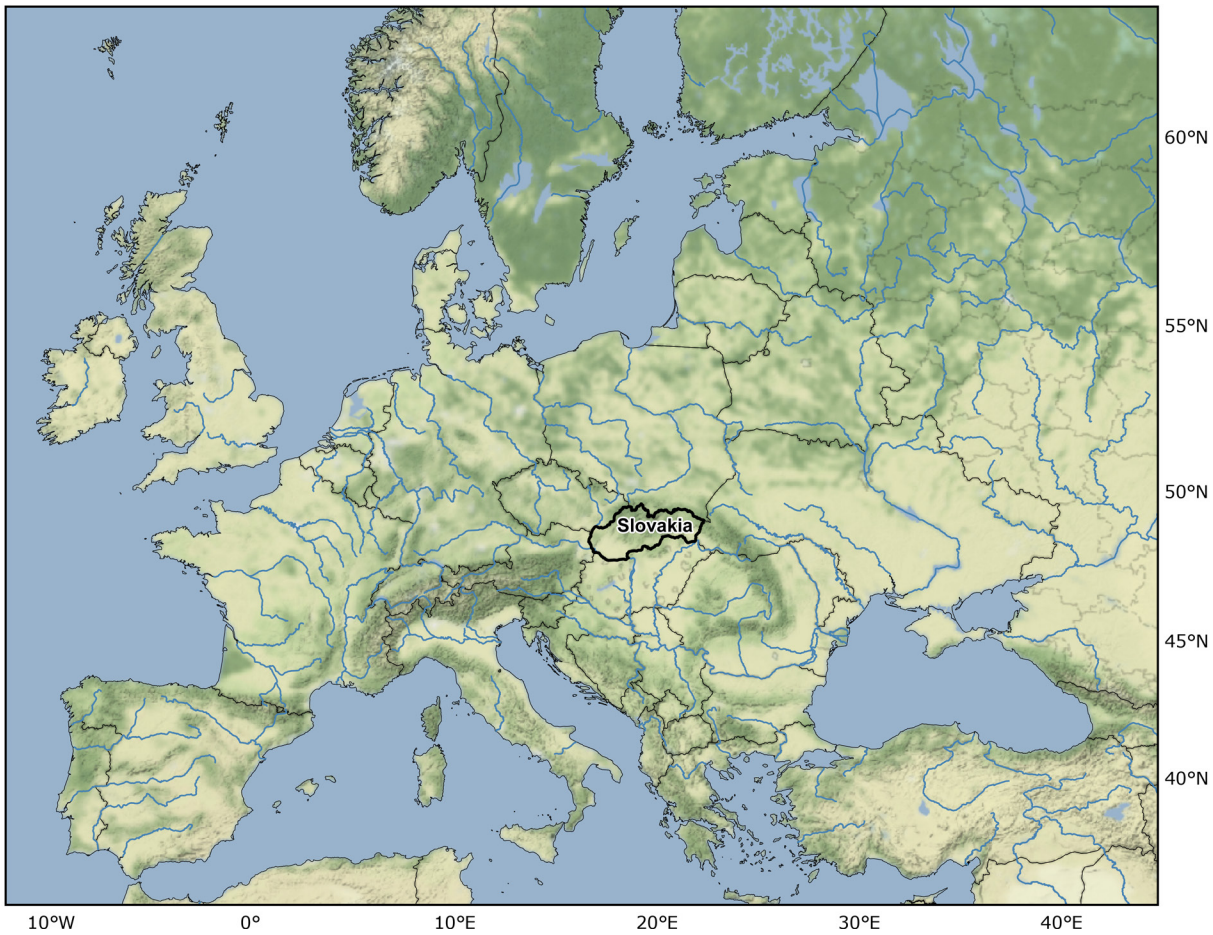

Fig. 1. Map of Europe showing the localization of Slovakia. Map tiles by ©Stamen Design, under a Creative Commons Attribution (CC BY 3.0) license. Data by OpenStreetMap, under ODbL.

1000–2500× magnification with a high-power oil immersion objective and differential interference contrast optics. Habitus and taxonomically important features were captured by a Canon EOS 80D camera. Illustrations were prepared in Inkscape ver. 0.92.4 and figure plates were assembled in Adobe Photoshop CC. Morphologically studied specimens were sampled for molecular analyses whenever possible, using the strategy described elsewhere (Križanová & Vďačný 2021).

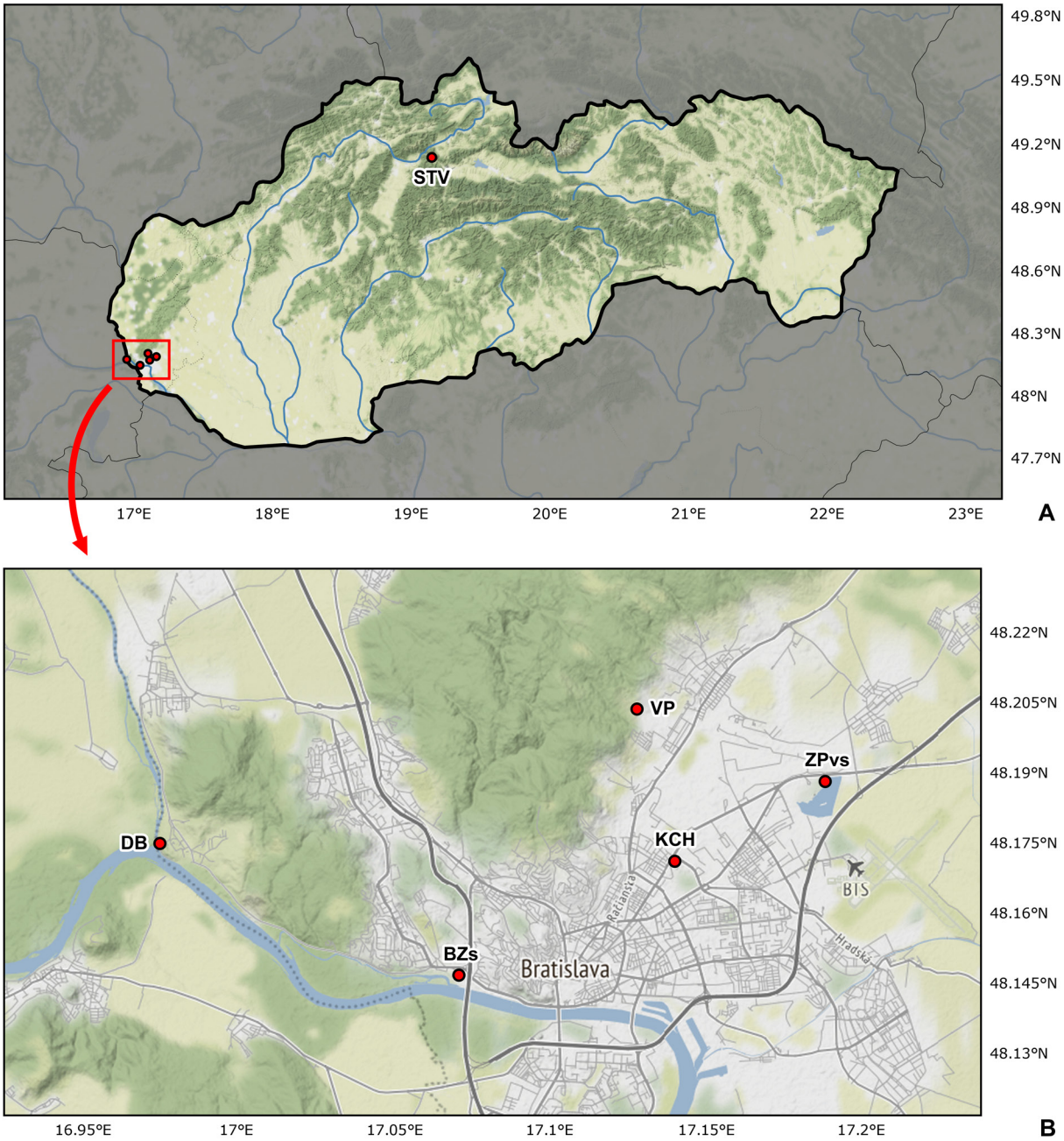

Fig. 2. Sampling sites of nine new gastrotrich species discovered in Slovakia. **A**. One locality (STV) was situated in northern Slovakia, while five localities were concentrated in the capital city of Bratislava (marked by the red rectangle). **B**. Detail of the Bratislava district showing the localization of five sampling sites. Map tiles by ©Stamen Design, under a Creative Commons Attribution (CC BY 3.0) license. Data by OpenStreetMap, under ODbL.

Morphological taxonomic methods followed Kisielewski (1981, 1991), Kolicka (2019a), and Kolicka *et al*. (2016, 2018). Properly oriented specimens and well visible morphological traits were measured from photomicrographs with the calibrated software ImageJ ver. 1.53. Since preserved gastrotrichs are less suitable for examination of taxonomically important characters, all measurements were based on a series of photomicrographs of living narcotized specimens (Kisielewski 1997b; Balsamo *et al.* 2008, 2014; Garraffoni *et al.* 2019b). Morphometric parameters are given in micrometers (µm), ratio characters are expressed as a percentage (%) of the body length, and distances from the anterior end are provided as percentage units (U) of the total body length (Kisielewski 1981, 1991, 1997b; Hummon *et al.* 1992). The calculation of pharynx formulae followed Kisielewski (1991) and Kolicka (2019a) while the ratio of the pharynx to intestine length was adopted from Kolicka *et al.* (2016). The measurement scheme of scales and spines is shown in Figure 3A–B. Angle α is made up of the anterior and the posterior lobe, while angle β is formed by the posterior lobes. The value d is defined as the distance from the tip of the lateral denticle to the apex of the spine. The calculation of the d-ratio is as follows:

$$d\text{-ratio} = \frac{d}{spine\ length} \times 100\%$$

Specimens from type series are no longer available because they were destroyed during microscopic examination with a compound microscope and/or were lyzed during DNA extraction. We used the isolated DNA as type material of the new species, which is in accordance with Article 72.5.1 of the ICZN (1999).

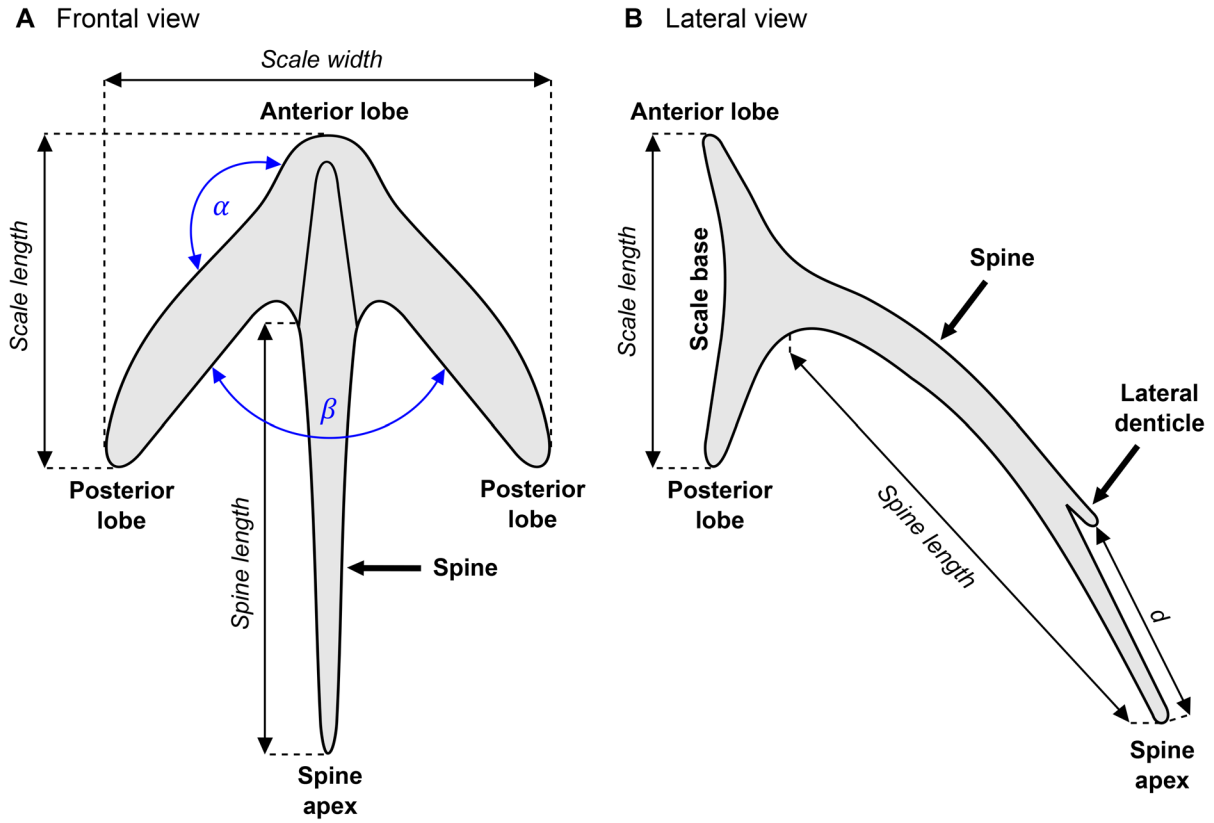

Fig. 3. Terminology and measurement scheme for scales and spines. **A**. Frontal view. **B**. Lateral view.

According to this article, any part of an animal is eligible to be a name-bearing type. To provide a more objective framework for recognition of the new species, we use morphological and molecular (rDNA cistron along with the barcoding cytochrome *c* oxidase subunit I sequences) data to diagnose new species. DNA sequences have been deposited in GenBank (https://www.ncbi.nlm.nih.gov/ nucleotide/), while DNA samples have been stored in the Natural History Museum, Vajanského nábrežie 2, 810 06 Bratislava, Slovak Republic. Illustrations and photomicrographs of holotype and paratype specimens (ICZN 2017: Article 73, Recommendation 73G, Declaration 45) are available on the webserver of the Department of Zoology, Comenius University in Bratislava, Slovak Republic (https://fns.uniba.sk/en/gastrotricha/).

The generic name *Chaetonotus*, derived from the Greek noun '*χαίτη*' ('*khaítē*' [f]; 'flowing hair'), is abbreviated as '*Ch.*'. The Greek letter chi *χ* is transliterated to Latin as *ch* according to the ISO 843 transliteration system, an international standard for the transliteration and/or transcription of Greek characters into Latin characters. The abbreviation of the subgeneric name *Hystricochaetonotus* is '*H.*'. These generic and subgeneric abbreviations were used also by Kisielewski (1981, 1991, 1997a) and Schwank (1990).

Molecular methods

Processing of gastrotrichs for molecular analyses followed our previous study (Križanová & Vďačný 2021). Briefly, each sample contained only a single worm that was lyzed in 180 µl of CLD buffer (Promega, Fitchburg, Wisconsin, United States). Genomic DNA was extracted with the Relia Prep™ Blood gDNA Miniprep System (Promega). The nuclear 18S, ITS region, and 28S as well as the mitochondrial gene coding for cytochrome *c* oxidase subunit I (COI) were amplified using the primers and protocols described by Križanová & Vďačný (2021). PCR products were electrophoresed in 1% agarose gel and 1X TBE buffer at 80 V for 50 min and visualized with the GoodView™ nucleic acid stain (SBS Genetech Co. Ltd., Beijing, China) under UV transillumination. PCR products were enzymatically purified using the calf intestinal alkaline phosphatase and exonuclease I, *E. coli* (New England Biolabs® Inc., Ipswich, Massachusetts, USA). When electrophoresis revealed non-specific amplification, the desired PCR products were extracted from the agarose gel and purified with the NucleoSpin Gel and PCR clean-up kit (Macherey-Nagel, Düren, Germany). All molecular markers were sequenced bidirectionally on an ABI 3730 automatic sequencer (Macrogen Europe B.V., Amsterdam, The Netherlands), using the Sanger dideoxynucleotide chain termination method. The quality of electropherograms was assessed in Chromas ver. 2.33 (Technelysium Pty Ltd, South Brisbane, Australia) and high-quality DNA fragments were assembled into contigs in BioEdit ver. 7.2.5 (Hall 1999).

Barcoding analyses

Nucleotide positions in the rRNA cistron suitable for species diagnoses (i.e., molecular autapomorphies of individual species) were identified within the secondary structure-based alignments (see below) using a custom Python script. The ordinal number of the position in the reference alignments is followed by the nucleotide character in the molecular diagnoses. Deletions are marked by dashes (–). Species-specific (i.e., unique codons) in COI were detected with a custom Python script as well. The codon ordinal numbers are followed by the corresponding span of nucleotide positions in parentheses. Reference alignments are provided in Supp. file 1: Alignments 1–4. 2D-based alignments were prepared with the help of the package 4SALE ver. 1.7.1 (Seibel *et al.* 2006), considering both the primary and the secondary structure information. The CBCAnalyzer option (Wolf *et al.* 2005), as implemented in 4SALE, was employed to count and reveal the localization of compensatory base changes (CBC) in a pair-wise manner.

Pairwise *p*-distances were calculated separately for each molecular marker, whereby mutually exclusive ambiguity nucleotide positions and alignment gaps were considered since alignments were based on secondary structures or predicted amino acid sequences. Histograms of intra- and interspecific distances were constructed for each molecular marker using a custom Python script and Matplotlib (Hunter 2007).

Secondary structure predictions

The secondary structures of the 18S and 5.8S–28S rRNA molecules were predicted with R2DT (Sweeney *et al.* 2021). The R2DT package analyses RNA sequences using covariance models, taking into account a library of over 3000 templates representing the majority of known structured RNAs. The generated 2D layouts are consistent with 3D ribosomal structures and hence account also for the presence of non-canonical base pairs along with Watson-Crick pairings (Petrov *et al.* 2014). Since helix 25 of the 28S rRNA molecule is highly divergent, its secondary structure was studied also using the thermodynamic and homology modeling on the Mfold web server ver. 3.0 (http://www.unafold.org/) (Zuker 2003). The helix number system of rRNA molecules followed Petrov *et al.* (2014).

The common folding pattern of ITS2 molecules was found by running the multilign and TurboFold algorithms on the RNAstructure webserver (http://rna.urmc.rochester.edu/RNAstructureWeb) (Mathews 2004). Consequently, ITS2 molecules were folded on the Mfold web server, using the free-energy minimization approach and homology modeling. The 50%-majority rule consensus ITS2 secondary structure model was built in 4SALE based on the 2D-based alignment. The online program WebLogo ver. 2.8.2 (https://weblogo.berkeley.edu/) (Crooks *et al.* 2004) served to prepare the visualization of the nucleotide frequencies at individual positions of ITS2 helices with the relative entropy method. The total length, GC content, length of helices, unpaired bases in bulges and loops, number of bulges, and GU pairings were counted and statistically evaluated. Gibbs free energy ΔG of the ITS2 molecules was calculated with the webserver program RNAeval ver. 2.4.13 (http://rna.tbi.univie.ac.at/cgi-bin/RNAWebSuite/RNAeval.cgi) (Lorenz *et al.* 2011, 2016). The tertiary structure of ITS2 molecules was predicted from the secondary structure with RNAComposer ver. 1.0 (http://rnacomposer.cs.put.poznan.pl/) (Popenda *et al.* 2012).

2D layouts of gastrotrich rRNAs and ITS2 molecules were visualized with R2DT, TRAVeLer (Elias & Hoksza 2017), and Varna ver. 3.93 (Darty *et al.* 2009). Resulting scalable vector graphic (SVG) files were processed in Inkscape ver. 0.92.4.

Phylogenetic analyses

Taxon sampling mostly followed Kånneby *et al.* (2012) and Kolicka *et al.* (2020), but only chaetonotids having sequences from 18S, 28S, and COI were included in phylogenetic analyses as specified in our previous study (Križanová & Vďačný 2021). All sequences, except for the newly obtained ones, were retrieved from GenBank (https://www.ncbi.nlm.nih.gov/genbank/) and their accession numbers are provided in Supp. file 1: Table S1. The nuclear rRNA gene sequences were aligned on the MAFFT ver. 7 server (https://mafft.cbrc.jp/alignment/server/) (Katoh *et al.* 2019), using the G-INS-i strategy, the 200PAM/κ=2 scoring matrix, and the gap opening penalty at 1.53. The mitochondrial protein-coding COI sequences were aligned with MEGA X (Kumar *et al.* 2018), using the invertebrate mitochondrial genetic code and the Muscle codon algorithm.

Two probabilistic methods, maximum likelihood and Bayesian inference, were utilized to build phylogenetic trees. Maximum likelihood (ML) analyses were carried out in IQ-TREE ver. 1.6.10 (Nguyen *et al.* 2015) on the webserver (http://iqtree.cibiv.univie.ac.at/) (Trifinopoulos *et al.* 2016), while Bayesian inferences (BI) were performed in the program MrBayes ver. 3.2.7 (Ronquist *et al.* 2012). Settings in ML analyses were as follows: (1) the best substitution model, as selected under the Bayesian information criterion by the in-built program, was assigned to each molecular marker, (2) the edge-unlinked partition model that accounts for heterotachy (rate variation across sites and lineages) and allows each partition to have its own set of branch lengths, (3) thousand ultrafast bootstrap pseudo-replicates, (4) the bnni algorithm that reduces overestimating bootstrap support (Hoang *et al.* 2018), and (5) all other parameters were left default. Settings of Bayesian analyses were as follows: (1) prior parameters of evolutionary models as estimated with IQ-TREE were implemented with the 'prset'

command, (2) all model parameters were unlinked across partitions, (3) five million Markov chain Monte Carlo (MCMC) simulations, (4) a sampling frequency of trees and parameters at one hundred, and (5) a relative burn-in fraction of 25%. Convergence of the MCMC analyses was confirmed with the in-built diagnostics of the program MrBayes. All trees were computed as unrooted and were rooted in FigTree ver. 1.4.3 (http://tree.bio.ed.ac.uk/software/figtree/).

Abbreviations

5.8S = 5.8S rRNA molecule (gene)
18S = 18S (small subunit) rRNA molecule (gene)
28S = 28S (large subunit) rRNA molecule (gene)
ag = adhesive gland
an = anus
at = adhesive tube(s)
BI = Bayesian inference
BZs = greenhouse pond in Botanical Garden of Comenius University
CBC = compensatory base change
ceph = cephalion
cg = cerebral ganglion
COI = cytochrome *c* oxidase subunit I
cp = ciliary patch(es)
ct = cuticular tooth
das = differentiated anterior section of intestine
DB = temporary pond in the floodplain area of the River Morava
epi = epipleurae
GC = guanosine-cytosine content
hs = hypostomium
hyp = hypopleurae
int = intestine
ITS2 = internal transcribed spacer 2
KCH = Kuchajda lake
ld = lateral denticle
m = mouth
me = mature egg
mb = mouth basket
mem = membrane
Ma = millions of years (Mega annum)
ML = maximum likelihood
nt = nucleotide(s)
ov = ovary
ph = pharynx
pij = pharyngeal–intestinal junction
prn = protonephridia
ps = posteriormost lateral trunk spines
rr = rod-like reinforcements
s = sensoric bristle (setola)
sc = sensoric cilia
sg = salivary gland
sp = spine
STV = River Váh near the village of Stankovany
tb = transversal band(s)
vcb = ventral ciliary band(s)

VP = Vajspeterský potok creek
X = organ X
ZPvs = Zlaté Piesky lake

Results

Diversity and occurrence

We investigated the gastrotrich fauna in a variety of water bodies in Slovakia (Central Europe) during the years 2019–2021. Altogether, nine new species were detected at six localities: *Ch.* (*H.*) *arcanus* sp. nov., *Ch.* (*H.*) *avarus* sp. nov., *Ch.* (*H.*) *gulosus* sp. nov., *Ch.* (*H.*) *iratus* sp. nov., *Ch.* (*H.*) *luxus* sp. nov., *Ch.* (*H.*) *mirabilis* sp. nov., *Ch.* (*H.*) *optabilis* sp. nov., *Ch.* (*H.*) *slavicus* sp. nov., and *Ch.* (*H.*) *superbus* sp. nov. Two species (*Ch.* (*H.*) *luxus* sp. nov. and *Ch.* (*H.*) *superbus* sp. nov.) were detected at two localities, while all other species were found only at a single spot each. Interestingly, two or three species co-occurred at four out of the six localities studied (Table 1).

Molecular identification

In total, 72 new sequences were obtained from the nine new *Chaetonotus* (*Hystricochaetonotus*) species (Table 2). They can be unambiguously distinguished by the primary structure of ITS2, 28S, and COI sequences. According to the present barcoding analyses, 28S can serve as a pre-barcode and ITS2 and COI as barcodes (Fig. 4B–D). Our two-step barcoding approach thus comprises a preliminary identification using a universal eukaryotic barcode (28S), called the pre-barcode, followed by a more precise species-level assignment using group-specific barcodes (ITS2 and COI). Based on the present barcoding analysis, a combination of ITS2 and COI is preferred but not required for the determination of species within the subgenus *Hystricochaetonotus*. These two barcodes thus can be used for species identification also separately.

Table 1. Occurrence of nine new species of the subgenus *Hystricochaetonotus* Schwank, 1990 at six collection sites. [a] For abbreviations of collection sites, see Material and methods. Plus sign (+) means presence, minus sign (–) absence.

Species	Collection site[a]					
	BZs	**DB**	**KCH**	**STV**	**VP**	**ZPvs**
Ch. (*H.*) *arcanus* sp. nov.	–	–	–	+	–	–
Ch. (*H.*) *avarus* sp. nov.	–	–	–	–	+	–
Ch. (*H.*) *gulosus* sp. nov.	–	–	–	–	+	–
Ch. (*H.*) *iratus* sp. nov.	–	–	–	+	–	–
Ch. (*H.*) *luxus* sp. nov.	–	–	–	–	+	+
Ch. (*H.*) *mirabilis* sp. nov.	+	–	–	–	–	–
Ch. (*H.*) *optabilis* sp. nov.	–	+	–	–	–	–
Ch. (*H.*) *slavicus* sp. nov.	–	+	–	–	–	–
Ch. (*H.*) *superbus* sp. nov.	–	–	+	–	–	+

Table 2. GenBank accession numbers of nuclear and mitochondrial gene sequences of nine new species of the subgenus *Hystricochaetonotus* Schwank, 1990.

Species	Specimen[a]	18S rRNA gene	ITS region-28S rRNA gene	COI gene
Ch. (*H.*) *mirabilis* sp. nov.	BZs 02[b]	OM421704	OM421680	OM424059
	BZs 15	OM421705	OM421681	OM424060
	BZs 16	OM421706	OM421682	OM424061
	BZs 17	OM421707	OM421683	OM424062
Ch. (*H.*) *superbus* sp. nov.	ZPvs 55[c]	OM421708	OM421684	OM424063
	KCH 61	OM421709	OM421685	OM424064
Ch. (*H.*) *optabilis* sp. nov.	DB 34[d]	OM421710	OM421686[k]	OM424065
	DB 35	OM421711	OM421687[k]	OM424066
	DB 36	OM421712	OM421688[k]	OM424067
Ch. (*H.*) *avarus* sp. nov.	VP 32[e]	OM421713	OM421689[k]	OM424068
Ch. (*H.*) *luxus* sp. nov.	ZPvs 20[f]	OM421714	OM421690	OM424069
	ZPvs 22	OM421715	OM421691	OM424070
	ZPvs 23	OM421716	OM421692	OM424071
	ZPvs 24	OM421717	OM421693	OM424072
	ZPvs 25	OM421718	OM421694	OM424073
	VP 28	OM421719	OM421695	OM424074
Ch. (*H.*) *iratus* sp. nov.	STV 65[g]	OM421720	OM421696	OM424075
Ch. (*H.*) *gulosus* sp. nov.	VP 18[h]	OM421721	OM421697	OM424076
	VP 31	OM421722	OM421698	OM424077
Ch. (*H.*) *arcanus* sp. nov.	STV 67[i]	OM421723	OM421699	OM424078
Ch. (*H.*) *slavicus* sp. nov.	DB 40[j]	OM421724	OM421700	OM424079
	DB 41	OM421725	OM421701	OM424080
	DB 42	OM421726	OM421702	OM424081
	DB 43	OM421727	OM421703	OM424082

[a] Specimen code consists of a locality and an isolate code. For abbreviations of locality codes, see Material and methods.

[b] Genomic DNA of the holotype specimen BZs 02 has been deposited in the Natural History Museum in Bratislava, Slovakia (ID Collection Code 01427888).

[c] Genomic DNA of the holotype specimen ZPvs 55 has been deposited in the Natural History Museum in Bratislava, Slovakia (ID Collection Code 01427126).

[d] Genomic DNA of the holotype specimen DB 34 has been deposited in the Natural History Museum in Bratislava, Slovakia (ID Collection Code 01427607).

[e] Genomic DNA of the holotype specimen VP 32 has been deposited in the Natural History Museum in Bratislava, Slovakia (ID Collection Code 01427566).

[f] Genomic DNA of the holotype specimen ZPvs 20 has been deposited in the Natural History Museum in Bratislava, Slovakia (ID Collection Code 01427593).

[g] Genomic DNA of the holotype specimen STV 65 has been deposited in the Natural History Museum in Bratislava, Slovakia (ID Collection Code 01427609).

[h] Genomic DNA of the holotype specimen VP 18 has been deposited in the Natural History Museum in Bratislava, Slovakia (ID Collection Code 01427574).

[i] Genomic DNA of the holotype specimen STV 67 has been deposited in the Natural History Museum in Bratislava, Slovakia (ID Collection Code 01427571).

[j] Genomic DNA of the holotype specimen DB 40 has been deposited in the Natural History Museum in Bratislava, Slovakia (ID Collection Code 01427570).

[k] These sequences contain only first two domains of 28S.

The length of the 18S rRNA gene is from 1815 nt in *Ch.* (*H.*) *mirabilis* sp. nov. to 1821 nt in *Ch.* (*H.*) *optabilis* sp. nov. The GC content ranges only from 46.51% in *Ch.* (*H.*) *optabilis* sp. nov. to 48.98% in *Ch.* (*H.*) *superbus* sp. nov. Sequences within species were identical except for *Ch.* (*H.*) *luxus* sp. nov. and *Ch.* (*H.*) *optabilis* sp. nov. in which the sequence identities ranged from 99.89% to 100%. In addition, two heterozygotes were detected in the former species, which had cytosine and guanosine at position 1729 in helix 44. This position is apparently polymorphic in *Ch.* (*H.*) *luxus* sp. nov. Both nucleotide states are involved in a noncanonical interaction that retains the RNA helical structure. Interspecies *p*-distances typically spanned a range of 0.05–4.39%, whereby no difference was found only between *Ch.* (*H.*) *luxus* sp. nov. and *Ch.* (*H.*) *iratus* sp. nov. Nevertheless, due to some overlap between intra- and interspecies distances, 18S cannot be used as a reliable DNA barcode for this group of gastrotrichs (Fig. 4A). The 18S secondary structure models of the nine new gastrotrichs are shown in Figure 5 and Supp. file 1: Figs S1–S8. Diagnostic autapomorphies are marked by arrows. The distinctness of the majority of species is also strengthened by 1–16 CBCs (Table 3).

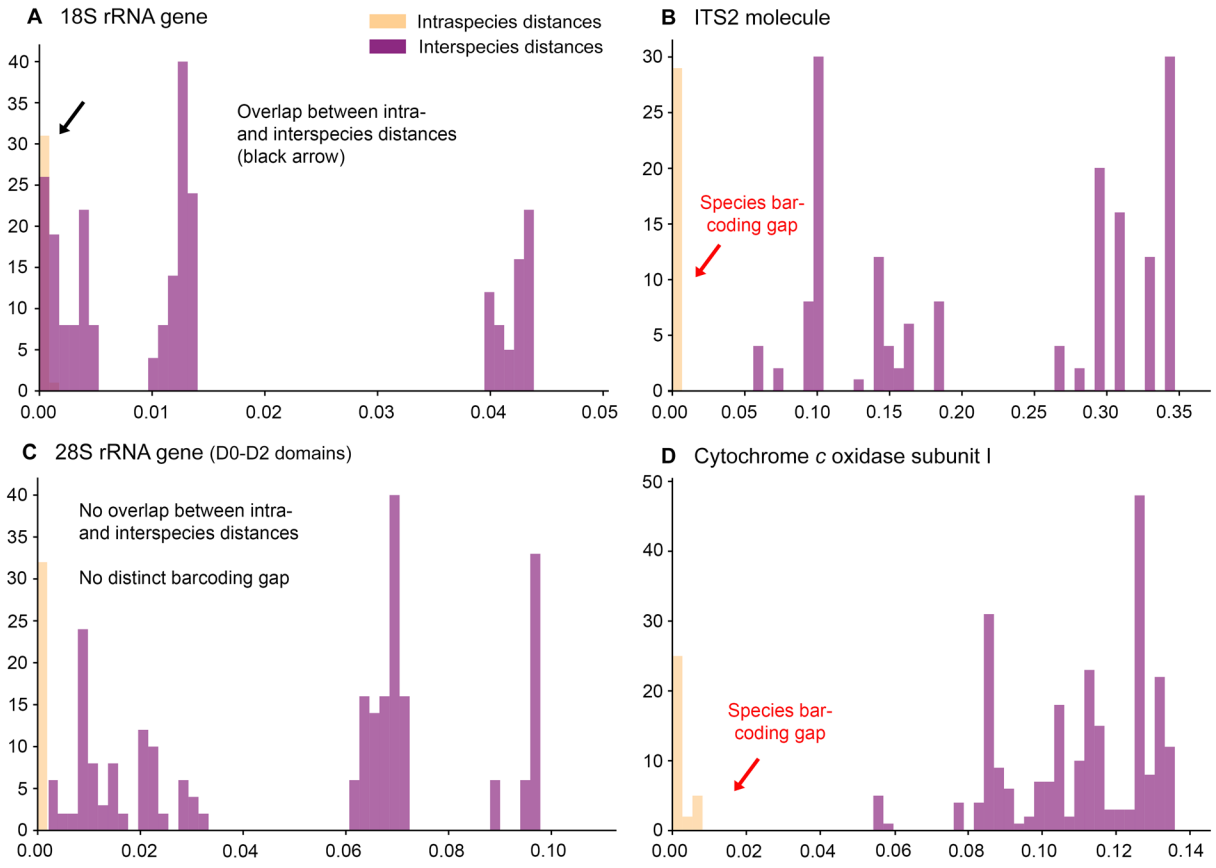

Fig. 4. Histograms showing intra- and interspecies *p*-distances of four molecular markers studied in nine new gastrotrich species. **A**. Barcoding analysis of 18S rRNA gene sequences. The black arrow marks the overlap between intra- and interspecies *p*-distances. **B**. Barcoding analysis of ITS2 molecules. Sequences are identical within species (red arrow), while interspecies *p*-distances range from 5.88% to as much as 34.76%. **C**. Barcoding analysis of the first two domains of 28S rRNA gene. Although there is no overlap between intra- and interspecies *p*-distances, no distinct barcoding gap is recognizable. **D**. Barcoding analysis of COI showing the distinct gap between intra- and interspecies *p*-distances (red arrow).

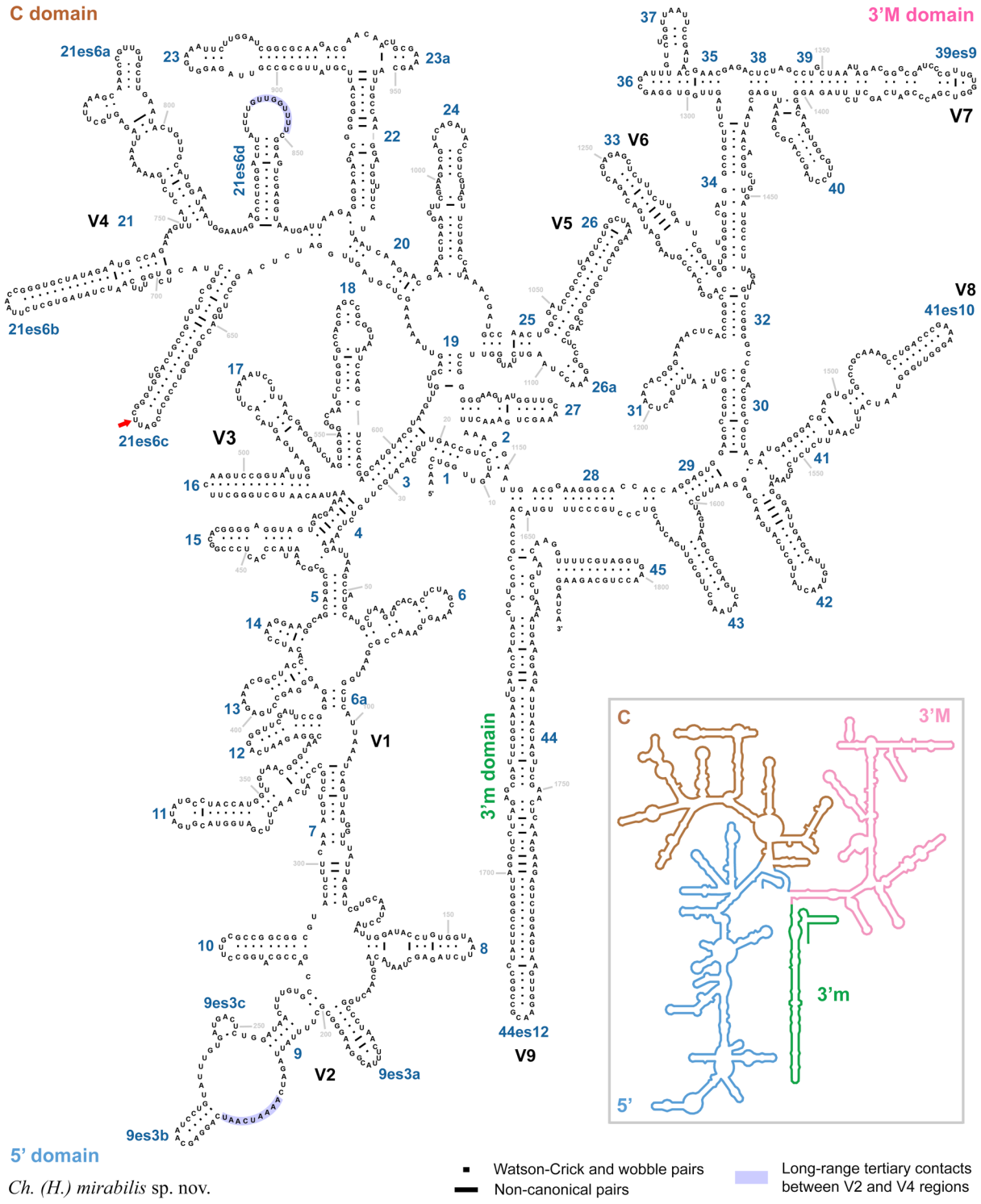

Ch. (H.) mirabilis sp. nov.

Fig. 5. Secondary structure of the 18S rRNA molecule of *Chaetonotus* (*Hystricochaetonotus*) *mirabilis* sp. nov. The single diagnostic molecular autapomorphy (red arrow) is situated in the terminal loop of helix 21es6c in the V4 region of the C domain. Note the long-range tertiary contacts between the V2 and V4 regions (highlighted in pink). The reference 18S secondary structure map of *Saccharomyces cerevisiae* Meyen ex E.C.Hansen (inset) is from http://apollo.chemistry.gatech.edu/RibosomeGallery (Petrov *et al.* 2014).

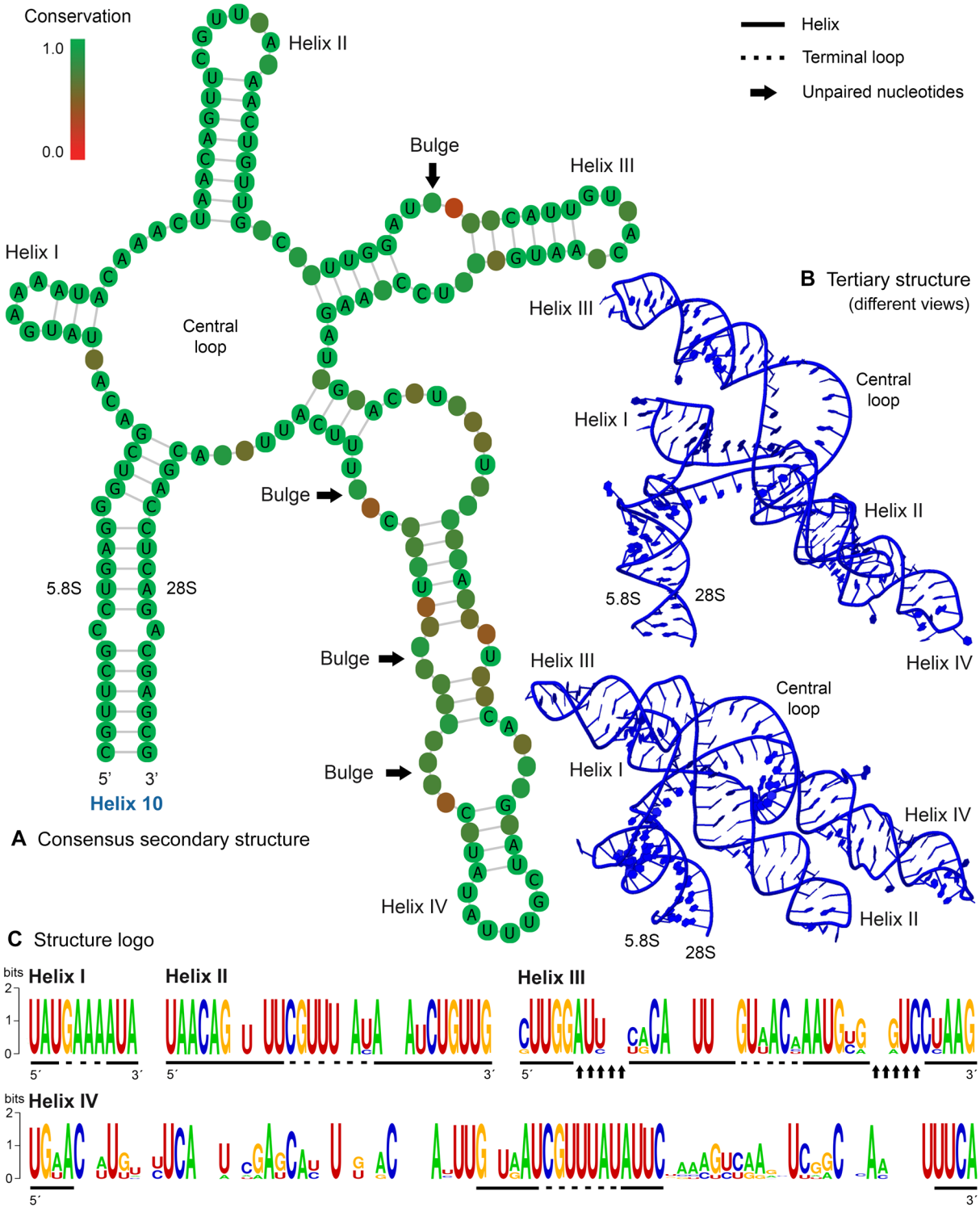

Fig. 6. ITS2 of the subgenus *Hystricochaetonotus* Schwank, 1990. **A**. Putative consensus secondary structure. The central loop radiates four unequally long helices. The first two helices are highly conserved, while the two following helices are much less conserved. For localization of helix 10, which is made by the interaction of 3'-end of 5.8S and 5'-end of 28S, see Fig. 7. **B**. Two different views on the tertiary structure, showing that helices II and IV run in parallel. **C**. Structure logos of helices I–IV. The height of a base is proportional to its frequency in the multiple sequence alignment.

Table 3. Numbers of CBCs in the 18S, ITS2, and 28S molecules of nine new species of the subgenus *Hystricochaetonotus* Schwank, 1990. A dash (–) indicates missing ITS2 sequences from *Ch.* (*H.*) *avarus* sp. nov. and *Ch.* (*H.*) *optabilis* sp. nov.

		1.	2.	3.	4.	5.	6.	7.	8.
1.	*Ch.* (*H.*) *mirabilis* sp. nov.								
2.	*Ch.* (*H.*) *gulosus* sp. nov.	2/4/11							
3.	*Ch.* (*H.*) *luxus* sp. nov.	3/4/12	1/0/2						
4.	*Ch.* (*H.*) *avarus* sp. nov.	3/–/10	1/–/2	2/–/2					
5.	*Ch.* (*H.*) *optabilis* sp. nov.	13/–/11	15/–/17	16/–/18	14/–/18				
6.	*Ch.* (*H.*) *slavicus* sp. nov.	3/4/12	1/0/2	0/0/0	2/–/2	16/–/18			
7.	*Ch.* (*H.*) *superbus* sp. nov.	0/4/1	2/4/10	3/4/10	3/–/9	13/–/11	3/4/10		
8.	*Ch.* (*H.*) *iratus* sp. nov.	3/2/12	1/1/2	0/1/0	2/–/2	16/–/18	0/1/0	3/3/10	
9.	*Ch.* (*H.*) *arcanus* sp. nov.	3/3/12	1/0/2	0/0/0	2/–/2	16/–/17	0/0/0	3/3/10	0/1/1

The ITS2 transcripts were comparatively short, ranging from 150 to 164 ribonucleotides with a GC content of 30.52–35.95% (Table 4). All gastrotrichs shared a loop model consisting of a 17–37 nt-long central loop and four helices (Fig. 6A). Helix I is the shortest and most conservative, displaying a motif 5'-UAU vs AUA-3' in the stem and a terminal tetraloop. Helix II is also rather conservative, carrying a motif 5'-UAACAG vs CUGUUG-3' at its base (Fig. 6C). This helix is typically composed of eight rarely ten (*Ch.* (*H.*) *superbus* sp. nov., Supp. file 1: Fig. S9B) or eleven (*Ch.* (*H.*) *mirabilis* sp. nov., Supp. file 1: Fig. S9A) pairs. In addition, there is a pyrimidine mismatch in *Ch.* (*H.*) *superbus* sp. nov. (Supp. file 1: Fig. S9B, opposed arrows). The terminal loop of helix II consists of six to eight ribonucleotides. Helix III is less conservative and contains 11–13 pairs, a single bulge, and 4 or 6 nucleotides in the terminal loop. Helix IV is the longest having as many as 46–72 ribonucleotides. It is the most variable helix concerning both the primary and the secondary structure. Only the terminal part of this helix is somewhat conserved, displaying a motif 5'-RAU vs AUY-3' in front of the terminal loop. Interestingly, there are no variable positions in the terminal loop of helix IV (Fig. 6A, C). ITS2 sequences were consistently identical within a species. Interspecies *p*-distances ranged from 5.88% to as much as 34.76%, making the ITS2 molecule an optimal barcode for species identification (Fig. 4B). Moreover, both the primary and secondary structures unambiguously define each species (Supp. file 1: Figs S9–S12) and up to four CBCs have been recognized between species (Table 3).

The amplified region of the 28S rRNA gene covers a portion of domain 0 (helix 25a), the whole domain I (helices 2–25es7), and a part of domain II (helices 27–35a). Sequences within species were identical except for *Ch.* (*H.*) *slavicus* sp. nov. in which the sequence identities ranged from 99.91% to 100%. Interspecies *p*-distances varied from 0.26% to 9.78%. Since the gap between intra- and interspecies distances is very small (i.e., the maximum intraspecies distance is 0.09% while the minimum interspecies distance is 0.26%), 28S is suitable only as a DNA pre-barcode (Fig. 4C). Despite this, each species could be unambiguously distinguished by both the primary and the secondary structure of the first two domains of the 28S rRNA molecule. Species-specific mutations tend to accumulate in helices 25es7–25es7c, which are hence taxonomically most important. Secondary structure models of the nine new gastrotrichs are shown in Figure 7 and Supp. file 1: Figs S13–S20. Diagnostic autapomorphies are marked by arrows. The distinctness of the majority of species is also strengthened by 1–18 CBCs (Table 3).

The amplified region of the COI gene is invariably 677 nt long and has a GC content of 42.25–44.46%. According to the present barcoding analyses, the intraspecies *p*-distances range only from 0.00% to 0.59% whereas the interspecies distances vary from 5.63% to 13.59%. Such a big gap between intra-

Table 4. Characterization of ITS2 molecules of seven new species of the subgenus *Hystricochaetonotus* Schwank, 1990.

Taxon	Total length	GC content (%)	Length of helix				Number of unpaired bases in							No. of bulges in helix IV	No. of GU pairings	ΔG (37°C, kcal/mol)
			I	II	III	IV	Central loop	Terminal loop of helix I	Terminal loop of helix II	Terminal loop of helix III	Terminal loop of helix IV	Bulge(s) of helix III	Bulges of helix IV			
Ch. (*H.*) *arcanus* sp. nov.	153	33.33	10	23	34	67	19	4	7	6	7	6	12	4	7	–27.40
Ch. (*H.*) *gulosus* sp. nov.	150	32.00	10	23	34	66	17	4	7	4	7	4	13	4	6	–28.60
Ch. (*H.*) *iratus* sp. nov.	164	35.37	10	23	40	72	19	4	7	6	7	8	25	4	2	–32.90
Ch. (*H.*) *luxus* sp. nov.	162	33.95	10	24	38	71	19	4	8	4	7	8	28	3	3	–30.60
Ch. (*H.*) *mirabilis* sp. nov.	154	30.52	10	28	33	46	37	4	6	6	7	5	5	2	7	–25.10
Ch. (*H.*) *slavicus* sp. nov.	153	35.95	10	23	34	67	19	4	7	6	7	4	20	4	3	–31.40
Ch. (*H.*) *superbus* sp. nov.	155	32.26	10	28	35	58	24	4	6	4	7	7	9	2	5	–29.60
Minimum	150	30.52	10	23	33	46	17	4	6	4	7	4	5	2	2	–32.90
Maximum	164	35.95	10	28	40	72	37	4	8	6	7	8	28	4	7	–25.10
Arithmetic mean	155.9	33.34	10	24.6	35.4	63.9	22	4	6.9	5.1	7	6	16	3.3	4.7	–29.37
Standard deviation	5.15	1.92	0.00	2.37	2.57	9.08	6.95	0.00	0.69	1.07	0.00	1.73	8.52	0.95	2.06	2.61

and interspecies distances (more than one order of magnitude) makes COI to be a very suitable DNA barcode for the subgenus *Hystricochaetonotus* (Fig. 4D).

Phylogenetic analyses

The multi-gene phylogenetic analyses resulted in well-resolved trees (Figs 8–9). Each new gastrotrich species was depicted as a separate branch both in the ML and Bayesian trees. All nine new species consistently clustered together in a fully statistically supported clade comprising multiple species assigned to the subgenus *Hystrichochaetonotus* (*Ch.* (*H.*) *aemilianus*, *Ch.* (*H.*) *borealis*, *Ch.* (*H.*) *hornsundi* and *Ch.* (*H.*) cf. *hornsundi*, *Ch.* (*H.*) cf. *hystrix* and *Ch.* (*H.*) aff. *euhystrix*, *Ch.* (*H.*) *persimilis* and *Ch.* (*H.*) aff. *persimilis*) and the subgenus *Chaetonotus* (*Ch.* (*Ch.*) *bombardus* and *Ch.* (*Ch.*) aff. *bombardus*)

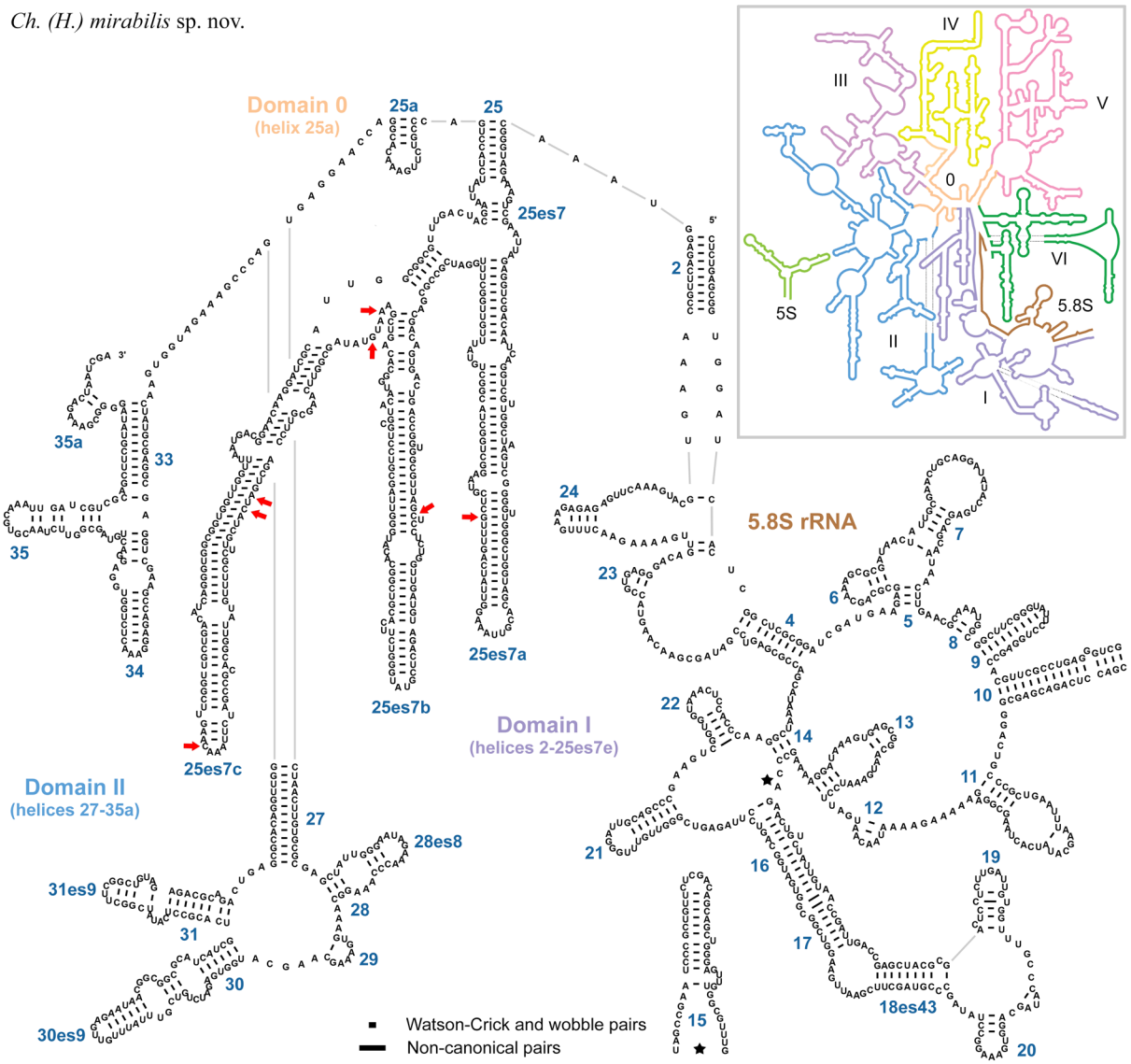

Fig. 7. Secondary structure of the first two domains of the 5.8–28S rRNA molecule of *Chaetonotus* (*Hystricochaetonotus*) *mirabilis* sp. nov. Diagnostic molecular autapomorphies are marked by red arrows. The reference 28S secondary structure map of *Saccharomyces cerevisiae* Meyen ex E.C.Hansen (inset) is from http://apollo.chemistry.gatech.edu/RibosomeGallery (Petrov *et al.* 2014).

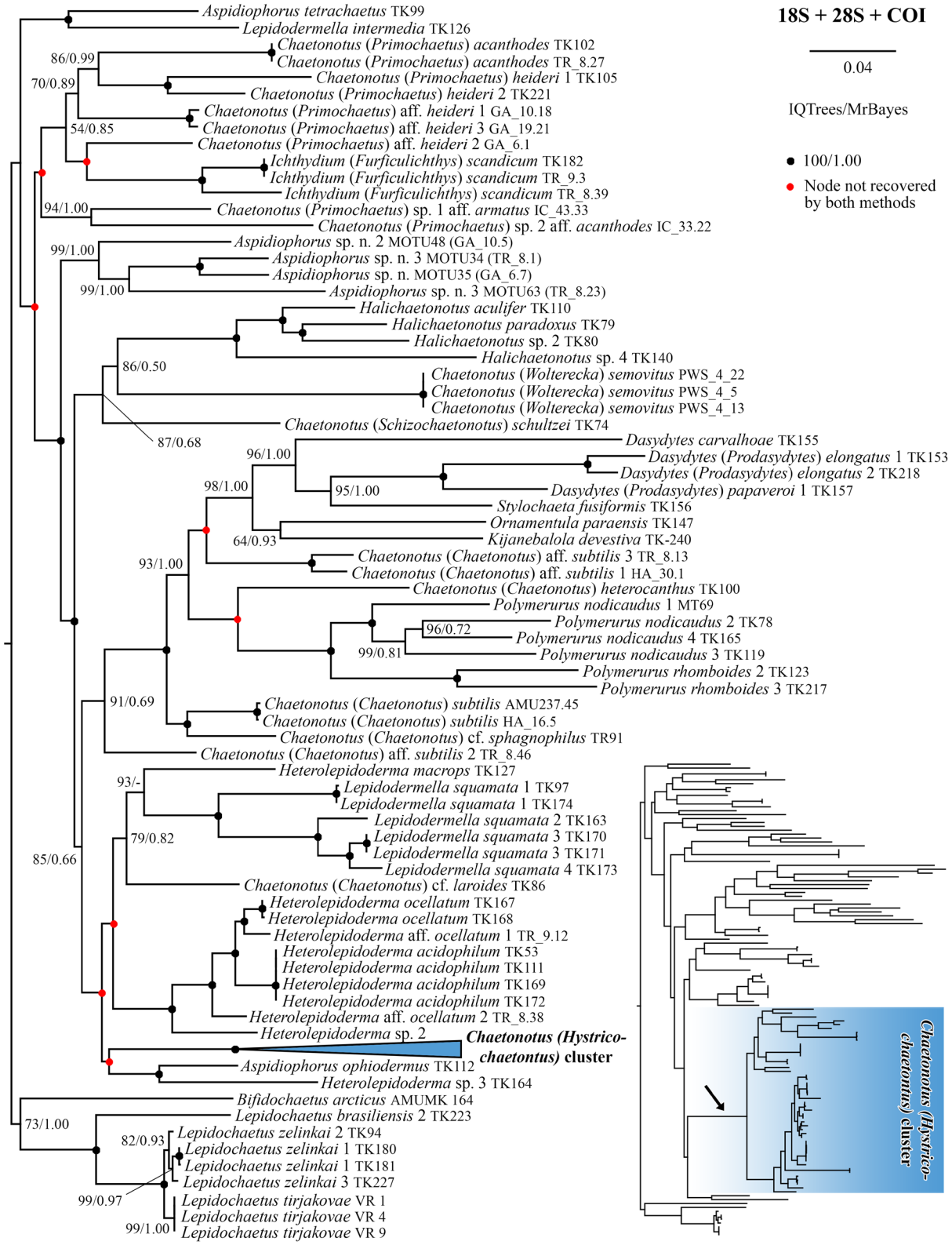

Fig. 8. Phylogenetic tree based on 18S, 28S, and COI sequences, showing the systematic positions of the *Chaetonotus* (*Hystricochaetonotus*) cluster (arrow). This clade is collapsed in the three, highlighted in the inset phylogram, and presented in detail in Fig. 9. ML bootstrap values and posterior probabilities were mapped onto the best ML tree.

(Fig. 9). This species-rich clade was separated from other chaetonotids included in phylogenetic analyses by a very distinct and comparatively long branch (Fig. 8, arrow). This split was well recognizable also when 18S, 28S, and COI were analyzed separately (data not shown). Thus, both nuclear and mitochondrial genes strongly corroborate the long independent evolution of this diverse clade.

This clade was consistently divided into two statistically well-supported lineages. The first group comprised *Ch. mirabilis* sp. nov., *Ch. superbus* sp. nov., *Ch. optabilis* sp. nov., *Ch. aemilianus*, *Ch.* cf. *hystrix*, *Ch.* aff. *euhystrix*, and *Ch.* aff. *bombardus* (94% ML, 0.98 BI). As concerns the three new species, *Ch. mirabilis* sp. nov. and *Ch. superbus* sp. nov. clustered together (100% ML, 1.00 BI)

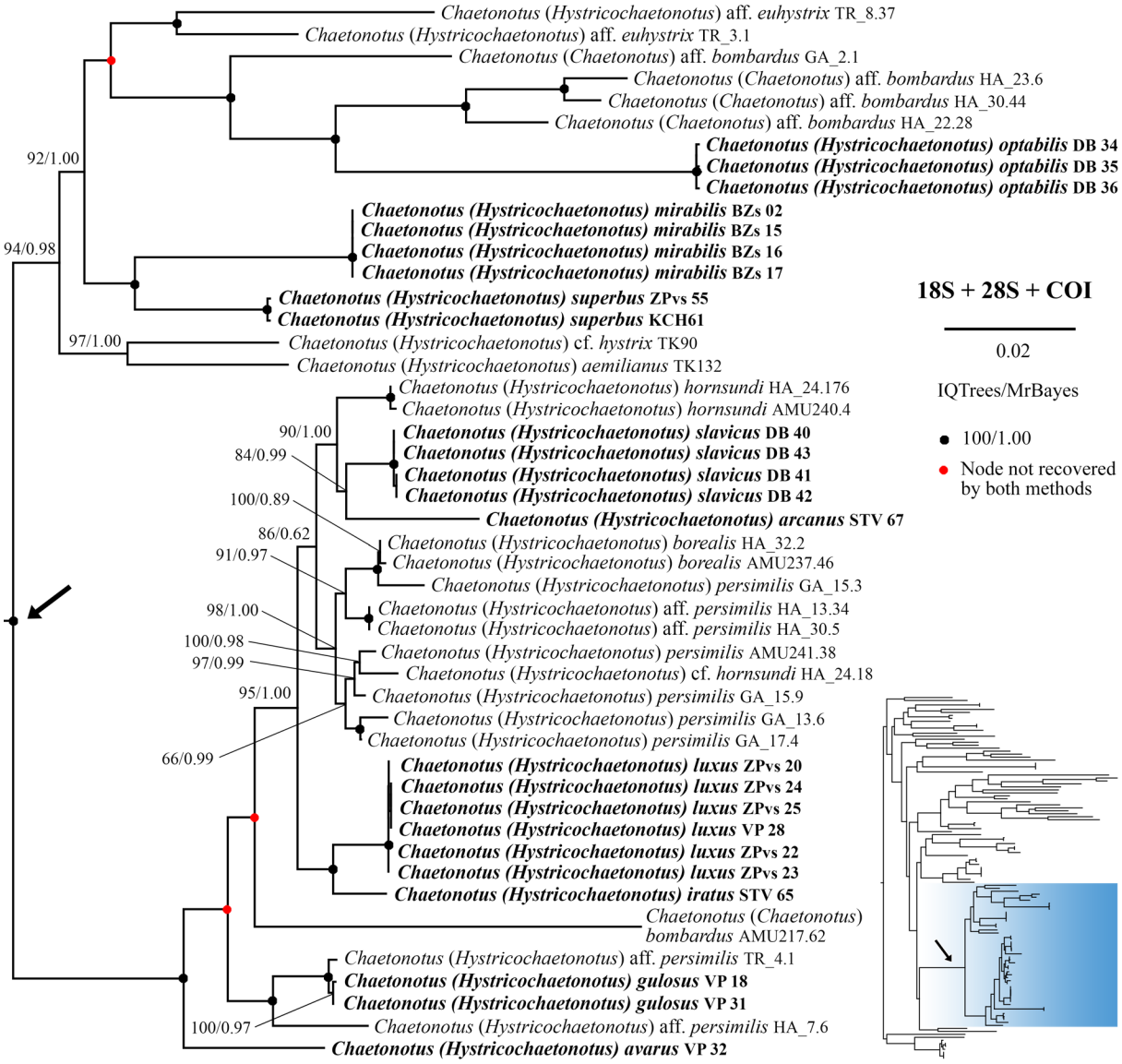

Fig. 9. Phylogenetic subtree based on 18S, 28S, and COI, showing the systematic positions of the nine new species within the *Chaetonotus* (*Hystricochaetonotus*) cluster. Arrows mark the same node in the subtree and the inset phylogram. The whole tree is presented in Fig. 8. The *Chaetonotus* (*Hystricochaetonotus*) cluster is highlighted in the inset phylogram. ML bootstrap values and posterior probabilities were mapped onto the best ML tree.

while *Ch. optabilis* sp. nov. grouped with *Ch.* aff. *bombardus* (100% ML, 1.00 BI). The second lineage united the six remaining new species and *Ch. borealis*, *Ch. hornsundi*, *Ch.* cf. *hornsundi*, *Ch. persimilis*, *Ch.* aff. *persimilis*, and *Ch. bombardus* (100% ML, 1.00 BI). With regard to the new species, *Ch. avarus* sp. nov. represented a separate lineage, *Ch. gulosus* sp. nov. grouped with *Ch.* aff. *persimilis* TR_4.1 (100% ML, 1.00 BI), *Ch. luxus* sp. nov. and *Ch. iratus* sp. nov. clustered together (100% ML, 1.00 BI), and *Ch. arcanus* sp. nov. and *Ch. slavicus* sp. nov. formed a monophylum (84% ML, 0.99 BI) that was placed in a sister position to *Ch. hornsundi* (80% ML, 1.00 BI) (Fig. 9).

Taxonomic account

Phylum Gastrotricha Mečnikow, 1865
Order Chaetonotida Remane, 1925 (sensu Rao & Clausen 1970)
Suborder Paucitubulatina d'Hondt, 1971
Family Chaetonotidae Gosse, 1864 (sensu Garraffoni *et al.* 2017)
Genus *Chaetonotus* Ehrenberg, 1830
Subgenus *Hystricochaetonotus* Schwank, 1990

Chaetonotus* (*Hystricochaetonotus*) *mirabilis sp. nov.
urn:lsid:zoobank.org:act:F959427F-762B-4344-A1E4-7D491DD99225
Figs 10–14; Supp. file 1: Table S2

Morphological diagnosis

Body slender and about 83–107 µm long. Head wider than neck, separated from trunk by a distinct neck constriction. Cephalion clearly demarcated, epipleurae and hypopleurae only inconspicuously marked in head outline. Trunk widest at ca U62, gradually tapers towards furca base (U85). Mouth ventral, with two cuticular teeth. Pharynx with anterior and posterior dilatations. Intestine straight, with a marked anterior section. Scales spined, three-lobed, not overlapping, distributed in 10–12 columns, 17 scales per column. Dorsal surface covered from anterior end of hypopleurae (ca U6) to neck constriction with fairly small scales bearing short spines. Neck caries broader scales with longer spines. Anterior trunk region bears similarly shaped, slightly bigger scales with posterior lobes closer together. Dorsolateral and lateral scales with elongated base and posterior lobes more divergent, spine with an inconspicuous denticle. Mid-trunk to terminal trunk region covered by (i) five horizontal rows of big, anteriorly tapered scales carrying very elongated, massive spines with a denticle and membrane and (ii) two horizontal rows of smaller, anteriorly rounded scales carrying significantly shorter spines with a denticle. Furca base short, lateral margins vaulted, furcal indentation U-shaped, adhesive tubes well-developed, diverging posteriorly. Furca base and branches covered with three-lobed, spined scales and oblong, keeled scales.

Molecular diagnosis

18S rRNA gene: 672 T, 1072 –. ITS2: 26 G, 28 A, 40 G, 41 T, 53 G, 60 C, 62 T, 84 A, 96 A, 107 –, 117 T, 131 A, 132 A, 133 A, 136 –, 137 –, 139 C, 156 G, 157 T, 159 T, 168 A, 173 –. 28S rRNA gene: 530 G, 608 C, 687 A, 690 G, 717 A, 719 C, 756 C. Cytochrome *c* oxidase subunit I (codon ordinal numbers are followed by the corresponding span of nucleotide positions in parentheses): 23 (67–69) ATT, 28 (82–84) CTT, 44 (130–132) GTC, 45 (133–135) GTA, 63 (187–189) GGA, 72 (214–216) CTT, 82 (244–246) CCA, 97 (289–291) AGT, 98 (292–294) TTA, 100 (298–300) CTT, 103 (307–309) GCG, 129 (385–387) AGG, 142 (424–426) GCA, 146 (436–438) TTG, 155 (463–465) ACC, 156 (466–468) CTA, 162 (484–486) GGT, 165 (493–495) TTT, 167 (499–501) CGT, 170 (508–510) TTA, 179 (535–537) GTT, 184 (550–552) CTG, 190 (568–570) GCC, 212 (634–636) GGA, 221 (661–663) CTA.

Reference molecules are shown in Figures 5, 7, and Supp. file 1: Fig. S9A. All diagnostic molecular autapomorphies are marked by arrows. Reference alignments with corresponding nucleotide positions are in Supp. file 1: Alignments 1–4.

The *p*-distance from species described in the present study is 0.22–4.06% in 18S, 18.19–34.22% in ITS2, 2.23–7.12% in 28S, and 11.37–13.15% in COI. There are 2–13 CBCs (except for *Ch.* (*H*). *superbus* sp. nov., where there are no CBCs) in the 18S rRNA molecule, 2–4 CBCs in the ITS2 molecule, and 1–12 CBCs in the first two domains of the 28S rRNA molecule.

Etymology

The Latin adjective '*mirabil·is*, *-is*, *-e*' [m, f, n] ('marvelous, extraordinary') refers to the extraordinary long dorsal spines.

Material examined

Holotype

SLOVAKIA • adult (photomicrographs, hologenophore); Greenhouse pond, Botanical Garden, Karlova Ves, Bratislava, Podunajská rovina plain (type locality); 48°08′46.8″ N, 17°04′22.6″ E; CU-FNS-11-09-19/HO.

Photomicrographs of the holotype are available at the Department of Zoology, Comenius University in Bratislava at https://fns.uniba.sk/en/gastrotricha/. The holotype is shown in Fig. 12.

Paratypes

SLOVAKIA • 2 adults (photomicrographs); same collection data as for holotype; CU-FNS-25-10-19/PA-1, CU-FNS-02-10-19/PA-2.

Photomicrographs of paratype specimens are available at the Department of Zoology, Comenius University in Bratislava at https://fns.uniba.sk/en/gastrotricha/. Paratypes are shown in Figs 13–14.

Type material

A DNA sample of the holotype specimen BZs 02 has been deposited in the Natural History Museum, Vajanského nábrežie 2, 810 06 Bratislava, Slovakia (ID Collection Code 01427888).

Type locality

Greenhouse pond, Botanical Garden of Comenius University, Karlova Ves, Bratislava, Podunajská rovina plain, Slovakia, 48°08′46.8″ N, 17°04′22.6″ E.

Gene sequences

The nuclear 18S and ITS1-5.8S-ITS2-28S rDNA sequences as well as the mitochondrial COI sequence of the holotype specimen BZs 02 have been deposited in GenBank under the following accession numbers: OM421704, OM421680, and OM424059, respectively.

Description

Habitus. *Chaetonotus* (*Hystricochaetonotus*) *mirabilis* sp. nov. is about 83–107 µm long and has a slender body that is tenpin-shaped, with a clearly defined head region, a narrowing neck, and a slightly bulbous trunk (Figs 10A–B, G, 12A–C). Body width is 10–19 µm at U10, 11.2–11.6 µm at U50, and 17.5–18.5 µm at U60. The head is relatively wide, with a plate-like, rounded cephalion. The neck (ca U12–U27) is clearly demarcated and smoothly continues to the trunk region, i.e., a distinct neck constriction is formed. The trunk is nearly as wide as the head, gradually dilating from about U39 to U62 where it reaches the maximum width. Then it gradually tapers towards U84 where vaulted margins of the furca branches start to form. Dorsal sensory bristles (setolae) arise from the cuticle in two pairs at U25 and U75 (Figs 14A, 16C). The furcal indentation is broadly U-shaped. The furca branches are

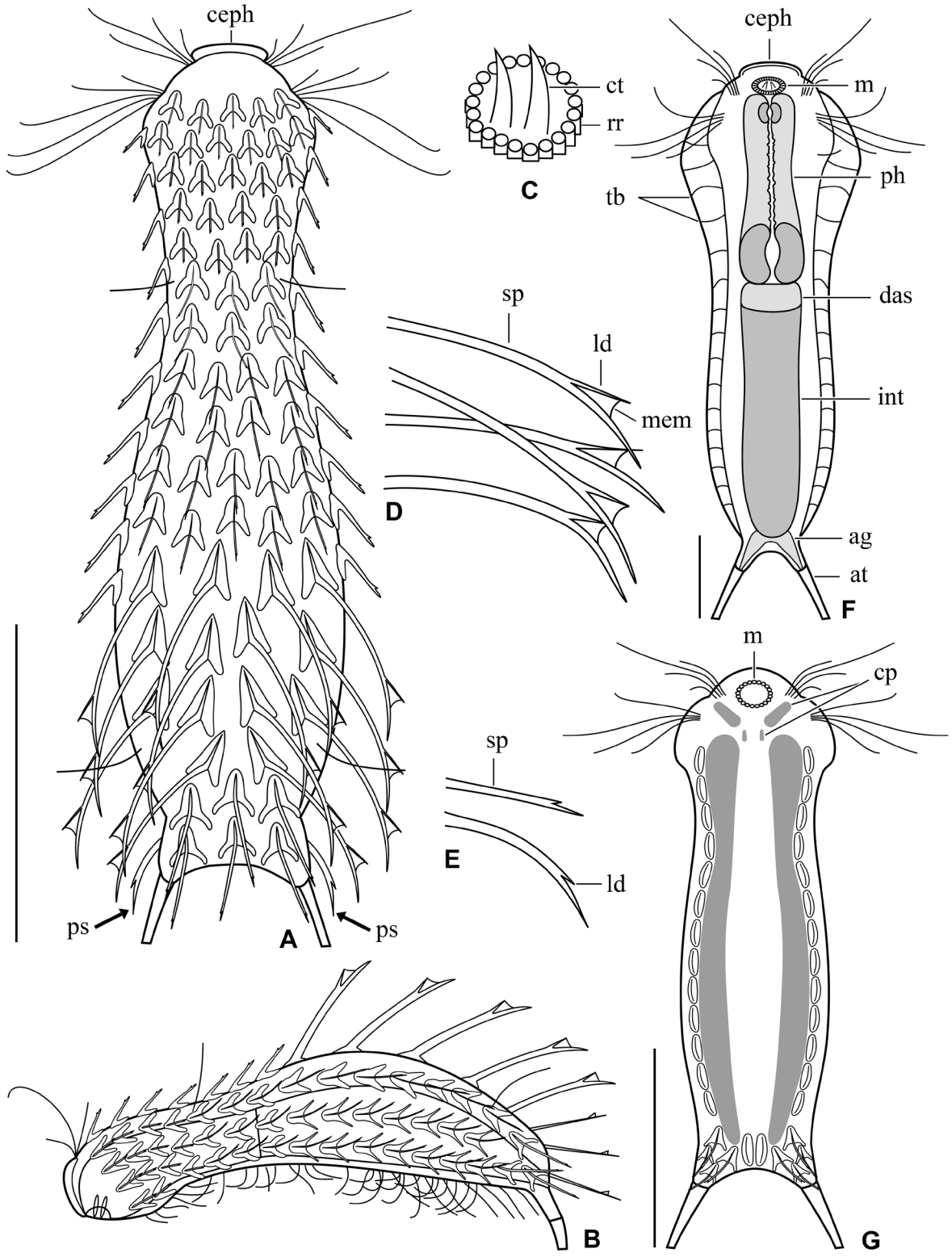

Fig. 10. *Chaetonotus* (*Hystricochaetonotus*) *mirabilis* sp. nov. **A–B**. Dorsal and lateral overviews showing the scale and spine pattern. **C**. Detail showing the cuticular teeth protruding from the mouth ring. **D**. Elongated dorsal spines with a membrane. **E**. Terminal dorsal spines. **F**. Internal morphology of a strongly squeezed specimen (body shape hence not representative). **G**. Ventral overview. Scale bars: A = 30 μm; F–G = 20 μm.

set apart and diverge posteriorly. Well-developed adhesive tubes are 9.4–10.5 µm long, they are straight and narrow (Fig. 17G).

Head. The head is roughly five-lobed. The cephalion (U1–U2) is rounded, 0.4–0.9 µm wide, clearly demarcated in the body outline, appears as a lens in the ventral view, and has a free posterior (dorsal) edge (Figs 10A–B, F, 12B, 13A–C). The epipleurae are approximately at U3–U5 and the hypopleurae are at ca U6–U9. Notches separating the epipleurae from the hypopleurae are very shallow, causing that they are only inconspicuously marked in the head outline (Fig. 13A, E). Two pairs of cephalic ciliary tufts emerge laterally between the cephalion and the epipleurae edge (ca U3) as well as between the epi- and the hypopleurae edge (U5) (Figs 10A, F–G, 12A–C, 13A, E). The hypostomium is absent and the under-mouth area carries only ciliary patches. Each field is composed of several irregular groups of basal

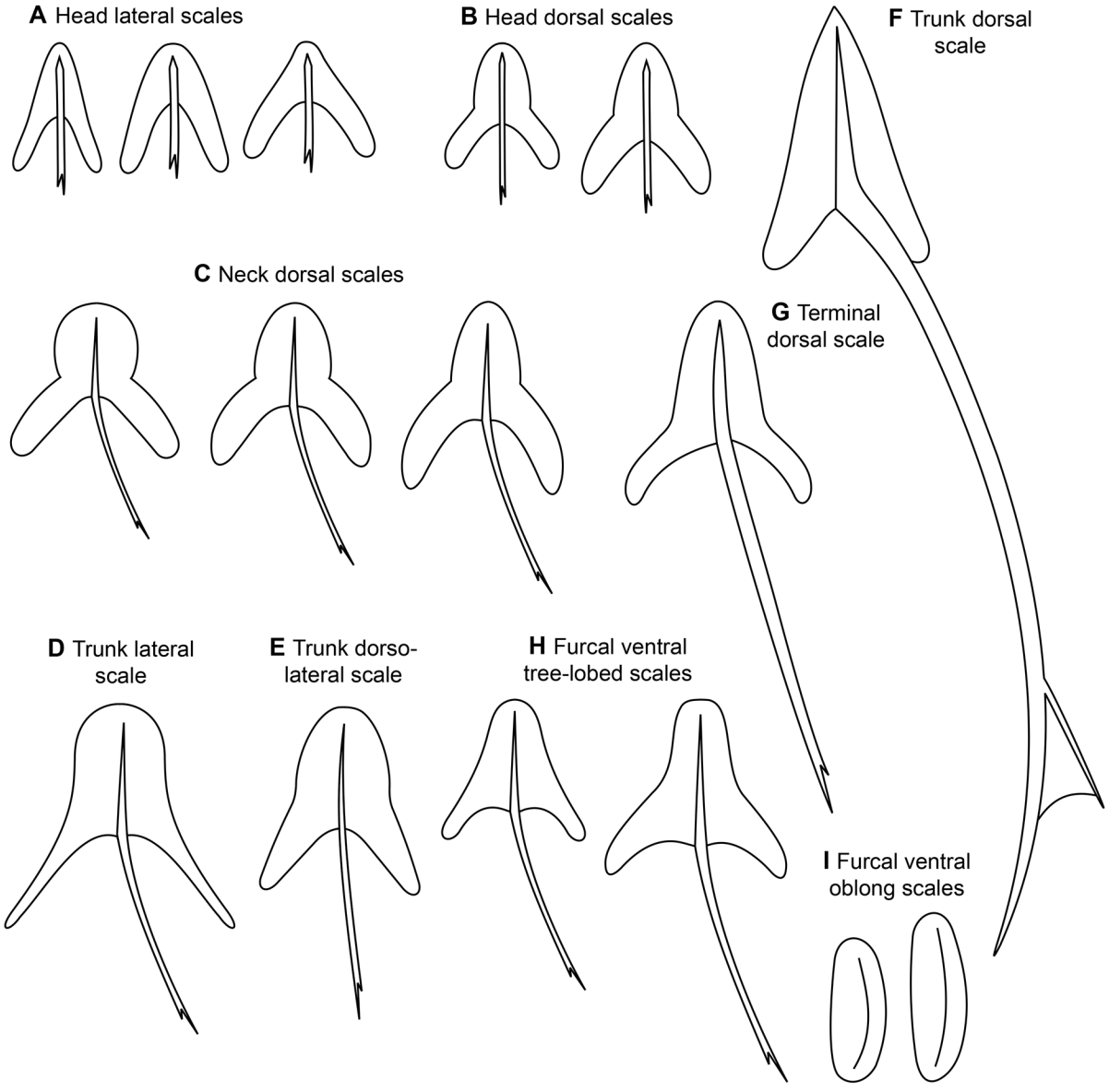

Fig. 11. Scales of *Chaetonotus* (*Hystricochaetonotus*) *mirabilis* sp. nov. **A**. Head lateral scales. **B**. Head dorsal scales. **C**. Neck dorsal scales. **D**. Trunk lateral scale. **E**. Trunk dorsolateral scale. **F**. Trunk dorsal scale. **G**. Terminal dorsal scale. **H**. Furcal ventral three-lobed scales. **I**. Furcal ventral oblong scales.

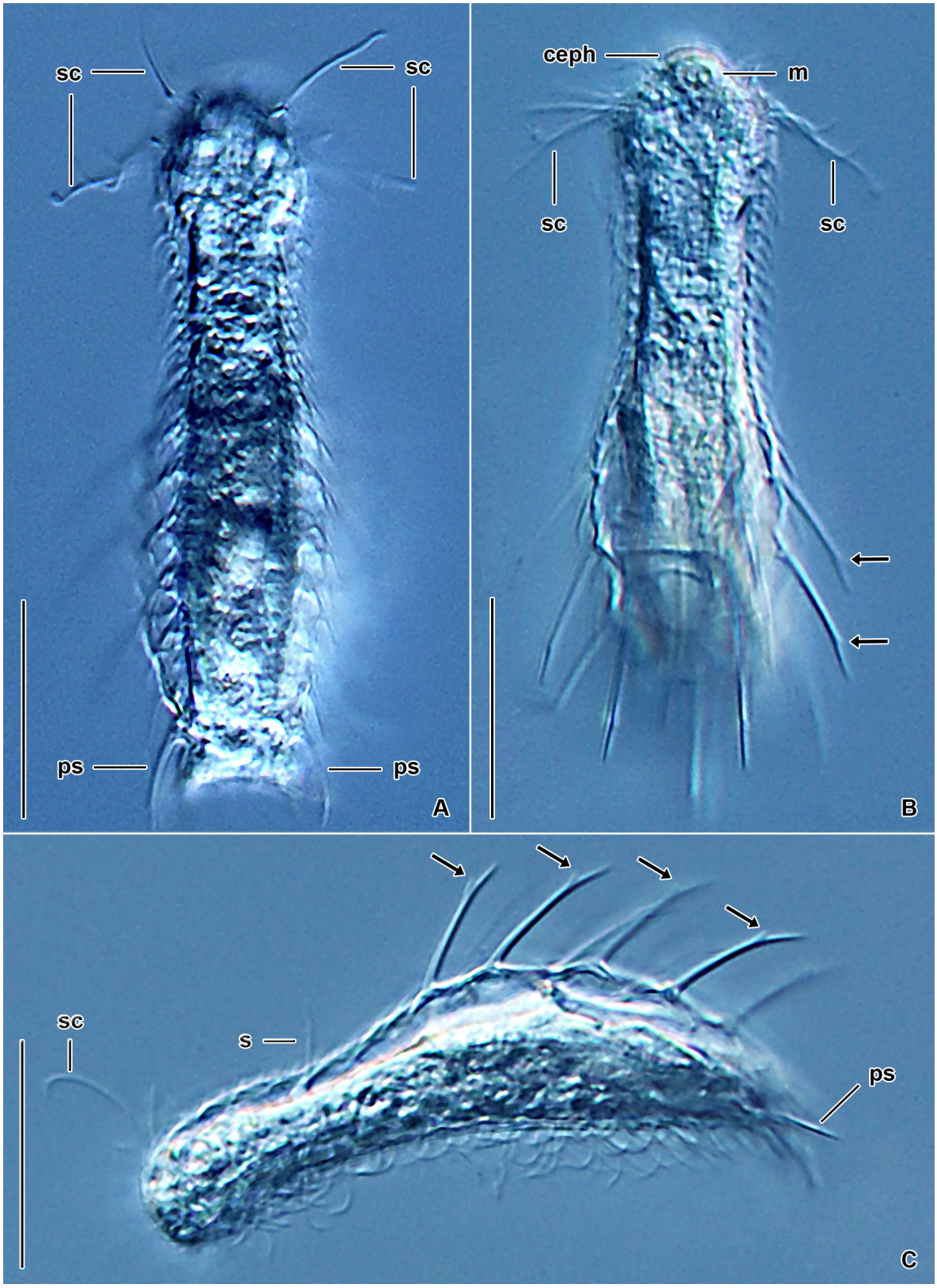

Fig. 12. *Chaetonotus* (*Hystricochaetonotus*) *mirabilis* sp. nov., holotype (CU-FNS-11-09-19/HO), differential interference contrast. **A–B**. Optical sections showing the general body organization. **C**. Lateral overview. Arrows in (B) and (C) mark the lateral denticle of spines. Scale bars = 30 µm.

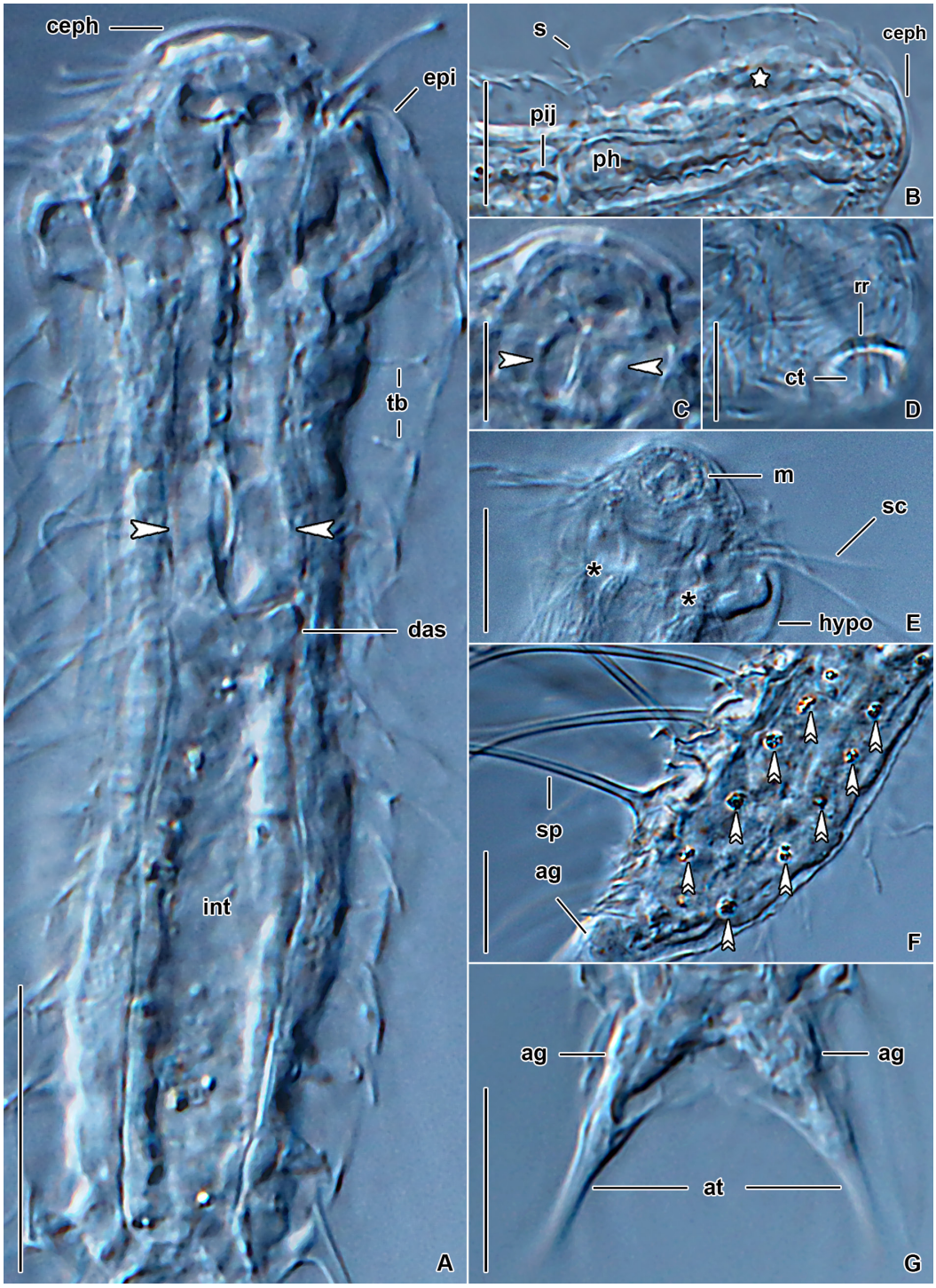

Fig. 13. *Chaetonotus* (*Hystricochaetonotus*) *mirabilis* sp. nov., differential interference contrast. **A, C, E, G**. Paratype (CU-FNS-25-10-19/PA-1). **B, D, F**. Paratype (CU-FNS-02-10-19/PA-2). **A**. Internal morphology. Opposed arrowheads denote posterior pharyngeal dilatations. **B**. Lateral view of the anterior body region. White star marks the cerebral ganglion. **C**. Anterior pharyngeal dilatations (opposed arrowheads). **D**. A pair of cuticular teeth is situated in the center of the mouth ring. **E**. Ventral view of the head region. Asterisks mark the beginning of the ventral ciliary bands. **F**. The intestine contains highly refractive and regularly arranged structures (white double arrowheads). **G**. Furca with a U-shaped indentation and adhesive glands. Scale bars: A = 15 µm; B, E–G = 10 µm; C–D = 5 µm.

bodies (kinetosomes). The mouth ring is oval, 5.0–5.5 µm in the largest diameter, located subterminally at U2–U4. There are strong but short, rod-like reinforcements lining the walls of the mouth ring as well as an inner pair of cuticular teeth located in the center of the mouth opening (Figs 10C, 13D).

Internal morphology. The pharynx extends from ca U5 to U30, is 26–30 µm long and 5.3–7.8 µm wide, sinuous, and has marked anterior and posterior dilatations (Figs 10F, 13A, C, white arrowheads). The posterior dilatation (ca U20–U30) is larger than the anterior one (ca U5–U8) (Supp. file 1: Table S2). The pharynx is connected to the straight intestine through a pharyngeal–intestinal junction (Fig. 13B). The intestine runs from U31 to U84 and has a separate, well-differentiated anterior section (U31–U33) (Figs 10F, 13A). There are highly refractive and regularly arranged structures well recognizable in the lateral view of the intestine (Figs 13F, 14G, double white arrowheads). Transversal bands connected to the base of dorsal scales are recognizable from ca U10 (Figs 10F, 13A). The adhesive gland (ca U85–U91) is placed right behind the terminal part of the intestine, it is broadly pyriform forming a short dichotomy at the subtle furca base (Figs 10F, 13G).

Scales. Almost the entire body is covered by not overlapping three-lobed scales that adhere to the basal cuticle layer along their whole perimeter. Scales are distributed in a minimum of 10–12 longitudinal rows, with 17 scales in the central row. Central dorsal and dorsolateral longitudinal rows of scales begin at the level of the anterior edge of the hypopleurae (ca U6), lateral rows start at their posterior end (ca U9). Ventral and ventrolateral rows are hardly visible due to the highly pronounced dorsal spines (for further explanation, see below). Head scales (ca U6–U25) are fairly small, i.e., 3.3–4.1 × 1.9–3.9 µm in size. Two types could be recognized: (i) lateral boomerang-shaped scales with a subtle anterior lobe, the transition between anterior and posterior lobes is indistinct and continuous, α = 170–177°, and β = 70–85° (Fig. 11A) and (ii) dorsal/dorsolateral scales with a distinctly elongated anterior lobe and a smaller angle α ranging from 146 to 169°, angle β spans a wide range of 68–108°, and the transition between anterior and posterior lobes is marked (Figs 11B, 14B). Neck dorsal scales are 3.2–5.1 × 2.0–2.7 µm in size. They are anteriorly more broadly rounded, their angle α is slightly smaller (153–163°), β is closer to the right angle (82–91°) than in head scales, and the transition between anterior and posterior lobes is marked (Figs 11C, 14A). This type of scale terminates right at the anterior border of the trunk region (ca U26–U39). The trunk region is covered by four types of scales: (i) lateral scales (U37–U50) with a tongue-shaped anterior lobe and comparatively narrow posterior lobes, α = 149–150°, and β = 76–82°, the transition between anterior and posterior lobes is indistinct and continuous (Figs 11D, 14F); (ii) dorsolateral scales (U50–U81) with a tongue-shaped anterior lobe and wider posterior lobes being closer together, α = 147–158°, β = 68–76°, the transition between anterior and posterior lobes is indistinct (Figs 11E, 14A, C); (iii) dorsal big scales (U50–U78) with a tapered, triangular anterior lobe and narrowly rounded posterior lobes, α = 175–179°, β = 57–68°, the transition between anterior and posterior lobes is also indistinct (Figs 11F, 14A); and (iv) dorsal smaller scales (U80–U90) with an anteriorly rounded anterior lobe, the transition between anterior and posterior lobes is marked (Figs 11G, 14D).

Spines. All spines bear a lateral denticle and gradually narrow towards the distal end. Three main types could be distinguished. The most common type of spines emerges from the head (2.7–3.7 µm long), neck (4.5–7.1 µm long), trunk dorsolateral (4.0–6.8 µm long), and lateral scales (6.8–8.8 µm long). The lateral denticle is minute and its tip is distant only 0.7–0.9 µm from the spine apex, which corresponds to a *d*-ratio of 25.3–31.2%. Lateral spines are, however, slightly thinner (0.32–0.35 µm vs 0.30–0.43 µm) and their subterminal denticle is rather inconspicuous and much closer to the spine apex (*d*-ratio 8–10%) in comparison with head, neck, and dorsolateral spines. The second type is represented by the prominent, elongated spines carrying a conspicuous denticle (2.6–5.6 µm long) associated with a membrane (Figs 10D, 11F, 12B–C, 13F, 14A, G). The denticle is 6.4–7.9 µm distant from the spine apex, which corresponds to a *d*-ratio of 18.2–22.6%. Type 2 spines are 20.7–35.9 µm long and comparatively wide (1.8–1.9 µm) at the base. Altogether only five horizontal rows of dorsal scales are equipped with

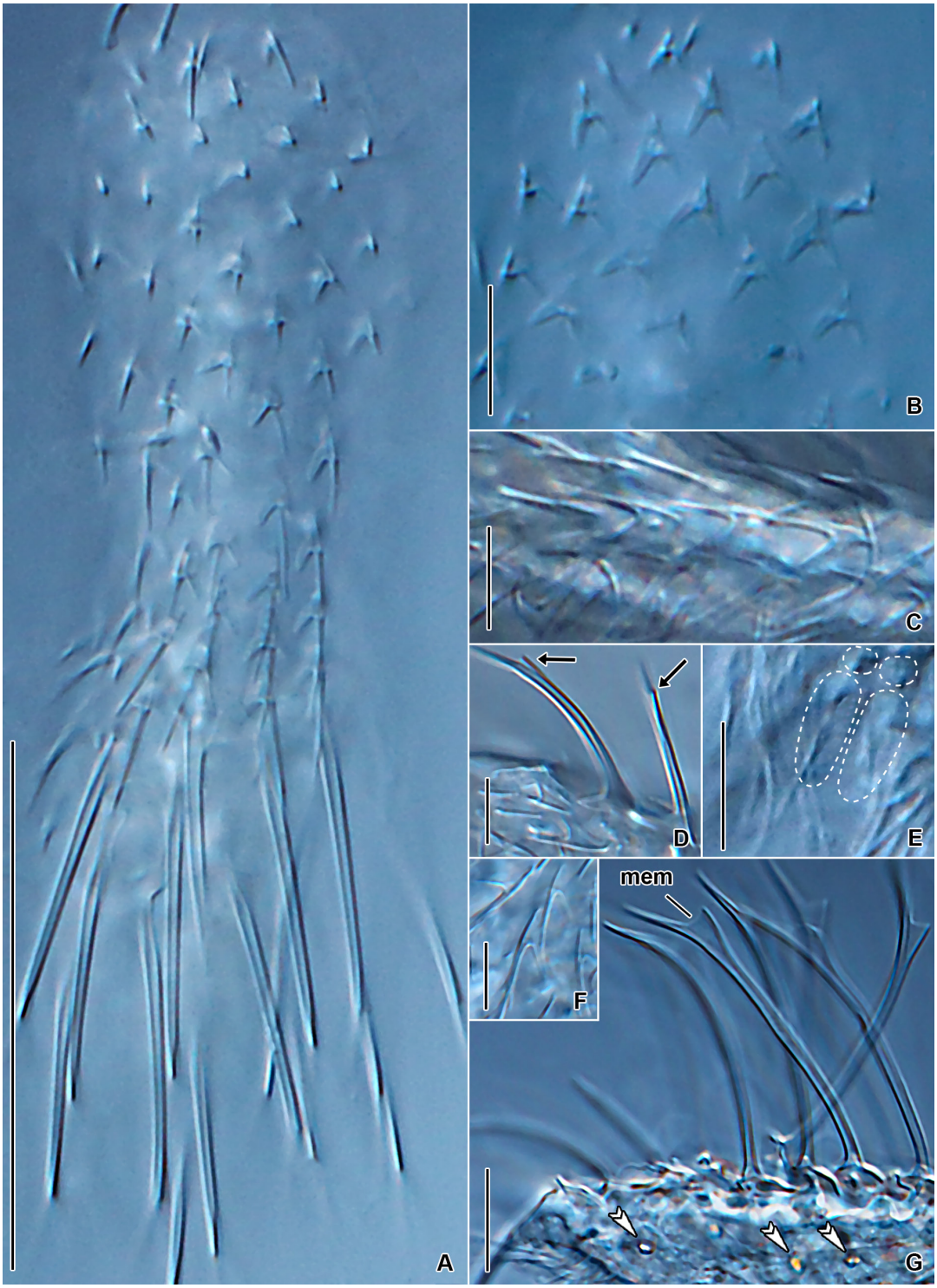

Fig. 14. *Chaetonotus* (*Hystricochaetonotus*) *mirabilis* sp. nov., differential interference contrast. **A–B, E**. Paratype (CU-FNS-25-10-19/PA-1). **C–D, F–G**. Paratype (CU-FNS-02-10-19/PA-2). **A**. Dorsal view showing the scale and spine pattern. **B**. Head scales. **C**. Neck and upper trunk dorsolateral scales. **D**. Terminal dorsal trunk scales with a lateral denticle (arrows). **E**. Ventral ciliary bands. White dashed lines mark upper-furcal scales. **F**. Lateral trunk scales. **G**. Dorsal trunk spines with a membrane. White double arrowheads mark the highly refractive bodies in the intestine. Scale bars: A = 30 µm; B–F = 5 µm; G = 10 µm.

this type of spines (U50–U78). The last type could be found only on the two terminal rows of dorsal scales on the furca base and branches. These spines are significantly shorter (13.0–18.4 µm vs 20.7–35.9 µm) and thinner (0.7–0.8 µm vs 1.1–1.6 µm) than the previous type. They are slightly curved and hair-like tapered distally. Although their denticle is well recognizable, it is not associated with a distinct membrane. The *d*-value is 2.9–4.4 µm and the *d*-ratio is 22.0–25.7% (Figs 10E, 11G, 14D).

Ventral ciliary bands and ventral interciliary field. Unfortunately, the ventral side could not be observed in detail due to the very long and strong type 2 spines that precluded turning over and squeezing the worms. Despite that, the following observations could be done. The longitudinal ciliary bands begin at ca U7 and run backward to ca U87. They are somewhat wider on the neck than on the trunk where they narrow slightly from ca U78. The ciliary bands are accompanied by a ventrolateral row of small (2.4–3.0 × 1.0–1.5 µm in size), oblong, and keeled scales that start at U7. The upper furcal region (U84–U90) carries two types of scales: (i) three-lobed, spined scales with a broadly rounded anterior lobe, narrowly rounded posterior lobes, α = 137–171°, and β = 59–72° (Figs 10G, 11H) and (ii) oblong and keeled scales being 1.5–3.9 × 0.7–1.5 µm in size (Figs 10G, 11I).

Chaetonotus* (*Hystricochaetonotus*) *superbus sp. nov.
urn:lsid:zoobank.org:act:781619BA-32C2-4336-A729-2BDA3E13C7D4
Figs 15–17; Supp. file 1: Table S3

Morphological diagnosis

Body stocky and about 107 µm long. Head wider than neck, separated from trunk by an inconspicuous neck constriction. Cephalion, epipleurae, and hypopleurae clearly demarcated. Trunk gradually widens from ca U37 to U60 and then gradually tapers towards furca base at U80. Mouth ventral, with delicate protruding structures, no cuticular teeth. Pharynx without dilatations. Intestine straight, with a marked anterior section. Scales spined, three-lobed, not overlapping, distributed in 10–12 columns, 15 scales per column. Spines with a short lateral denticle. Scales and spines increase gradually in size in a posterior direction. Dorsal surface covered by scales from posterior end of cephalion (ca U3) to furca base (ca U93). Furca base short, lateral margins of furca branches more or less straight, furcal indentation deeply U-shaped, adhesive tubes well-developed, almost parallel. Furca base and branches covered with oval, keeled scales.

Molecular diagnosis

18S rRNA gene: 341 C. ITS2: 26 T, 28 G, 40 A, 41 C, 50 T, 62 G, 78 C, 87 A, 96 C, 107 A, 108 A, 112 –, 116 G, 117 A, 118 A, 131 T, 139 T, 157 C, 167 T, 168 T. 28S rRNA gene: 317 A, 690 T, 797 T, 902 G. Cytochrome *c* oxidase subunit I (codon ordinal numbers are followed by the corresponding span of nucleotide positions in parentheses): 29 (85–87) AGT, 44 (130–132) GTA, 71 (211–213) CCA, 75 (223–225) GGT, 81 (241–243) TTT, 97 (289–291) TCT, 124 (370–372) GCT, 126 (376–378) GCC, 139 (415–417) CTA, 142 (424–426) GCC, 155 (463–465) ACT, 170 (508–510) CTG, 189 (565–567) TTC, 196 (586–588) CTG, 221 (661–663) CTG.

Reference molecules are shown in Supp. file 1: Figs S1, S9B, S13. All diagnostic molecular autapomorphies are marked by arrows. Reference alignments with corresponding nucleotide positions are in Supp. file 1: Alignments 1–4.

The *p*-distance from species described in the present study is 0.22–4.00% in 18S, 18.19–34.76% in ITS2, 2.23–6.70% in 28S, and 9.04–13.44% in COI. There are 2–13 CBCs (except for *Ch.* (*H*). *mirabilis* sp. nov., where there are no CBCs) in the 18S rRNA molecule, 3–4 CBCs in the ITS2 molecule, and 1–11 CBCs in the first two domains of the 28S rRNA molecule.

Etymology

The Latin adjective '*superb·us*, *-a*, *-um*' [m, f, n] ('proud') refers to the 'beautiful appearance' of the new species.

Material examined

Holotype

SLOVAKIA • adult (photomicrographs, hologenophore); Zlaté Piesky lake, municipal recreation area, Ružinov, Bratislava, Podunajská rovina plain; 48°11′17.1″ N, 17°11′24.3″ E; CU-FNS-22-06-20/PA.

Photomicrographs of the holotype are available at the Department of Zoology, Comenius University in Bratislava at https://fns.uniba.sk/en/gastrotricha/. The holotype is shown in Figs 16A, 17C–G.

Paratype

SLOVAKIA • adult (photomicrographs, hologenophore); Kuchajda lake, municipal recreation area, Nové Mesto, Bratislava, Podunajská rovina plain (type locality); 48°10′15.7″ N, 17°08′30.6″ E; CU-FNS-15-06-20/HO.

Photomicrographs of the paratype specimen are available at the Department of Zoology, Comenius University in Bratislava at https://fns.uniba.sk/en/gastrotricha/. The paratype is shown in Figs 16B, 17A–B.

Type material

A DNA sample of the holotype specimen ZPvs 55 has been deposited in the Natural History Museum, Vajanského nábrežie 2, 810 06 Bratislava, Slovakia (ID Collection Code 01427126).

Type locality

Zlaté Piesky lake, Ružinov, Bratislava, Podunajská rovina plain, Slovakia, 48°11′17.1″ N, 17°11′24.3″ E.

Gene sequences

The nuclear 18S and ITS1-5.8S-ITS2-28S rDNA sequences as well as the mitochondrial COI sequence of the holotype specimen ZPvs 55 have been deposited in GenBank under the following accession numbers: OM421708, OM421684, and OM424063, respectively.

Description

Habitus. *Chaetonotus* (*Hystricochaetonotus*) *superbus* sp. nov. is about 107 µm long and has a stocky body that is tenpin-shaped, with a clearly defined head region, a narrowing neck, and a rather bulbous trunk (Figs 15A, H, 16A). Body height in lateral view is 14.0–15.0 µm at U10, 15.0–15.4 µm at U50, and 16.1–17.0 µm at U60. The head is relatively wide, with a plate-like, rounded cephalion. The neck (ca U12–U27) smoothly continues to the trunk, which is significantly wider than the head, gradually dilates from about U37 to U60 where it reaches the maximum width. Then it gradually tapers towards U80 where curved margins of the furca branches begin to emerge. Dorsal sensory bristles arise from the cuticle in two pairs at U12 and U79 (Fig. 19A). The furcal indentation is deeply U-shaped. The furca branches are set apart and diverge posteriorly. Well-developed adhesive tubes are approximately 9 µm long, more or less straight, and run almost in parallel (Figs 15A, H, J, 16A).

Head. The head is five-lobed. The cephalion (U1–U2) is rounded, clearly demarcated in the body outline, appears as a lens in the ventral view, and has a free posterior (dorsal) edge (Figs 15A, H, J–K, 16B, 17C). The epipleurae are formed approximately at U3–U5 while the hypopleurae at ca U6–U13. The latter structures are well recognizable in the head outline (Figs 15A–B, 16A, black stars). Two pairs

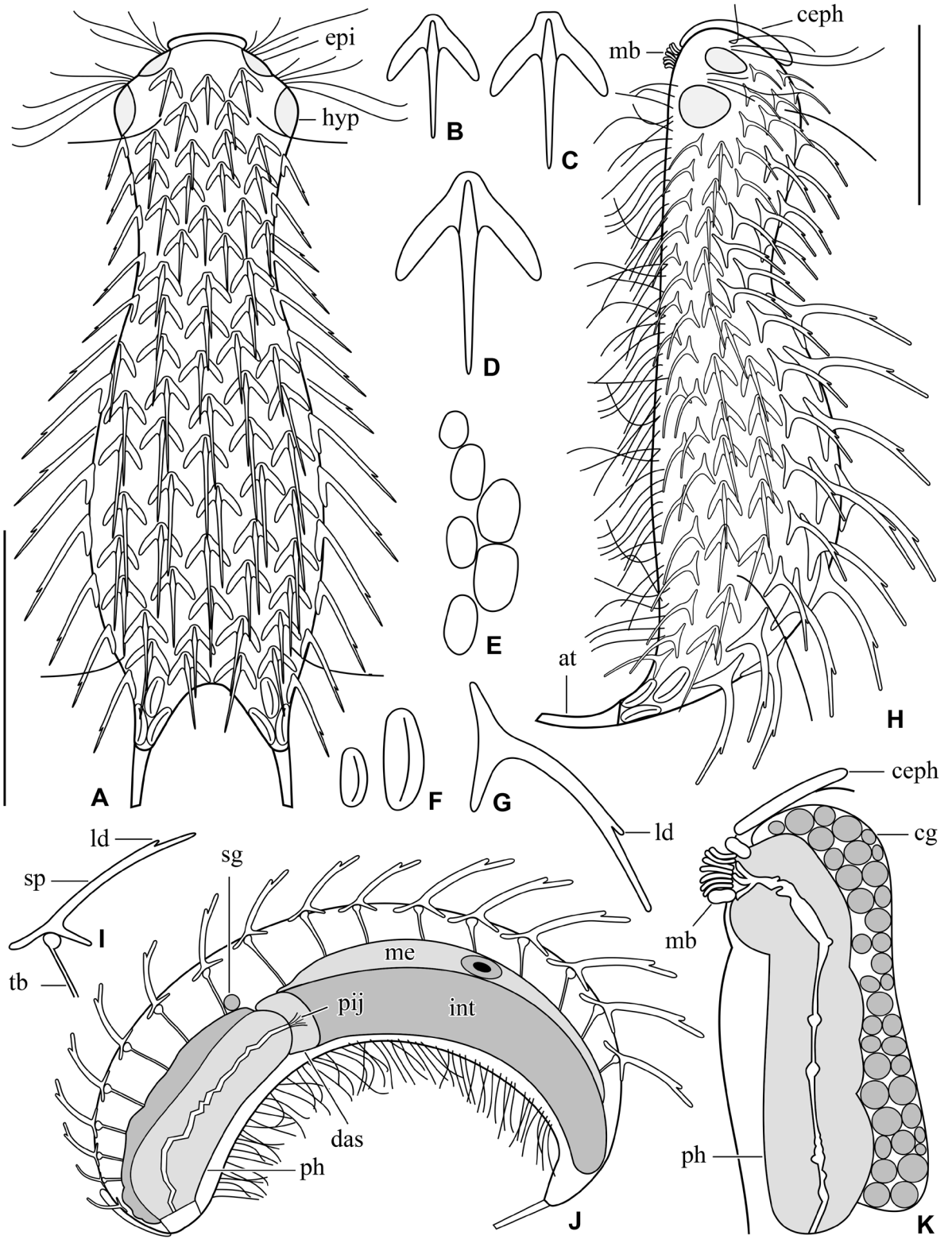

Fig. 15. *Chaetonotus* (*Hystricochaetonotus*) *superbus* sp. nov. **A**, **H**. Dorsal and lateral overviews showing the scale and spine pattern. **B**. Head scale. **C**. Neck scale. **D**. Trunk scale. **E**. Ventral scales. **F**. Upper-furcal dorsal scales. **G**. Lateral view of a trunk spined scale. **I**. Lateral view showing the connection of a transversal band to the base of a scale. **J**. Lateral overview showing the internal morphology. **K**. Lateral view of the anterior body region. Scale bars = 30 μm.

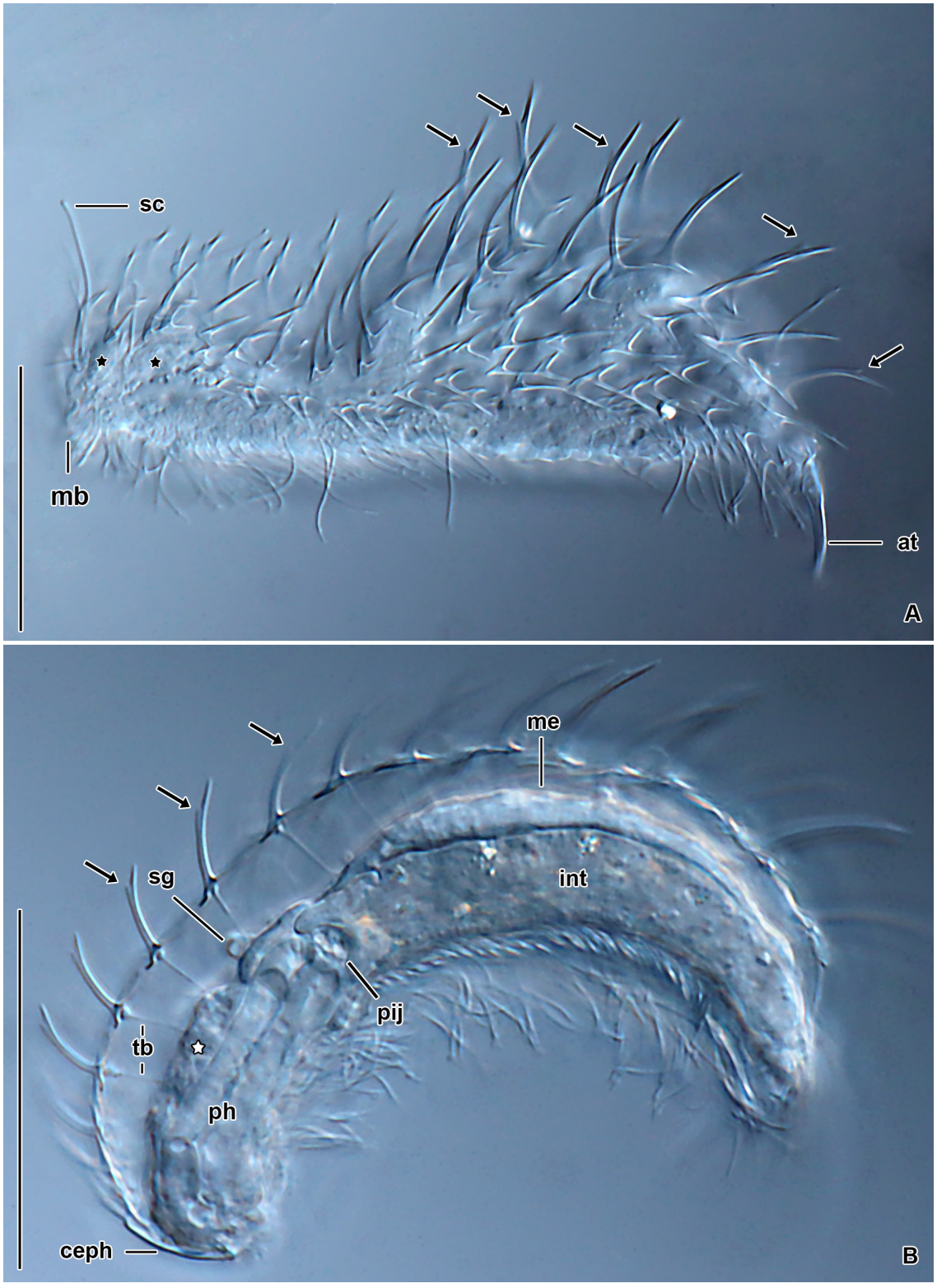

Fig. 16. *Chaetonotus* (*Hystricochaetonotus*) *superbus* sp. nov., differential interference contrast. **A**. Holotype (CU-FNS-15-06-20/HO), lateral overview showing the scale and spine pattern. **B**. Paratype (CU-FNS-22-06-20/PA), optical section showing the internal morphology in lateral view. Black stars in (A) mark the epipleurae and hypopleurae. White star in (B) marks the cerebral ganglion. Arrows mark the lateral denticle of spines. Scale bars = 30 µm.

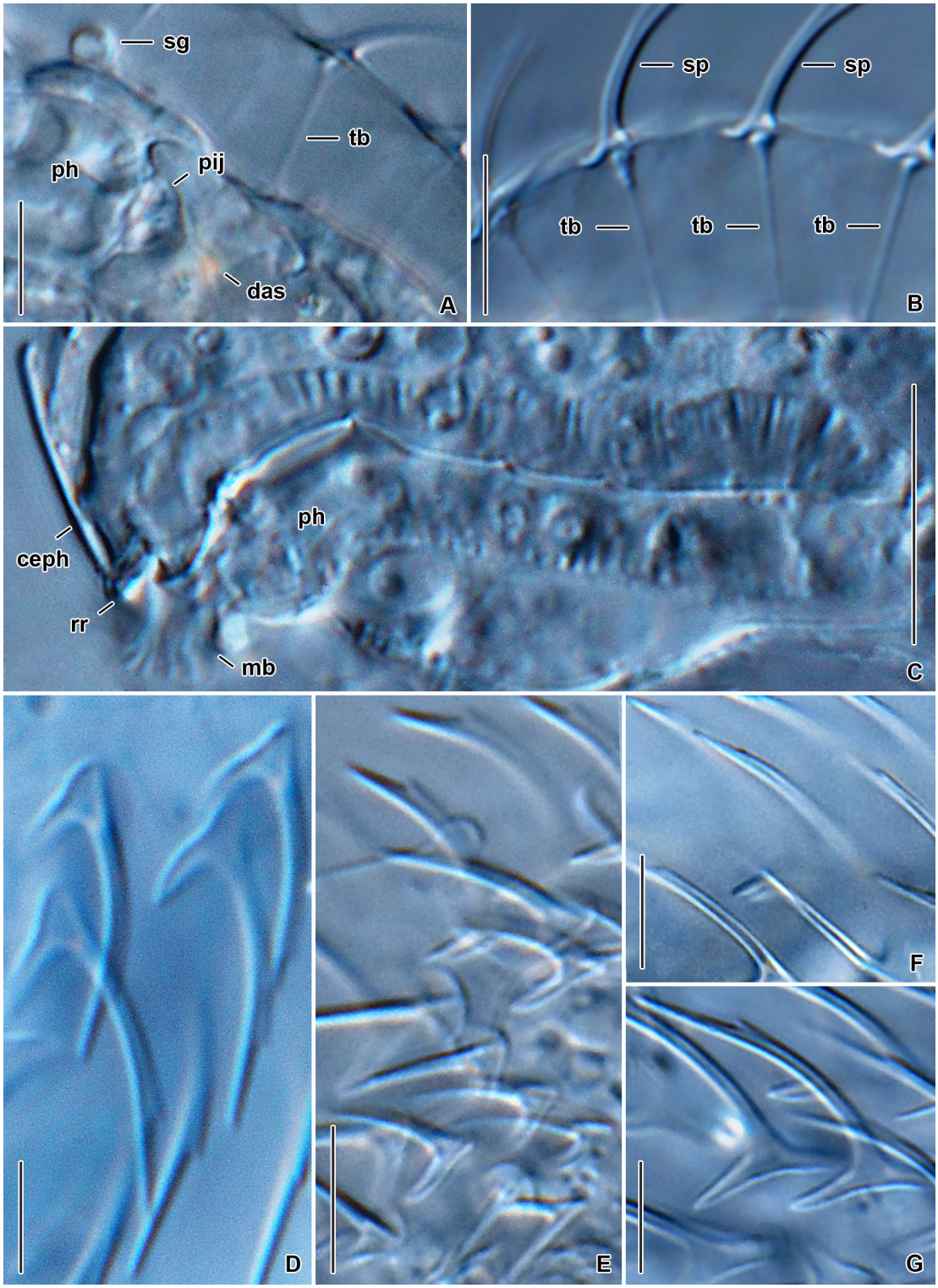

Fig. 17. *Chaetonotus* (*Hystricochaetonotus*) *superbus* sp. nov., differential interference contrast. **A–B**. Paratype (CU-FNS-22-06-20/PA). **C–G**. Holotype (CU-FNS-15-06-20/HO). **A**. Detail showing the salivary gland, pharyngeal-intestinal junction, and differentiated anterior section of the intestine. **B**. Detail showing the connection of transversal bands to the base of scales. **C**. Detail showing the anterior portion of the digestive tract. **D**. Head scales. **E**. Neck scales. **F**. Spines. **G**. Trunk spined scales. Scale bars: A–B, D–G = 5 µm; C = 10 µm.

of cephalic ciliary tufts emerge laterally between the cephalion and the epipleurae edge (ca U3) as well as between the epi- and the hypopleurae edge (U6) (Figs 15A, H, 16A). The hypostomium (ca U4–U6) is free of structures, lined only with ciliary patches. The mouth ring is oval, 4.4–4.9 µm in the largest diameter, located subterminally at U3–U6. There are strong, rod-like reinforcements lining the mouth walls and delicate structures protruding from the mouth ring (Figs 15H, K, 17C). Inner cuticular teeth are not present.

Internal morphology. The pharynx extends from ca U5 to U34, is 28–32 µm long and 5.9–8.3 µm wide, sinuous, and has no dilatations (Figs 15J, 16B, 17C). The cerebral ganglion appears as a mass surrounding the pharynx along its whole length (Fig. 15K). The salivary glands are recognizable as small hyaline balls situated at the dorsal side of the pharynx around at U33 (Figs 15J, 16B, 17A). The intestine runs from U35 to U82 and has a separate, well-differentiated anterior section (U35–U38) (Figs 15J, 16B). Transversal bands connected to the base of dorsal scales are well recognizable under DIC and secondary magnification of 2500× (Figs 15J, 16B, 17A–B). The adhesive gland (ca U85–U91) is placed right behind the terminal part of the intestine, forming a short dichotomy at the subtle furca base.

Scales. Almost the entire body is covered by not overlapping three-lobed scales that adhere to the basal cuticle layer along their whole perimeter. Scales are distributed in a minimum of 12 longitudinal rows, with 10 scales in the central row. Their size increases gradually in a posterior direction. Central dorsal and dorsolateral longitudinal rows of scales begin at the level of the anterior edge of the epipleurae (ca U5), while lateral rows start at the posterior end of the hypopleurae (ca U13). Ventral rows are hardly visible due to the thick, elongated dorsal spines (for further explanation, see below) and long locomotory cilia. Three main types of scales could be recognized with respect to the shape of the anterior lobe of scales: (i) head and upper-neck scales (U5–U28) with a small, rounded anterior lobe and elongated posterior lobes, α = 160–170°, and β = 89–98° (Figs 15B, 17E), (ii) lower-neck and anterior trunk scales (U29–42) with a truncated anterior lobe and elongated posterior lobes, α = 160–175°, and β = 76–93° (Figs 15C, 17D), and (iii) posterior trunk scales (U45–80) with a more broadly rounded anterior lobe and a larger angle β (101–110°) formed by the posterior lobes (Figs 15D, 17G). The transition between anterior and posterior lobes is indistinct and continuous in all scales.

Spines. All spines bear a distinct lateral denticle and gradually narrow towards their distal end. Keels start near the anterior margin of scales. Spines are not straight but distinctly curved (Figs 15A, G–J, 16A–B, 17D–G). They do not differentiate into various types, only their length changes in a posterior direction (Supp. file 1: Table S3). The most pronounced change occurs at the beginning of the trunk (Figs 15H, 16A), where dorsal spines increase significantly from 6.7–10.7 µm to 10.8–13.0 µm. The lateral denticle is comparatively distant from the spine apex, i.e., *d*-value ranges from 1.7–5.1 µm, which corresponds to a *d* ratio of 21.4–34.7%.

Ventral ciliary bands and ventral interciliary field. Unfortunately, the ventral side could not be observed in detail due to the thickness of the dorsal spines that precluded turning over and squeezing the worms. Moreover, the ventral locomotory cilia also hampered detailed observations of the ventral side. Despite these problems, the following observations could be done. The longitudinal ciliary bands begin at ca U10 and run backward to ca U85. The ciliary bands are accompanied by two ventrolateral rows of small (2.0–2.9 × 1.9–2.2 µm in size), three-lobed scales that start at U13. The interciliary field bears small (1.7–2.6 × 0.9–1.2 µm in size), oval scales without spines or keels (Fig. 15E). The upper furcal region (U84–U90) carries two types of scales: (i) lateral three-lobed, spined scales with a broadly rounded anterior lobe, narrowly rounded posterior lobes, α = ~140°, and β = ~73° and (ii) oblong and keeled scales being 0.84–1.2 × 1.47–1.72 µm in size (Fig. 15F).

Chaetonotus* (*Hystricochaetonotus*) *optabilis sp. nov.
urn:lsid:zoobank.org:act:0B0D89B0-6D24-4D99-A359-18C41CFA1BCE
Figs 18–22; Supp. file 1: Table S4

Morphological diagnosis

Body elongated and about 108–143 µm long. Head slightly wider than neck, separated from trunk by an inconspicuous neck constriction. Cephalion clearly demarcated, epipleurae and hypopleurae not recognizable. Trunk comparatively narrow, not broader than head, widest at ca U63, narrowest at ca U88. Mouth ventral, no cuticular teeth. Hypostomium bears a rectangular cuticular structure accompanied by two posterior lateral lamellae. Pharynx with anterior and posterior dilatations. Intestine straight, with a marked anterior section. Scales slightly overlapping, distributed in 16–18 columns, 40–45 scales per column. Dorsal surface covered from posterior end of cephalion (ca U1) to furca base (U94) with (i) spined, three-lobed scales with rounded anterior end and (ii) spined, three-lobed scales with truncated anterior end. Spines short, narrowed posteriorly, without denticles. Ventral side carries two broad ciliary bands and two pairs of ciliary fields around mouth and hypostomium. Interciliary filed bears (i) V-shaped scales without keels, (ii) bowl-shaped scales without keels, (iii) obtriangular scales with very minute keels, and (iv) narrowly obovate, keeled scales. Furca base longer than adhesive tubes, lateral margins more or less straight, furcal indentation deeply V-shaped, adhesive tubes diverging posteriorly. Dorsal side of furca base and branches covered with three-lobed scales, ventral side with oblong, spined scales and oval to broadly fusiform, keeled scales.

Molecular diagnosis

18S rRNA gene: 78 C, 148 T, 223 A, 225 A, 228 T, 235 A, 239 T, 240 T, 243 A, 264 A, 267 –, 282 T, 283 T, 286 A, 288 A, 336 T, 337 T, 338 C, 340 C, 345 A, 546 A, 639 A, 648 T, 649 A, 652 C, 656 T, 658 A, 664 T, 666 T, 676 A, 678 A, 681 T, 686 T, 688 A, 694 T, 714 T, 722 T, 733 A, 741 A, 1059 A, 1060 A, 1082 T, 1083 T, 1366 A, 1368 T, 1372 G, 1373 A, 1374 A, 1376 T, 1377 T, 1381 –, 1383 C, 1384 –, 1388 A, 1391 T, 1507 A, 1526 T, 1535 A, 1690 T, 1724 T, 1732 C, 1736 T. 28S rRNA gene: 275 A, 292 A, 309 T, 480 T, 485 T, 487 A, 489 –, 500 A, 504 A, 506 A, 520 C, 522 T, 543 A, 588 C, 589 C, 591 –, 599 T, 603 T, 608 A, 615 A, 628 C, 634 T, 645 A, 648 T, 652 T, 657 T, 661 A, 662 A, 688 T, 690 A, 698 A, 704 T, 706 A, 713 T, 722 A, 735 G, 742 T, 746 T, 764 A, 777 A, 784 T, 789 C, 791 A, 795 A, 798 A, 810 A, 813 T, 814 A, 819 A, 965 A, 966 C, 996 C. Cytochrome *c* oxidase subunit I (codon ordinal numbers are followed by the corresponding span of nucleotide positions in parentheses): 20 (58–60) CTA, 32 (94–96) AGT, 45 (133–135) GTC, 49 (145–147) GCT, 51 (151–153) GTC, 55 (163–165) TTC, 57 (169–171) GTT, 69 (205–207) CTA, 76 (226–228) GCG, 77 (229–231) CCA, 91 (271–273) TTA, 101 (301–303) GTG, 109 (325–327) GCC, 111 (331–333) ACA, 114 (340–342) ACG, 133 (397–399) GCT, 154 (460–462) ACC, 156 (466–468) TTA, 184 (550–552) TTG, 186 (556–558) TTA, 205 (613–615) AGG.

Reference molecules are shown in Supp. file 1: Figs S2 and S14. All diagnostic molecular autapomorphies are marked by arrows. Reference alignments with corresponding nucleotide positions are in Supp. file 1: Alignments 1–4.

The *p*-distance from species described in the present study is 4.00–4.39% in 18S, 6.78–9.79% in 28S, and 10.96–13.59% in COI. There are 13–16 CBCs in the 18S rRNA gene and 11–18 CBCs in the 28S rRNA gene.

Etymology

The Latin adjective '*optabil·is*, *-is*, *-e*' [m, f, n] ('desirable') refers to the very elegant appearance of the new species.

Material examined

Holotype

SLOVAKIA • adult (photomicrographs, hologenophore); temporary pond in the floodplain area of the River Morava, Devín, Bratislava, Podunajská rovina plain; 48°10′29.4″ N, 16°58′35.8″ E; CU-FNS-05-03-20-1/HO.

Photomicrographs of the holotype are available at the Department of Zoology, Comenius University in Bratislava at https://fns.uniba.sk/en/gastrotricha/. The holotype is shown in Figs 20B–C, 21C, 22B–C.

Paratypes

SLOVAKIA • 2 adults (photomicrographs, both hologenophores); same collection data as for holotype; CU-FNS-05-03-20-2/PA-1, CU-FNS-05-03-20-3/PA-2.

Photomicrographs of paratype specimens are available at the Department of Zoology, Comenius University in Bratislava at https://fns.uniba.sk/en/gastrotricha/. Paratypes are shown in Figs 20A, 21A–B, D, 22.

Type material

A DNA sample of the holotype specimen DB 34 has been deposited in the Natural History Museum, Vajanského nábrežie 2, 810 06 Bratislava, Slovakia (ID Collection Code 01427607).

Type locality

Ephemeral pond in the floodplain area of the River Morava near the foothill of the Devín castle, Bratislava, Podunajská rovina plain, Slovakia, 48°10′29.4″ N, 16°58′35.8″ E.

Gene sequences

The nuclear 18S and 28S rDNA sequences as well as the mitochondrial COI sequence of the holotype specimen DB 34 have been deposited in GenBank under the following accession numbers: OM421710, OM421686, and OM424065, respectively.

Description

Habitus. *Chaetonotus* (*Hystricochaetonotus*) *optabilis* sp. nov. is about 108–143 µm long and has a slender elongated body, with a head region slightly broader than the inconspicuous neck and a more or less bulbous trunk (Figs 18A, 19A, E, 20A). Body width is 18.8–21.7 µm at U10, 22.5–23.7 µm at U50, and 26.1–30.7 µm at U60. The head is relatively wide (11–15 µm at U6), with a plate-like, rounded cephalion. Epi- and hypopleurae are not recognizable. The neck (ca U12–U25) is only inconspicuously marked and smoothly continues to the trunk region. The trunk is about as narrow as the head, gradually dilating from approximately U38 to U63, where it reaches the maximum width. Then it gradually tapers towards U88, where the curved margins of the furca branches start to form. Dorsal sensory bristles were not observed. The furcal indentation is deeply V-shaped. The furca branches are set apart and diverge posteriorly. Well-developed adhesive tubes are approximately 9 µm long, they are straight and almost in parallel (Figs 18A, 19A, D–E, 21D, 22E).

Head. The cephalion (U1) is rounded, clearly demarcated in the body outline, appears as a lens in the ventral view (Figs 19A, E, 21A). Pairs of cephalic ciliary tufts emerge laterally at U4 and U6 (Figs 19A, E, 21A). The mouth ring is oval, 5.2–6.2 µm in the largest diameter, and is located subterminally at U2–U5. There are strong but short, rod-like reinforcements lining the walls of the mouth ring and inner delicate structures directed towards the center of the mouth ring. Inner cuticular teeth are not present (Figs 20A, 21B). The hypostomium (ca U5–U9) has a complex morphology, i.e., bears a rectangular

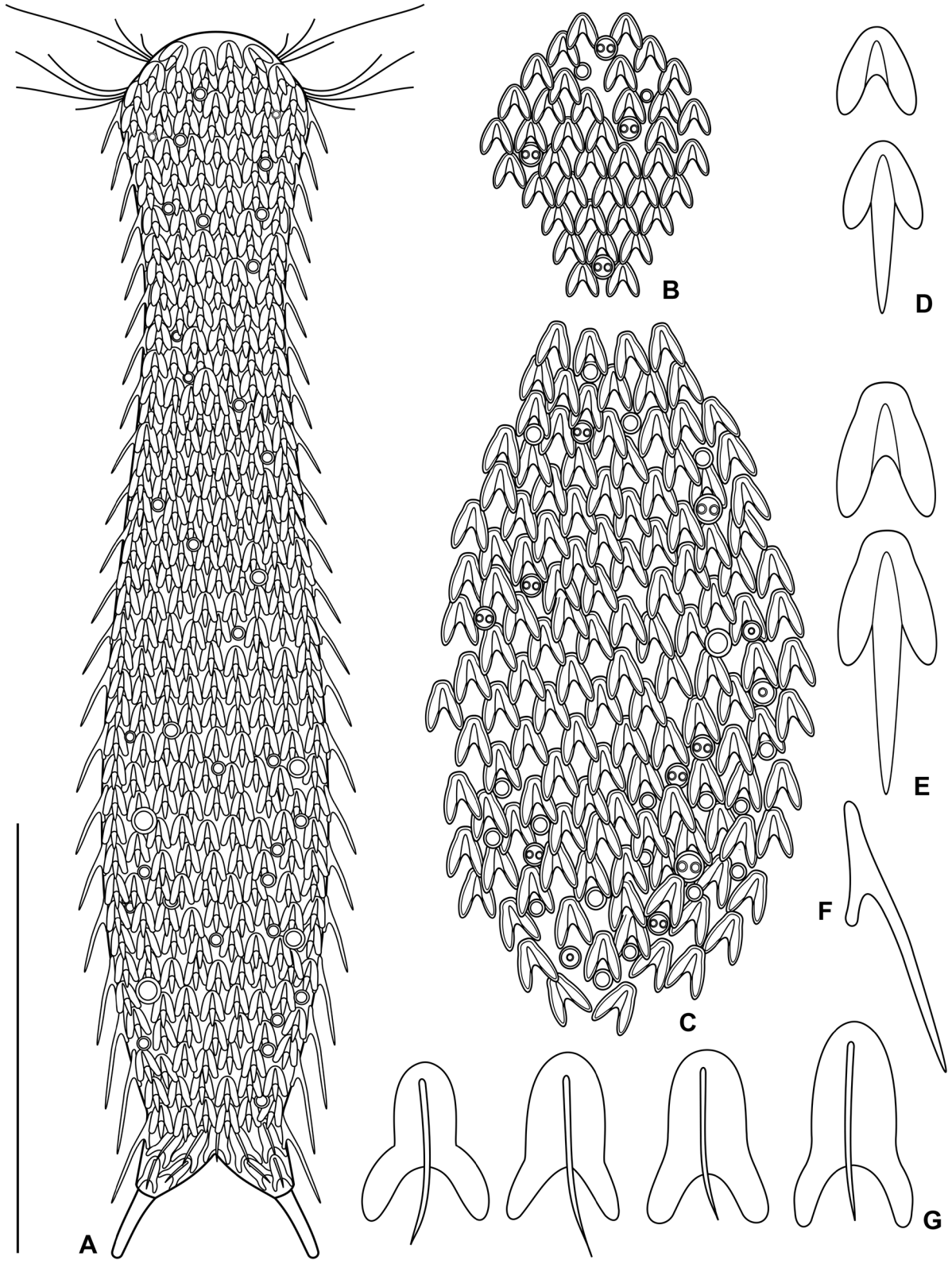

Fig. 18. *Chaetonotus* (*Hystricochaetonotus*) *optabilis* sp. nov. **A**. Dorsal overview showing the scale and spine pattern. **B**–**C**. Details showing the distribution of head and trunk scales. **D**–**E**. Head and trunk scales, the schematic drawing of the scale base is shown above that of spined scales. **F**. Lateral view of a trunk spined scale. **G**. Dorsal furcal scales. Scale bar = 30 μm.

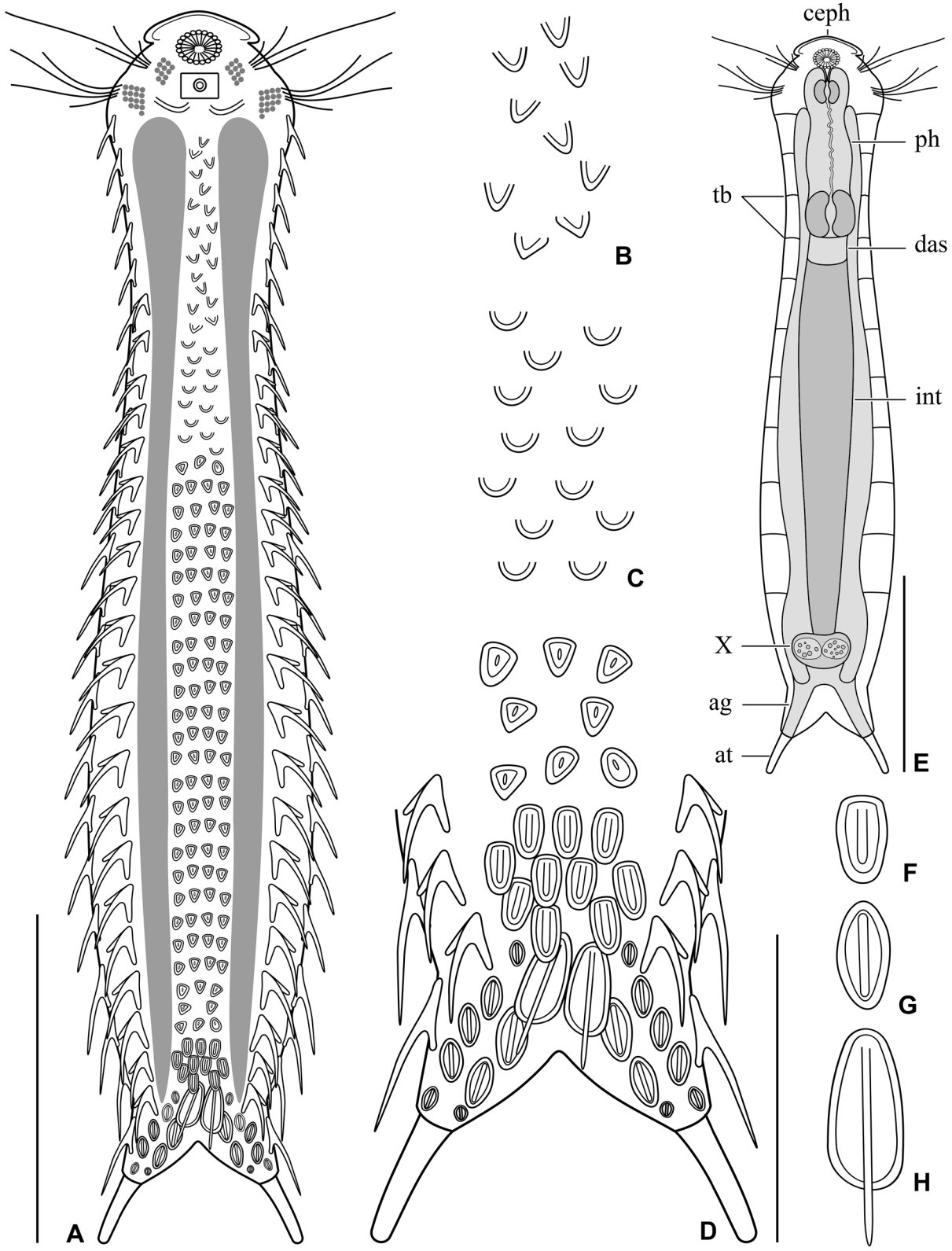

Fig. 19. *Chaetonotus* (*Hystricochaetonotus*) *optabilis* sp. nov. **A**. Ventral overview showing the scale and ciliary pattern. **B**. V-shaped scales without keels. **C**. Bowl-shaped scales without keels. **D**. Detail of the ventral posterior body region. **E**. Internal morphology. **F**. Narrowly obovate keeled scale. **G**. Fusiform keeled scale. **H**. Oblong spined scale. Scale bars: A, E = 30 µm; D = 10 µm.

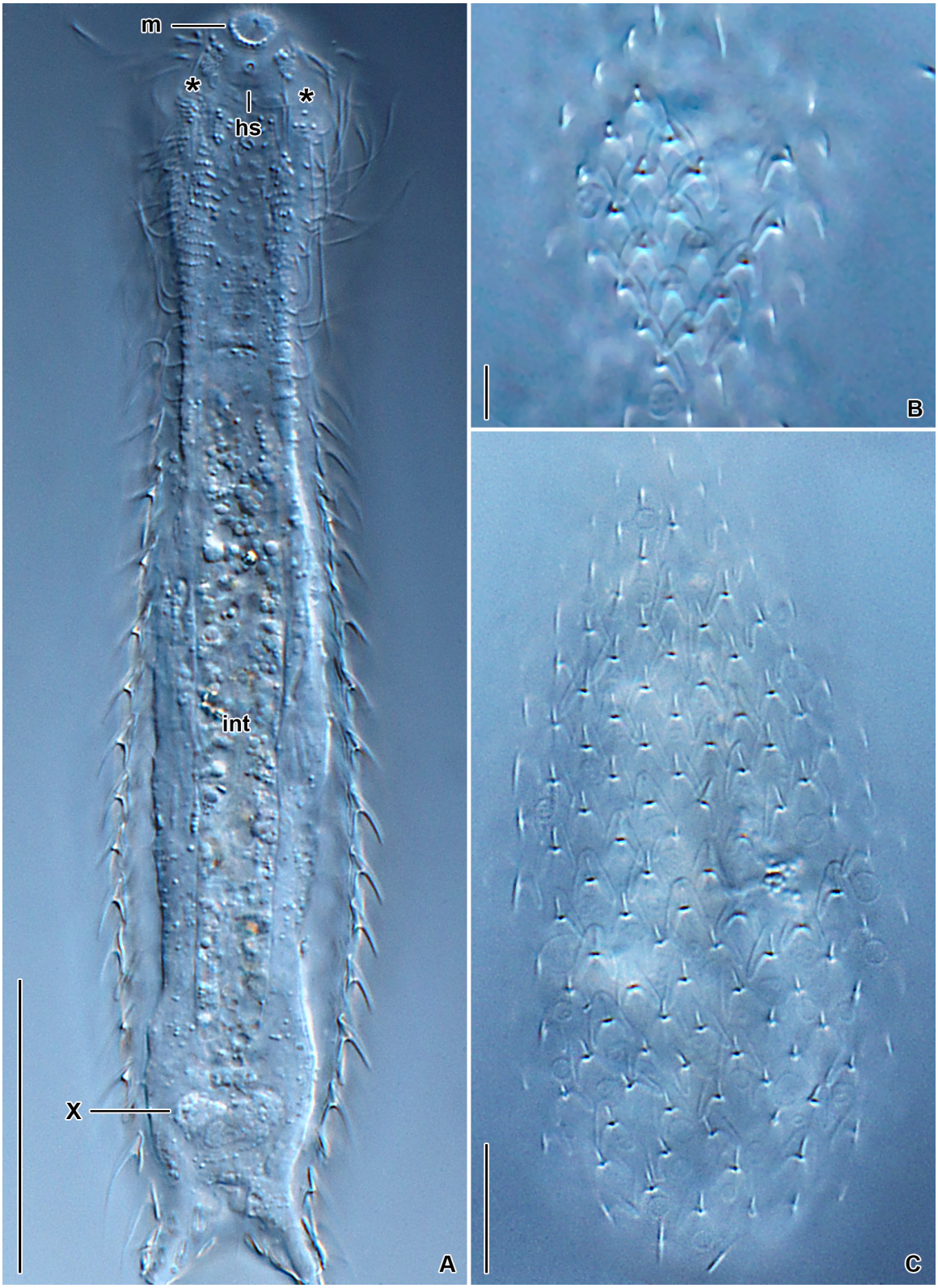

Fig. 20. *Chaetonotus* (*Hystricochaetonotus*) *optabilis* sp. nov., differential interference contrast. **A**. Paratype (CU-FNS-05-03-20-3/PA-2). **B–C**. Holotype (CU-FNS-05-03-20-1/HO). **A**. Overview showing the general body organization. Asterisks mark the beginning of the ventral ciliary bands. **B–C**. Surface views, showing the head and trunk scale patterns. Scale bars: A = 30 µm; B = 5 µm; C = 10 µm.

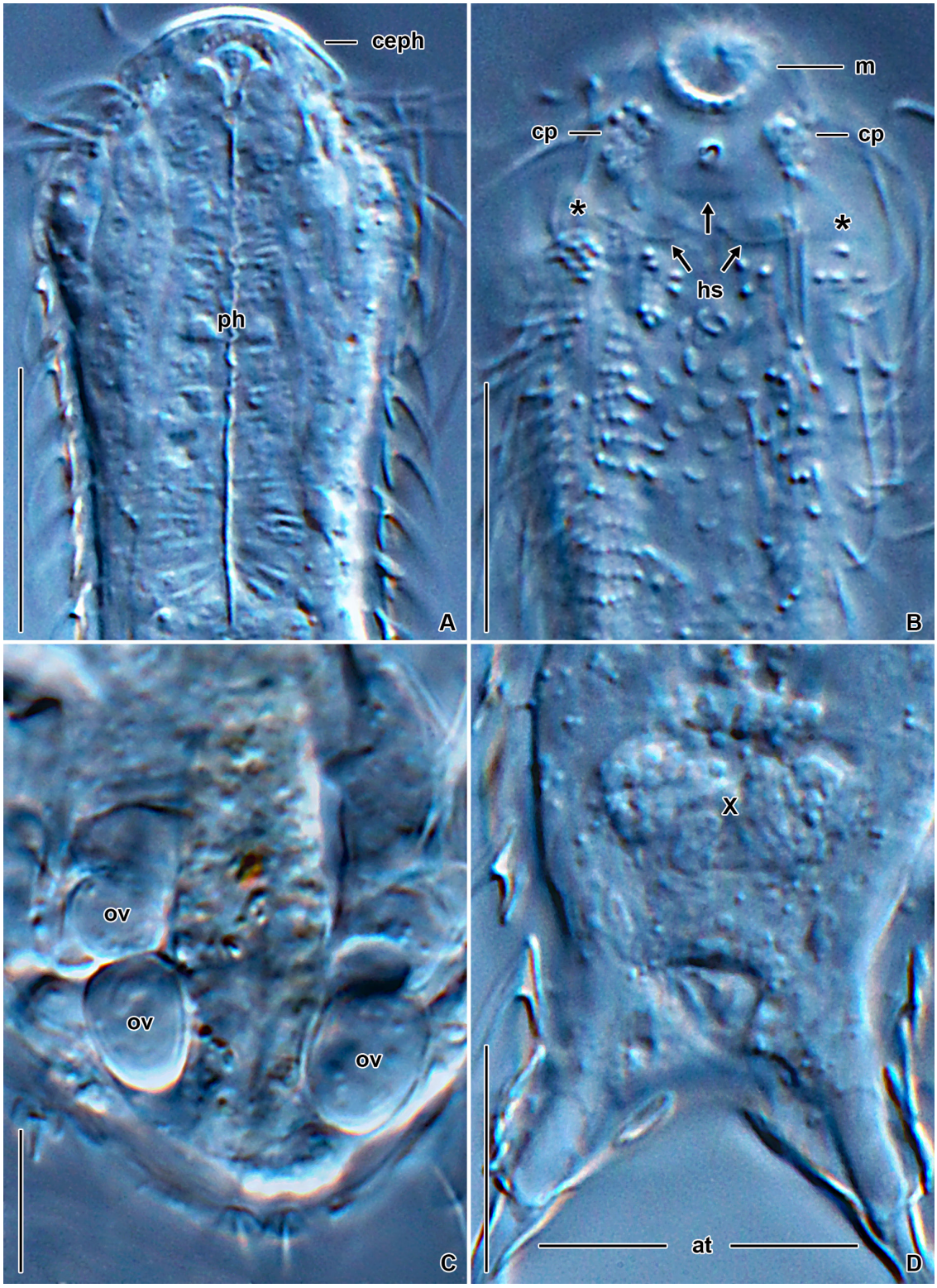

Fig. 21. *Chaetonotus* (*Hystricochaetonotus*) *optabilis* sp. nov., differential interference contrast. **A–B, D**. Paratype (CU-FNS-05-03-20-3/PA-2). **C**. Holotype (CU-FNS-05-03-20-1/HO). **A**. Detail of the anterior body region. **B**. Ventral view of the head region. Asterisks mark the beginning of the ventral ciliary bands, arrows mark the cuticular structures of the hypostomium. **C–D**. Details of the posterior body region, showing the ovaries and the organ X. Scale bars = 10 µm.

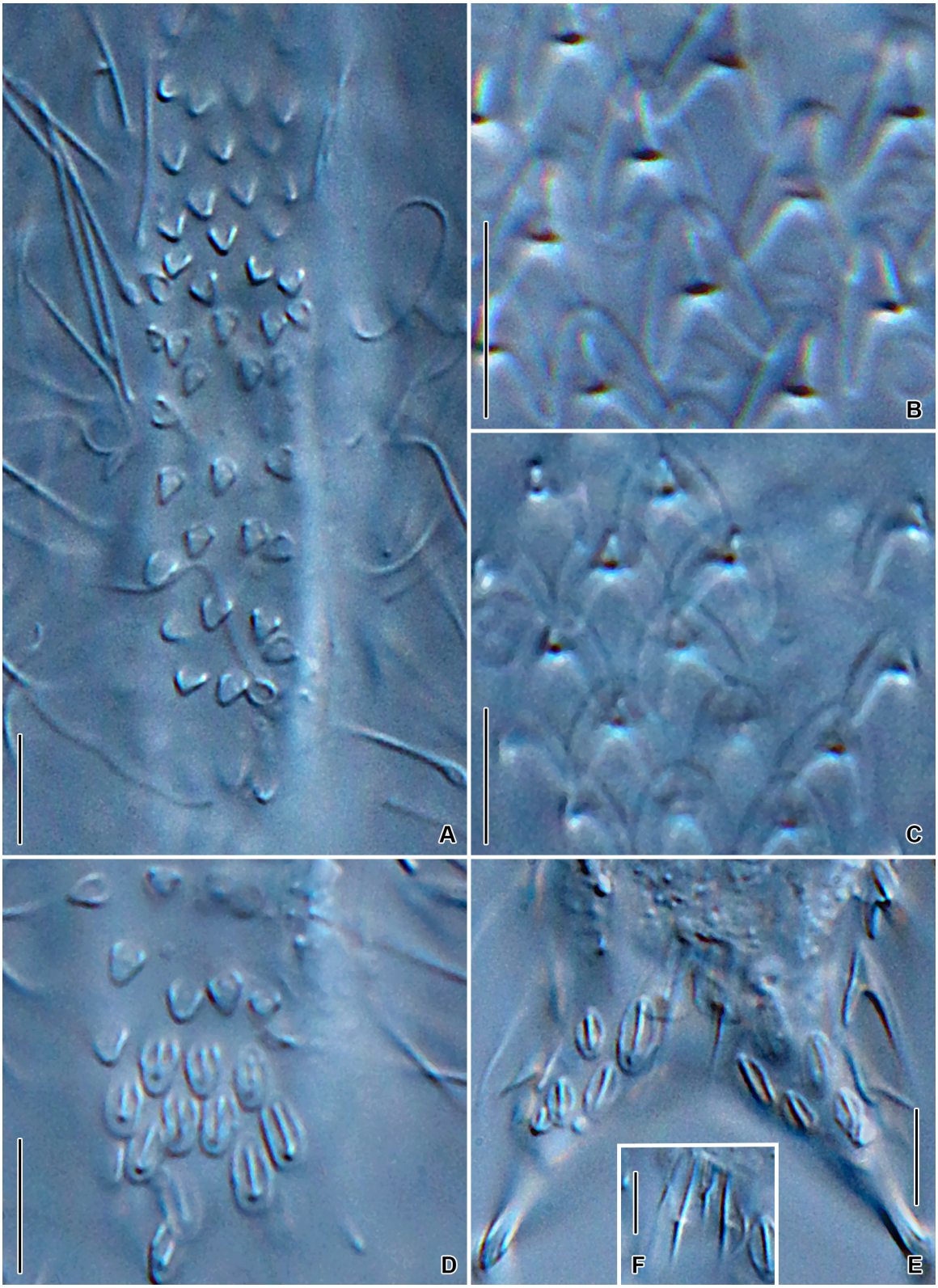

Fig. 22. *Chaetonotus* (*Hystricochaetonotus*) *optabilis* sp. nov., differential interference contrast. **A, D–F**. Paratype (CU-FNS-05-03-20-3/PA-2). **B–C**. Holotype (CU-FNS-05-03-20-1/HO). **A**. Scales in the ventral interciliary field. **B**. Trunk scales. **C**. Head scales. **D–E**. Details of the ventral posterior body region. **F**. Oblong spined scales. Scale bars: A–E = 5 µm; F = 2 µm.

plate (5.0 × 2.9 µm) with a small central protuberance and two lamellae situated posterior to the plate. The lateral sides of the hypostomium are lined by a relatively wide pair of sensoric ciliary patches from U3 to U8 (Figs 19A, 20A, 21B).

Internal morphology. The pharynx extends from ca U5 to U29, is 28.0–33.4 µm long and 7.3–7.8 µm wide, sinuous, and has marked anterior and posterior dilatations (Fig. 19E). The posterior dilatation (ca U20–U25) is larger than the anterior one (ca U7–U9) (Supp. file 1: Table S4). The intestine runs from U29 to U85 and has a separate, well-differentiated anterior section (U29–U33). Transversal bands connected to the base of dorsal scales are well recognizable (Fig. 19E). The adhesive gland (ca U85–U87) is placed right behind the terminal part of the intestine forming a short dichotomy at the subtle furca base. The organ X has a lemniscate shape and is situated ahead of adhesive glands (Figs 19E, 21D).

Scales. Almost the entire body is covered by slightly overlapping three-lobed scales that adhere to the basal cuticle layer along either all or most of their perimeter. Scales are distributed in 16–18 longitudinal rows, with 40–45 scales in the central row. Their size increases slightly in a posterior direction. Central dorsal and dorsolateral longitudinal rows of scales begin at the level of the anterior edge of the cephalion (ca U1), while lateral rows start at ca U6. They run almost along the whole body length (till U94). Ventrolateral rows commence at U23 due to the highly developed and wide anterior part of ciliary rows and terminate in the furcal region (at ca U91). Ventral rows start at U10, are staggered, and exhibit a horizontal zonation pattern. Given the shape of the anterior scale lobe, two main types were recognized: (i) head and neck scales (U1–U30), with a rounded anterior lobe and comparatively short posterior lobes, α = 180–196°, β = 47–68° (Figs 18B, D, 20B, 22C) and (ii) trunk and dorsal furca scales (U31–U93), with a truncated anterior lobe and longer posterior lobes, α = 162–188°, β = 58–85° (Figs 18C, E, 22B). Both types share an indistinct and continuous transition between the anterior and posterior lobes. Rounded structures (1.0–2.4 µm across) irregularly interspersed within type 1 and 2 scales were observed along the whole dorsal side (Figs 18A–C, 20B–C). As they were clearly recognizable only in a single specimen, we cannot exclude that these structures are artifacts. The V-shaped furcal indentation carries the fourth type of dorsal scales that are three-lobed and have a tongue-shaped anterior lobe, relatively narrow posterior lobes, α = 156–176°, β = 56–80°, and a marked transition between the anterior and posterior lobes (Fig. 18G).

Spines. Dorsal, dorsolateral, lateral, and ventrolateral scales bear simple, slightly curved spines that gradually narrow towards the distal end (Figs 18D–G, 20A). The spine emerges rather close to the anterior margin of scales. Spines do not differentiate into various types, only their length slightly increases in a posterior direction (Supp. file 1: Table S4). A lateral denticle is not formed. Ventral scales are spineless.

Ventral ciliary bands and ventral interciliary field. Ciliary bands start at U10, where they are conspicuously broad (Figs 19A, 21B, asterisks). However, they begin to narrow from U25 and terminate at U88. The ciliary bands are accompanied by two ventrolateral rows of three-lobed scales that extend from U22 to U91. They are 3.6–4.9 × 2.6–3.6 µm in size and have an indistinct and continuous transition between the anterior and posterior lobes (Fig. 19A). The ventral interciliary field bears four types of horizontally distributed scales: (i) minute (0.7–0.9 × 0.8–1.2 µm), V-shaped, double-edged scales without keels (U10–U30) (Fig. 19B); (ii) minute (0.8–1.1 × 0.8–1.3 µm), bowl-shaped, double-edged scales without keels (U31–U36) (Fig. 19C); (iii) small (1.3–2.0 × 1.0–1.5 µm), obtriangular, double-edged scales with a minute keel (U38–U81) (Figs 19D, 22A); and (iv) larger (1.7–3.4 × 1.0–1.5 µm), narrowly ovate, double-edged, keeled, and slightly overlapping scales arranged in three distinct rows (U82–U88) (Fig. 19D, F). The furcal region (U87–U93) carries two types of scales: (i) a pair of oblong, comparatively large (7.3–7.6 × 2.4–2.6 µm), spined scales, with a broadly rounded posterior end

(Figs 19D, H, 22F) and (ii) oval to broadly fusiform, rather small (1.0–4.1 × 1.0–1.8 µm), keeled scales (Figs 19D, G, 22E).

Chaetonotus* (*Hystricochaetonotus*) *avarus sp. nov.
urn:lsid:zoobank.org:act:7B146EA8-7E66-46A3-A4C2-8707A9C9EB56
Figs 23–27; Supp. file 1: Table S5

Morphological diagnosis

Body elongated and about 130 µm long. Head slightly wider than neck, separated from trunk by an inconspicuous neck constriction. Cephalion, epipleurae, and hypopleurae clearly demarcated. Trunk comparatively narrow, not broader than head, widest at ca U62, narrowest at ca U87. Mouth ventral, three cuticular teeth. Hypostomium bears a pentagonal cuticular structure with two protuberances. Pharynx without dilatations. Intestine straight, with a marked anterior section. Scales slightly overlapping, distributed in 14 columns, 30–32 scales per column. Dorsal surface covered with: (i) head scales small, with a subtle, well-delimited anterior lobe and comparatively long and diverging posterior lobes; (ii) neck scales boomerang-like, with a broadly rounded anterior lobe, elongated posterior lobes; (iii) dorsolateral neck scales with a well-delimited, broadly rounded anterior lobe and distinct transition between anterior and posterior lobes; (iv) main trunk scales with a rounded anterior end, posterior lobes comparatively long, narrowly rounded distally, and diverging; (v) posterior trunk scales with a conspicuously prolonged, tongue-shaped anterior lobe and relatively short posterior lobes tapering distally; and (vi) furca base scales with a narrower and more elongated anterior lobe and short posterior lobes very narrowly rounded or almost acute distally. Spines slightly increasing in length from head to posterior trunk region, gradually tapering to become hair-like terminally, without denticles. Ventrolateral spines shorter than dorsal ones. Ventral side carries two broad, anteriorly connected (U9–U27) ciliary bands. Interciliary field covered by (i) minute, tongue-like, keeled scales; (ii) small, roughly rectangular, keeled scales; (iii) oblong scales with a short spine; and (iv) a pair of big, elongated oval, keeled scales. Furca branches slightly longer than adhesive tubes, lateral margins more or less straight, furcal indentation deeply V-shaped, adhesive tubes short. Dorsal side of furca branches covered with elongated oval, keeled scales and ventral side of furca branches covered with (i) two pairs of three-lobed, spined scales, having an elongated, tongue-shaped anterior lobe and comparatively short, narrowly rounded to acute posterior lobes and (ii) cordiform, short-spined scales.

Molecular diagnosis

18S rRNA gene: 268 A, 1739 G. 28S rRNA gene: 128 C, 136 G, 447 G, 691 A, 737 C, 764 T, 765 A, 767 A. Cytochrome *c* oxidase subunit I (codon ordinal numbers are followed by the corresponding span of nucleotide positions in parentheses): 84 (250–252) CTA, 91 (271–273) CTA, 99 (295–297) CTA, 102 (304–306) TCG, 120 (358–360) TCC, 154 (460–462) ACT, 192 (574–576) GGA, 213 (637–639) GGG.

Reference molecules are shown in Supp. file 1: Figs S3 and S15. All diagnostic molecular autapomorphies are marked by arrows. Reference alignments with corresponding nucleotide positions are in Supp. file 1: Alignments 1–4.

The *p*-distance from species described in the present study is 0.38–4.17% in 18S, 2.49–9.44% in 28S, and 8.44–13.15% in COI. There are 1–14 CBCs in the 18S rRNA molecule and 2–18 CBCs in the first two domains of the 28S rRNA molecule.

Etymology

The Latin adjective '*avar·us*, *-a*, *-um*' [m, f, n] ('avaricious, covetous, greedy') refers to the three cuticular teeth of the new species.

Material examined

Holotype

SLOVAKIA • adult (the specimen was destroyed during DNA extraction); Vajspeterský potok creek, Rača, Bratislava, Podunajská rovina plain; 48°12′12.8″ N, 17°07′46.9″ E.

Paratypes

SLOVAKIA • 2 adults (photomicrographs); same collection data as for holotype; CU-FNS-25-02-20/PA-1, CU-FNS-26-02-20/PA-2.

Photomicrographs of paratype specimens are available at the Department of Zoology, Comenius University in Bratislava at https://fns.uniba.sk/en/gastrotricha/. Paratypes are shown in Figs 25–27.

Type material

A DNA sample of the holotype specimen VP 32 has been deposited in the Natural History Museum, Vajanského nábrežie 2, 810 06 Bratislava, Slovakia (ID Collection Code 01427566).

Type locality

Vajspeterský potok creek, Rača, Bratislava, Podunajská rovina plain, Slovakia, 48°12′12.8″ N, 17°07′46.9″ E.

Gene sequences

The nuclear 18S and 28S rDNA sequences as well as the mitochondrial COI sequence of the holotype specimen VP 32 have been deposited in GenBank under the following accession numbers: OM421713, OM421689, and OM424068, respectively.

Description

Habitus. *Chaetonotus* (*Hystricochaetonotus*) *avarus* sp. nov. is about 130 µm long and has a slender elongated body, with a head region slightly broader than the neck and trunk (Figs 23A, K, 24A, 25A–C). Body width is 22.0–23.0 µm at U10, 18.0–19.0 µm at U50, and 20.0–21.0 µm at U60. The head is relatively wide (11–15 µm at U6), with a plate-like cephalion. Epi- and hypopleurae are clearly demarcated in the head outline (Figs 23A, K, 24A, 25A–C, 26A). The neck (ca U14–U27) is only inconspicuously marked and smoothly continues to the trunk. In comparison with the head, the trunk is comparatively slender, gradually dilatating from about U35 to U55, where it reaches the maximum width. Then, the trunk gradually narrows towards U87, where more or less straight margins of the furca branches start to form. Dorsal sensory bristles arise from the cuticle in two pairs at U28 and U78 (Fig. 23A, L). The furcal indentation is deeply V-shaped. Well-developed adhesive tubes are approximately 6–12 µm long, they are straight and short (Figs 23A, K, 24A, H, 27E).

Head. The cephalion (U1) is clearly demarcated in the body outline, surrounds the mouth ventrally like a bib, and is distinctly flattened and lenticular in the dorsal view (Figs 23A, K, 24B, 25A–C, 26A, C). Two pairs of cephalic ciliary tufts emerge at U3 and U7. In addition, inverted V-shaped streaks of basal bodies extend from the level of the mouth to the posterior level of the hypostomium (Figs 24A, 26C). The mouth ring is oval, approximately 5.5 µm in the largest diameter, and located subapically at U2–U5. There are strong but short, rod-like reinforcements lining the walls of the mouth ring and inner delicate structures directed towards the center of the mouth ring (Fig. 26C). Three inner cuticular teeth are clearly visible, two are located laterally and one apically (Fig. 25A). The hypostomium (ca U5–U9) is rich in structures, i.e., it is composed of a pentagonal cuticular plate bearing two protuberances (Figs 24B, 26C).

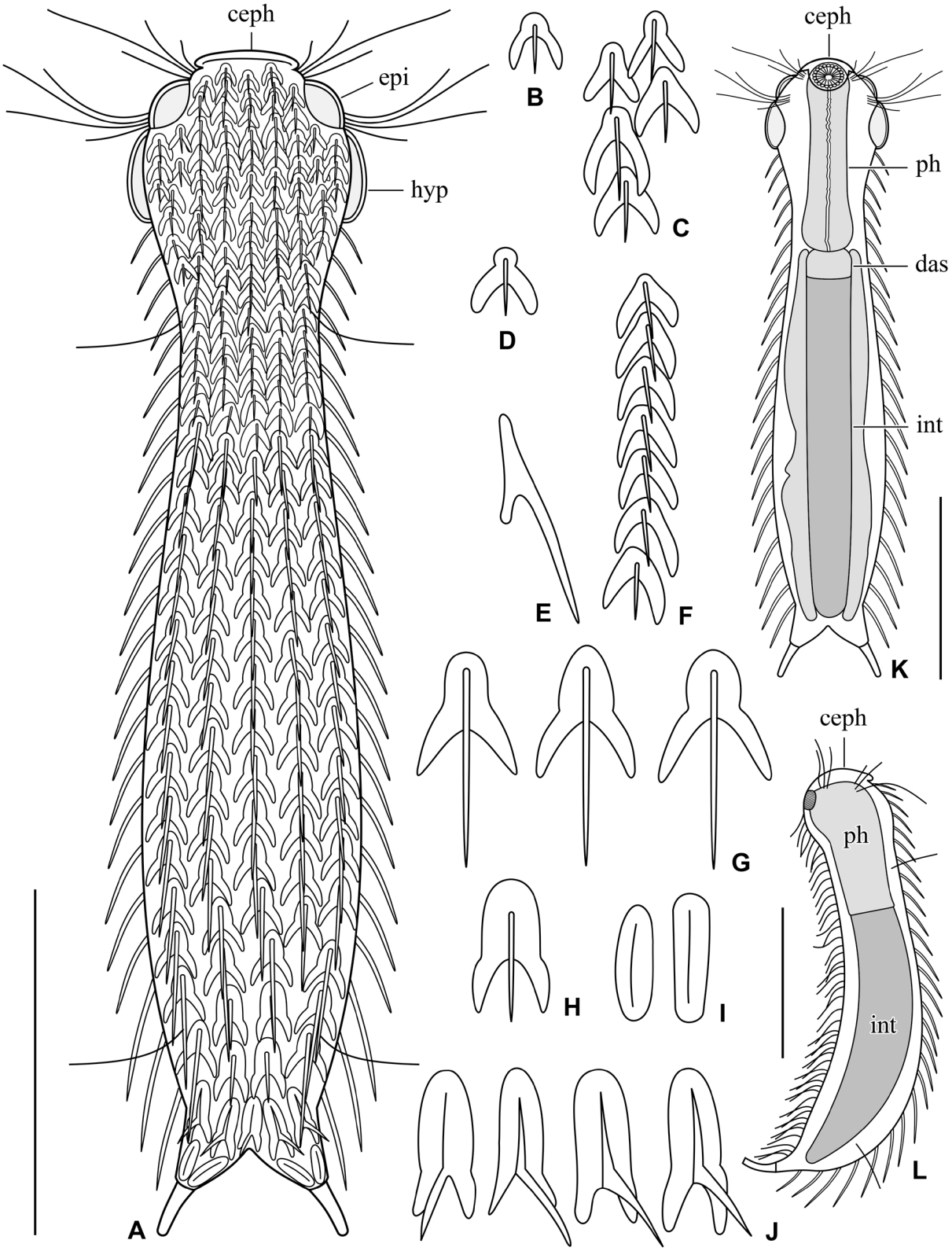

Fig. 23. *Chaetonotus* (*Hystricochaetonotus*) *avarus* sp. nov. **A**. Dorsal overview showing the scale and spine pattern. **B**–**C**. Head scales. **D**. Neck dorsolateral scale. **E**. Lateral view of a trunk spined scale. **F**. Neck central scales. **G**. Trunk scales. **H**. Posterior trunk scales. **I**. Dorsal furca branches scales. **J**. Dorsal furca base scales. **K**. Internal morphology. **L**. Lateral overview. Scale bars = 30 μm.

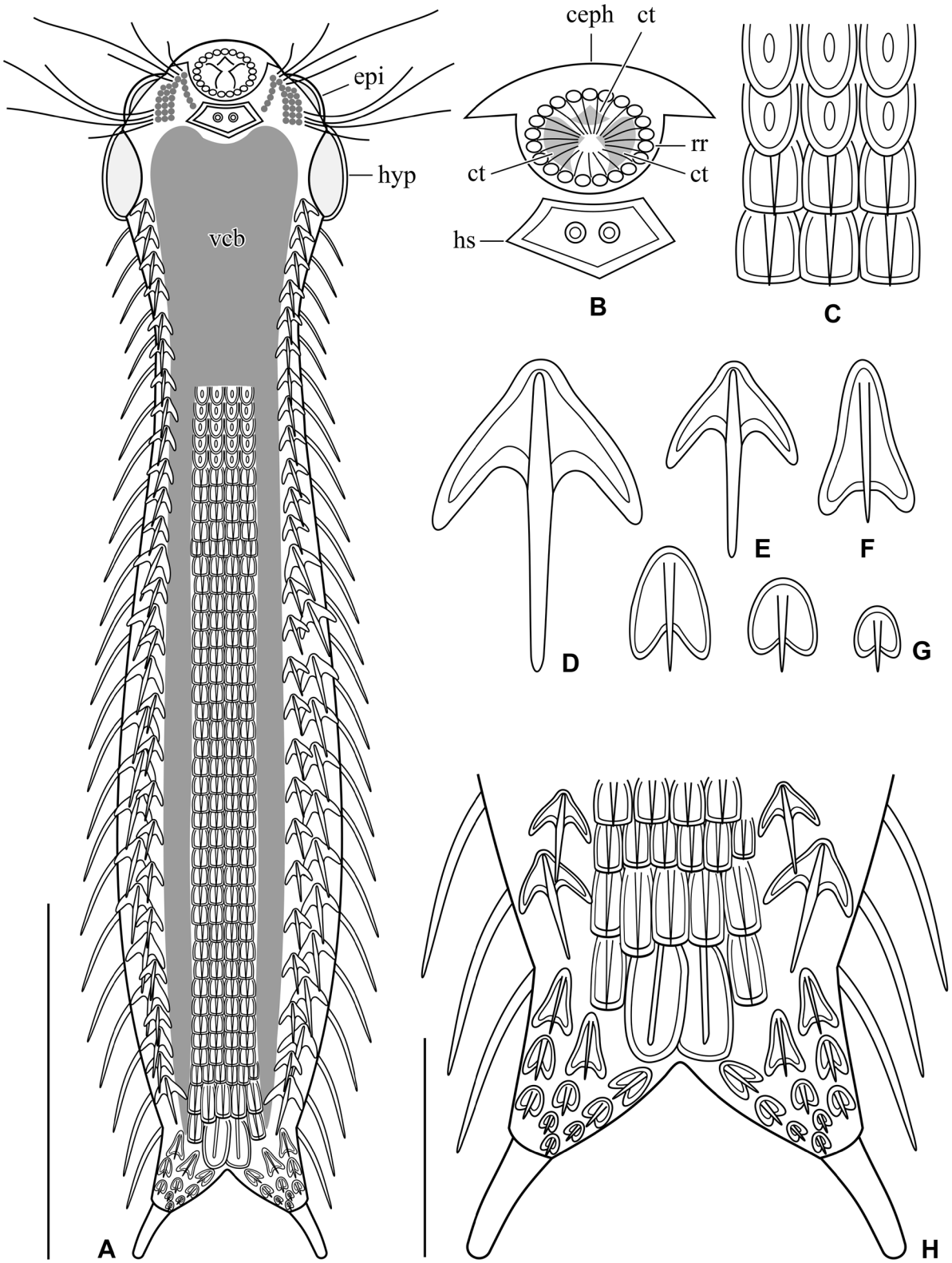

Fig. 24. *Chaetonotus* (*Hystricochaetonotus*) *avarus* sp. nov. **A**. Ventral overview showing the scale and ciliary pattern. **B**. Mouth region. **C**. Detail showing the transition region of two scale types in the interciliary field. **D**–**E**. Ventrolateral three-lobed scales. **F**. Ventral furcal three-lobed scales. **G**. Furcal cordiform scales. **H**. Detail of the terminal ventral region. Scale bars: A = 30 µm; H = 10 µm.

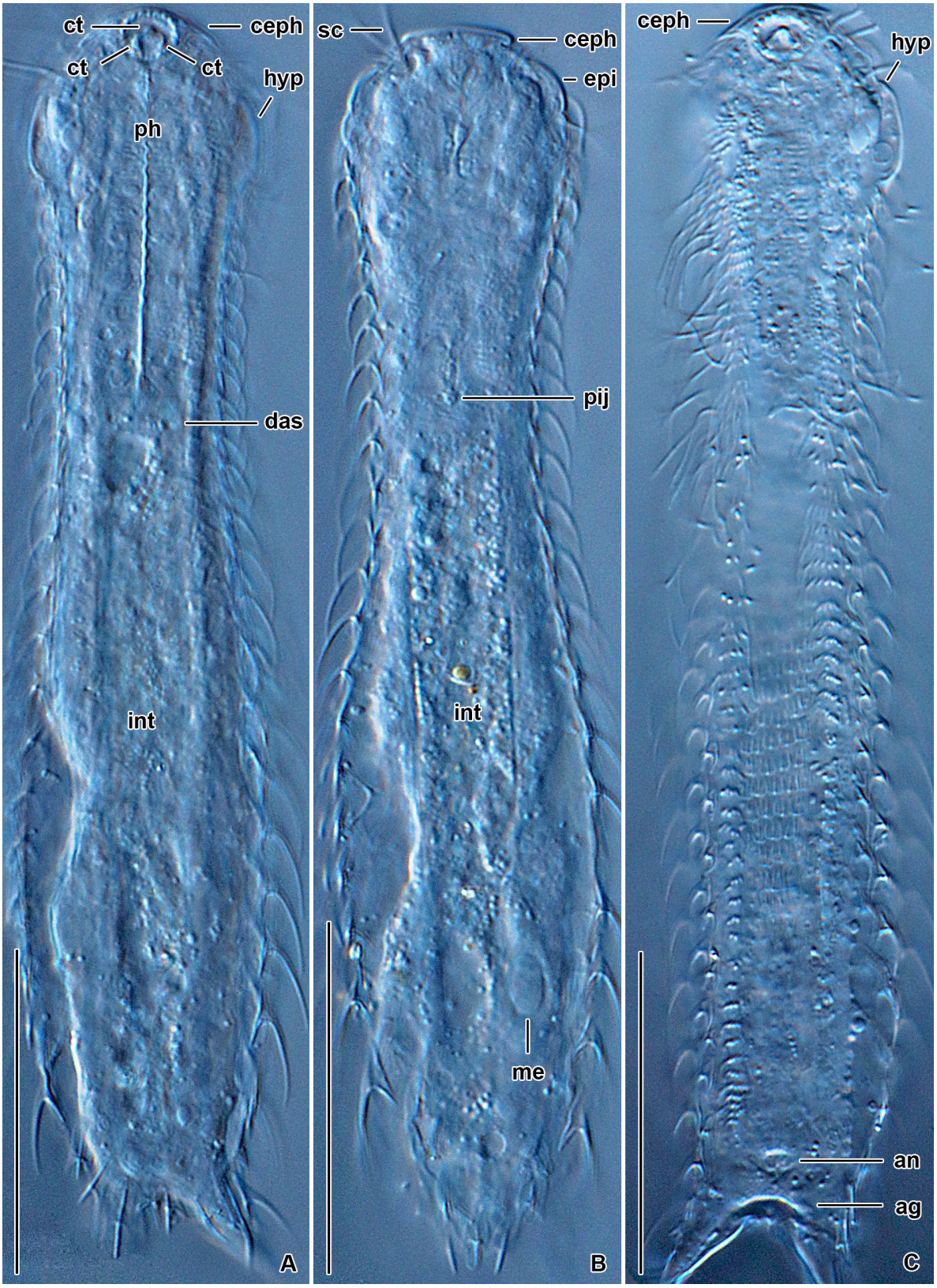

Fig. 25. *Chaetonotus* (*Hystricochaetonotus*) *avarus* sp. nov., paratype (CU-FNS-26-02-20/PA-2), differential interference contrast. **A**–**B**. Optical section showing the internal morphology. **C**. Ventral overview. Scale bars = 30 µm.

Internal morphology. The pharynx extends from ca U5 to U29, is almost 35 µm long and 7.4-9.1 µm wide, sinuous, and without dilatations (Figs 25A, 26A). The intestine runs from U29 to U85 and has a separate, well-differentiated anterior section (U29–U33). Transversal bands connected to the base of dorsal scales are well recognizable. The adhesive gland is placed right behind the terminal part of the intestine (ca U85–U87), forming a short dichotomy at the subtle furca base (Figs 23K–L, 25C).

Scales. Almost the entire body is covered by slightly overlapping, mostly three-lobed scales that adhere to the basal cuticle layer along either all or most of their perimeter. Scales are distributed in 14 longitudinal rows, with 30–32 scales in the central row. Their size increases slightly in a posterior direction. Central dorsal and dorsolateral longitudinal rows of scales begin at the level of the anterior edge of the cephalion (ca U1), while lateral rows start at ca U14 at the posterior edge of the hypopleurae. They run almost along the whole body length (till U92) (Figs 23A, 27B). Ventrolateral rows commence at U13 due to the highly developed hypopleurae and terminate in the furcal region at ca U85. Ventral rows commence rather far away from the anterior body end at U29, because of the strongly developed and apically completely fused bands of locomotory cilia (Figs 24A, 25C). Seven main types of dorsal scales were recognized. (i) Head scales (U2–U17) are small (3.1–4.1 × 1.6–3.0 µm) and have a subtle, well-delimited anterior lobe, comparatively long and diverging posterior lobes, α = 156–173°, β = 55–87° (Figs 23B–C, 27A). (ii) Dorsal neck scales (U17–U27) are boomerang-like with a broadly rounded anterior lobe, elongated posterior lobes, and an indistinct and continuous transition between the anterior and posterior lobes, α = 166–173°, β = 55–87° (Fig. 23F). (iii) Dorsolateral neck scales possess a well-delimited, broadly rounded anterior lobe, i.e., the transition between anterior and posterior lobes is distinct, α = ~171°, β = ~70° (Fig. 23D). (iv) The main trunk region bears distinctly bigger scales (5.3–9.3 × 3.1–6.1 µm) whose anterior end is rounded, posterior lobes are comparatively long, narrowly rounded, and diverging, the transition between anterior and posterior lobes is well marked, α = 146–176°, β = 86–102° (Fig. 23G). (v) Posterior trunk scales are 8.1–8.9 × 4.1–4.8 µm in size, their anterior lobe is conspicuously prolonged becoming tongue-shaped, while their posterior lobes are relatively short and taper towards the distal end, the transition between anterior and posterior lobes is slightly marked, α = 140–170°, β = 53–68° (Figs 23H, 27C). (vi) Furca base scales are 4.5–8.4 × 2.8–3.6 µm in size, their anterior lobe is slightly narrower and more elongated, posterior lobes are short and very narrowly rounded or almost acute distally, the lobe transition is less distinct than in the previous type, α = 149–163°, β = 69–78° (Fig. 23J). (vii) Furca branches carry elongated oval, keeled scales measuring 5.7–6.0 × 1.7–1.8 µm (Fig. 23I). These scales reach up to the apical margin of the adhesive tubes.

Spines. Dorsal, dorsolateral, lateral, and ventrolateral scales bear simple, slightly curved spines that gradually narrow towards the distal end (Figs 23A, E, K–L, 25A–B). The spine emerges rather close to the anterior margin of scales. Spines do not differentiate into various types, only their length slightly increases from 3.5 µm to 10.9 µm in a posterior direction (Supp. file 1: Table S4). A lateral denticle is not developed.

Ventral ciliary bands and ventral interciliary field. Ventral ciliary bands commence almost right behind the hypostomium. Their anterior region is conspicuously broad, causing both bands to be completely fused from U9 to U27 (Figs 24A, 26B–C). However, the middle distal part of the merged ciliary bands more or less follows the course of the posterior margin of the hypostomium, i.e., it is concave from ca U10 to U13. Basal bodies are densely packed and do not form regular rows in the anterior fused region of the ciliary bands. The anterior field of basal bodies splits into two distinct ventral bands about at U27. Locomotory cilia then become regularly arranged in more or less equidistantly spaced horizontal rows. Each row typically consists of seven narrowly spaced basal bodies from ca U28 to U83. Rows of basal bodies are lined up with horizontal rows of ventral scales. This regular pattern changes about at U84 where distances between horizontal ciliary rows gradually decrease. Also, the number of basal bodies per row gradually decreases and ciliary bands terminate at U88 (Figs 24A, 25C). The ciliary bands are accompanied by two ventrolateral rows of three-lobed scales, with an indistinct and continuous

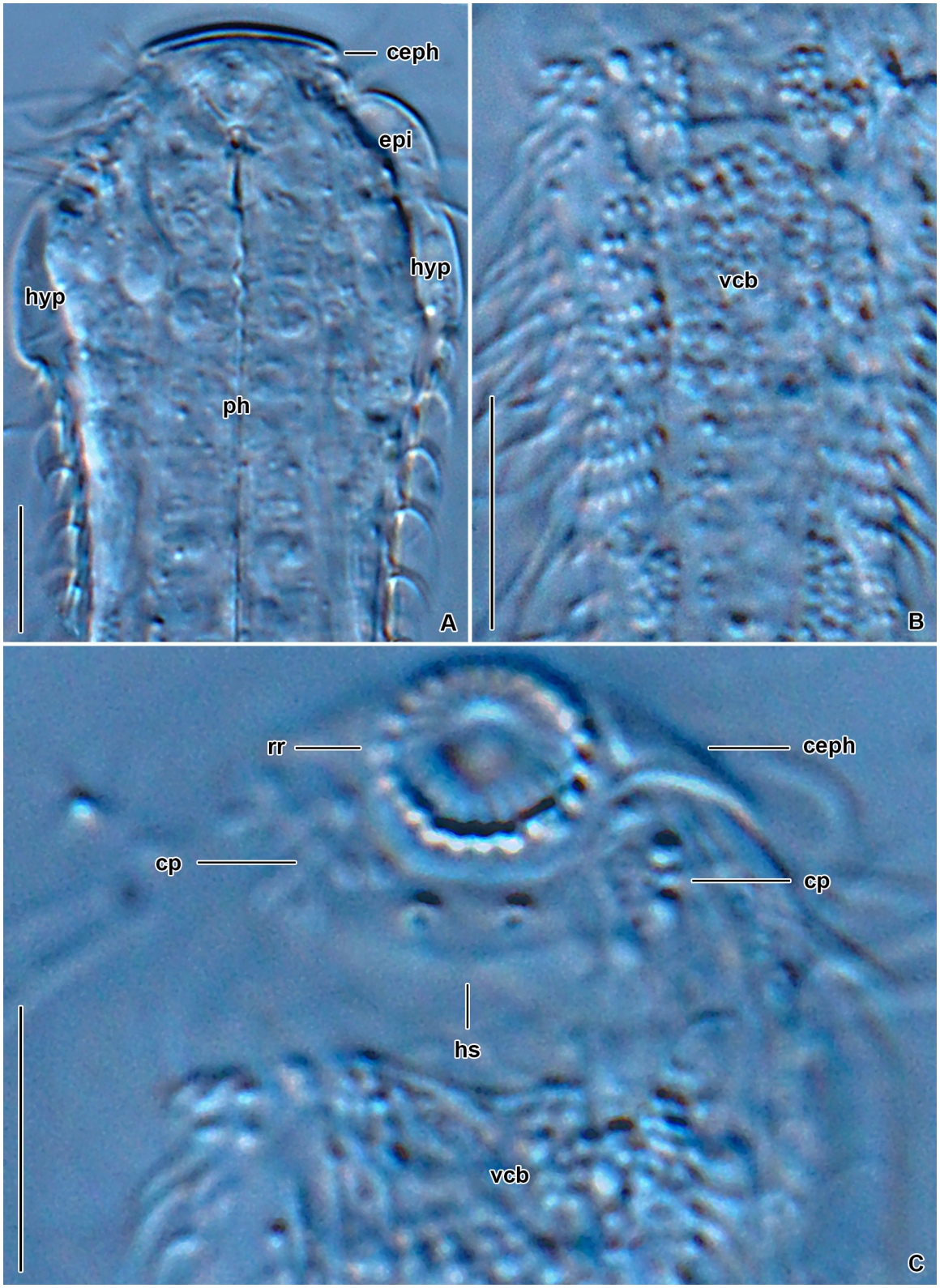

Fig. 26. *Chaetonotus* (*Hystricochaetonotus*) *avarus* sp. nov., paratype (CU-FNS-26-02-20/PA-2), differential interference contrast. **A**. Anterior body region. **B**. Anteriorly merged ventral ciliary bands. **C**. Detail of the mouth region. Hypostomium bears a pentagonal cuticular plate with two central protuberances. Scale bars = 10 µm.

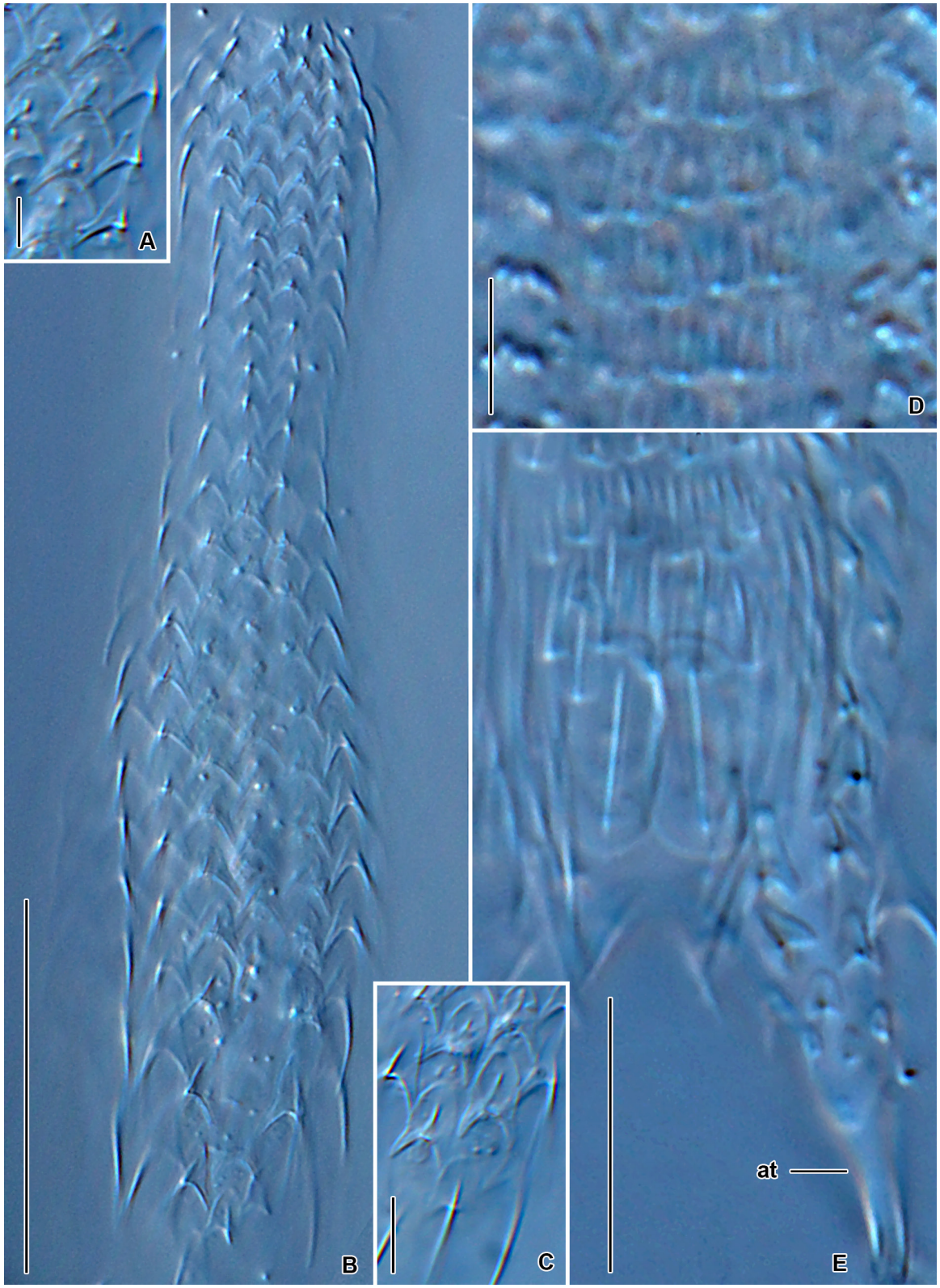

Fig. 27. *Chaetonotus* (*Hystricochaetonotus*) *avarus* sp. nov., paratype (CU-FNS-26-02-20/PA-2), differential interference contrast. **A**. Dorsal head scales. **B**. Overview showing the dorsal scale and spine pattern. **C**. Posterior trunk scales. **D**. Scales in the ventral interciliary field. **E**. Detail of the ventral posterior region. Scale bars: A, C–D = 5 µm; B = 30 µm; E = 15 µm.

transition between the anterior and posterior lobes (Fig. 24A). The inner row starts at U22 and consists of smaller scales (2.4–4.3 × 1.2–2.8 µm) (Fig. 24E), while the outer row begins at ca U40 and is built up from bigger scales (4.8–5.3 × 2.2–3.6 µm) (Fig. 24D). The ventral interciliary field bears four types of horizontally distributed scales: (i) minute (1.5–1.8 × 1.3–1.8 µm), tongue-like, double-edged scales with a minute keel (U28–U32); (ii) small (1.9–2.3 × 1.6–2.1 µm), roughly rectangular, double-edged scales with a keel (U33–U83) (Figs 24C, 27D); (iii) slightly bigger (3.9–4.4 × 1.0–1.5 µm), oblong, double-edged scales with a short spine (U83–U87); and (iv) a pair of big (6.1–7.8 × 2.0–3.2 µm), elongated oval scales with a keel (Figs 24H, 27E). All ventral interciliary field scales are anteriorly merged into the cuticle. The furca branches carry two types of scales (U88–U95): (i) two pairs of three-lobed, spined scales (3.2–5.0 × 1.1–2.0 µm), with an elongated, tongue-shaped anterior lobe and comparatively short, narrowly rounded to acute posterior lobes (Fig. 24F) and (ii) smaller (0.7–3.2 × 0.4–1.8 µm), cordiform, short-spined scales (Figs 24G–H, 27E).

Chaetonotus* (*Hystricochaetonotus*) *luxus sp. nov.
urn:lsid:zoobank.org:act:DD747096-A6E0-43F7-B462-349692AAFB65
Figs 28–30; Supp. file 1: Table S6

Morphological diagnosis

Body stocky and around 87–112 µm long. Head wider than neck, separated from trunk by a more or less distinct neck constriction. Cephalion, epipleurae, and hypopleurae clearly demarcated. Trunk widest at ca U55, gradually tapers towards furca base (U83). Mouth ventral, no cuticular teeth. Pharynx without dilatations. Intestine straight, with a marked anterior section. Scales spined, three-lobed, not overlapping, distributed in a minimum of 10 columns, 15 scales per column. Spines with a very short lateral denticle. Scales and spines increase gradually in size in a posterior direction. Dorsal surface covered with: (i) head and upper-neck scales with a small, narrowly rounded anterior lobe and elongated posterior lobes; (ii) lower-neck and anterior trunk scales with a slightly larger anterior lobe and elongated posterior lobes; (iii) posterior trunk scales with an elongated anterior lobe and posterior lobes about as long as anterior lobe; and (iv) posteriormost trunk scales with a tongue-shaped anterior lobe and short posterior lobes. Furca branches shorter than adhesive tubes, lateral margins more or less straight, furcal indentation U-shaped, adhesive tubes long and diverging posteriorly. Dorsal and lateral sides of furca branches covered with narrowly trapezoid, keeled scales with rounded edges and ventral side of furca base and branches covered with (i) a pair of oblong, keeled scales and (ii) three-lobed, spined scales, with an elongated anterior lobe and comparatively short, narrowly rounded posterior lobes, transition between anterior and posterior lobes continuous and indistinct.

Molecular diagnosis

ITS2: 36 T, 61 C, 71 T, 72 G, 126 T, 135 A, 164 C, 171 C, 175 A, 176 A, 177 A. Cytochrome *c* oxidase subunit I: 69 (205–207) CTG, 92 (274–276) TTG, 109 (325–327) GCG, 156 (466–468) GCT, 168 (502–504) CTA, 174 (520–522) GCC, 176 (526–528) TTA.

Reference molecules are shown in Supp. file 1: Figs S4, S10, S16. All diagnostic molecular autapomorphies are marked by arrows. Reference alignments with corresponding nucleotide positions are in Supp. file 1: Alignments 1–4.

The *p*-distance from species described in the present study is 0.00–4.33% in 18S, 10.16–34.22% in ITS2, 0.26–9.61% in 28S, and 5.63–12.70% in COI. There are 1–16 CBCs (except for *Ch.* (*H*). *slavicus* sp. nov., *Ch.* (*H*). *iratus* sp. nov., and *Ch.* (*H*). *arcanus* sp. nov. where there are no CBCs) in the 18S rRNA molecule, 1–4 CBCs (except for *Ch.* (*H*). *slavicus* sp. nov., *Ch.* (*H*). *gulosus* sp. nov., and *Ch.* (*H*). *arcanus* sp. nov. where there are no CBCs) in the ITS2 molecule, and 2–18 CBCs in the first two domains of the 28S rRNA gene (except for *Ch.* (*H*). *slavicus* sp. nov., *Ch.* (*H*). *iratus* sp. nov., and *Ch.* (*H*). *arcanus* sp. nov. where there are no CBCs).

Etymology

The Latin noun '*luxus*' [m] ('extravagance, luxury') refers to the 'extravagant' appearance of the new species. The species group name is treated as a noun in the nominative singular standing in apposition to the generic name (Article 11.9.1.2 of the ICZN 1999).

Material examined

Holotype

SLOVAKIA • adult (the specimen was destroyed during DNA extraction); Zlaté Piesky lake, municipal recreation area, Ružinov, Bratislava, Podunajská rovina plain; 48°11′17.1″ N, 17°11′24.3″ E.

Paratypes

SLOVAKIA • 2 adults (photomicrographs); same collection data as for the holotype; CU-FNS-17-02-20/PA-1, CU-FNS-18-02-20/PA-2.

Photomicrographs of paratype specimens are available at the Department of Zoology, Comenius University in Bratislava at https://fns.uniba.sk/en/gastrotricha/. Paratypes are shown in Fig. 30.

Type material

A DNA sample of the holotype specimen ZPvs 20 has been deposited in the Natural History Museum, Vajanského nábrežie 2, 810 06 Bratislava, Slovakia (ID Collection Code 01427593).

Type locality

Zlaté Piesky lake, municipal recreation area, Ružinov, Bratislava, Podunajská rovina plain, 48°11′17.1″ N, 17°11′24.3″ E.

Gene sequences

The nuclear 18S and ITS1-5.8S-ITS2-28S rDNA sequences as well as the mitochondrial COI sequence of the holotype specimen ZPvs 20 have been deposited in GenBank under the following accession numbers: OM421714, OM421690, and OM424069, respectively.

Description

Habitus. *Chaetonotus* (*Hystricochaetonotus*) *luxus* sp. nov. is about 87–112 µm long and has a stocky body that is more or less tenpin-shaped, with a clearly defined head region, a narrowing neck, and a rather bulbous trunk (Figs 28A, 29A). Body height in lateral view is 13.5–14.0 µm at U10, 16.5–16.8 µm at U50, and 18.0–18.2 µm at U60. The head is relatively wide, with a plate-like cephalion. The neck (ca U15–U28) smoothly continues to the trunk, which is significantly wider than the head, gradually dilates from about U37 to U60 where it reaches the maximum width. Then it gradually tapers towards U81, where curved margins of the furca branches begin to emerge. Dorsal sensory bristles were not observed. The furcal indentation is deeply U-shaped. The furca branches are set apart. Well-developed adhesive tubes are approximately 11–13 µm long, slightly curved in lateral view, and run almost in parallel (Figs 28A, H, 29A, D–E, 30A).

Head. The head is five-lobed. The cephalion (U1–U2) is rounded, clearly demarcated in the body outline, and has a free posterior (dorsal) edge. The epipleurae are formed approximately at U3–U5 while the hypopleurae at U6–U13. The latter structures are clearly demarcated in the head outline (Fig. 28A, H). Two pairs of cephalic ciliary tufts emerge laterally between the cephalion and the epipleurae edge (ca U3) as well as between the epi- and the hypopleurae edge (U6). The hypostomium (ca U4–U6) is free of structures. The mouth ring is oval, 3.2–6.0 µm in the largest diameter, located subterminally at U2–U6. There are strong but short rod-like reinforcements lining the walls of the mouth ring and inner

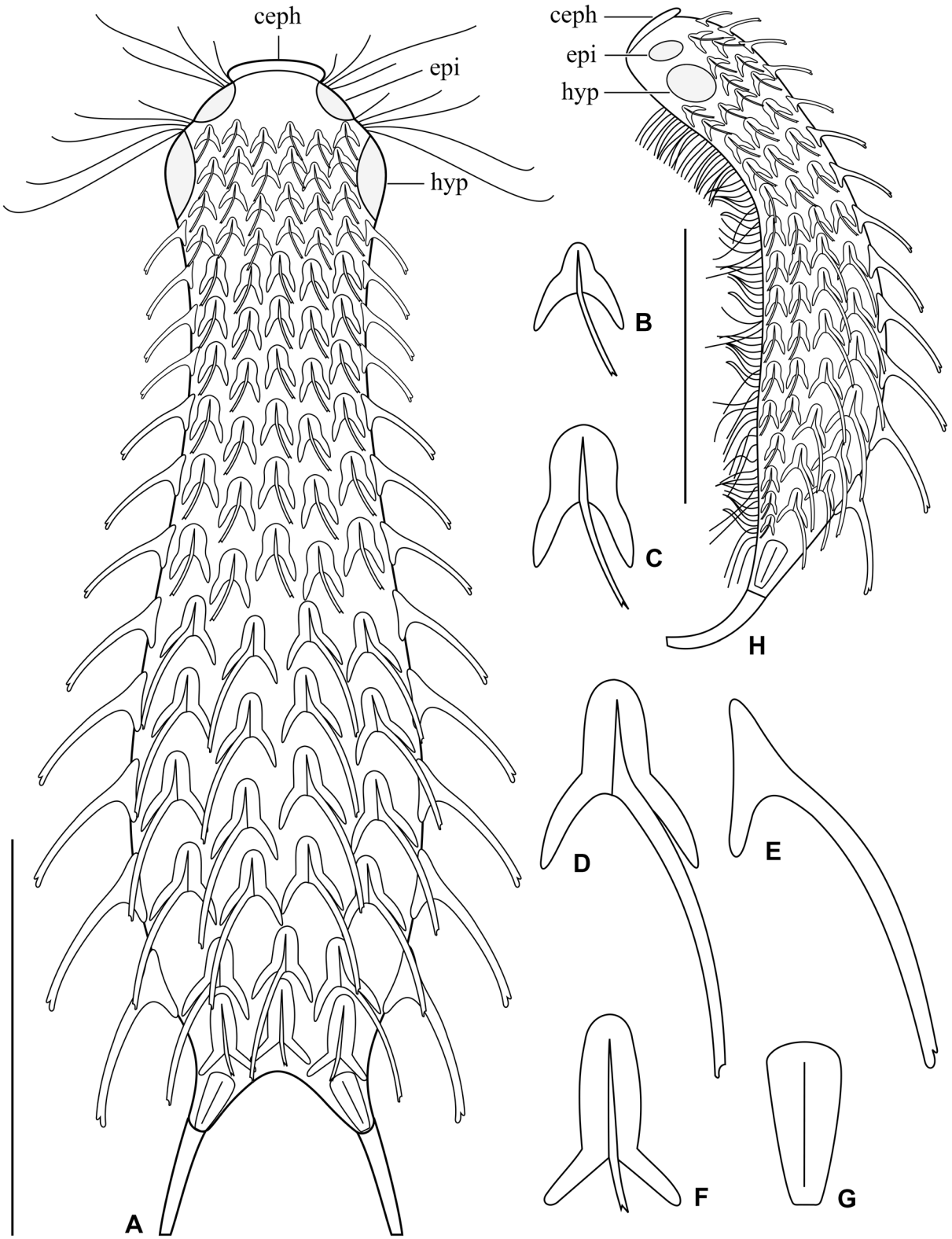

Fig. 28. *Chaetonotus* (*Hystricochaetonotus*) *luxus* sp. nov. **A**, **H**. Dorsal and lateral overviews showing the scale and spine pattern. **B**. Head scale. **C**. Neck and upper-trunk scale. **D**–**E**. Frontal and lateral views of a trunk spined scale. **F**. Posterior trunk scale. **G**. Dorsal furcal scale. Scale bars = 30 μm.

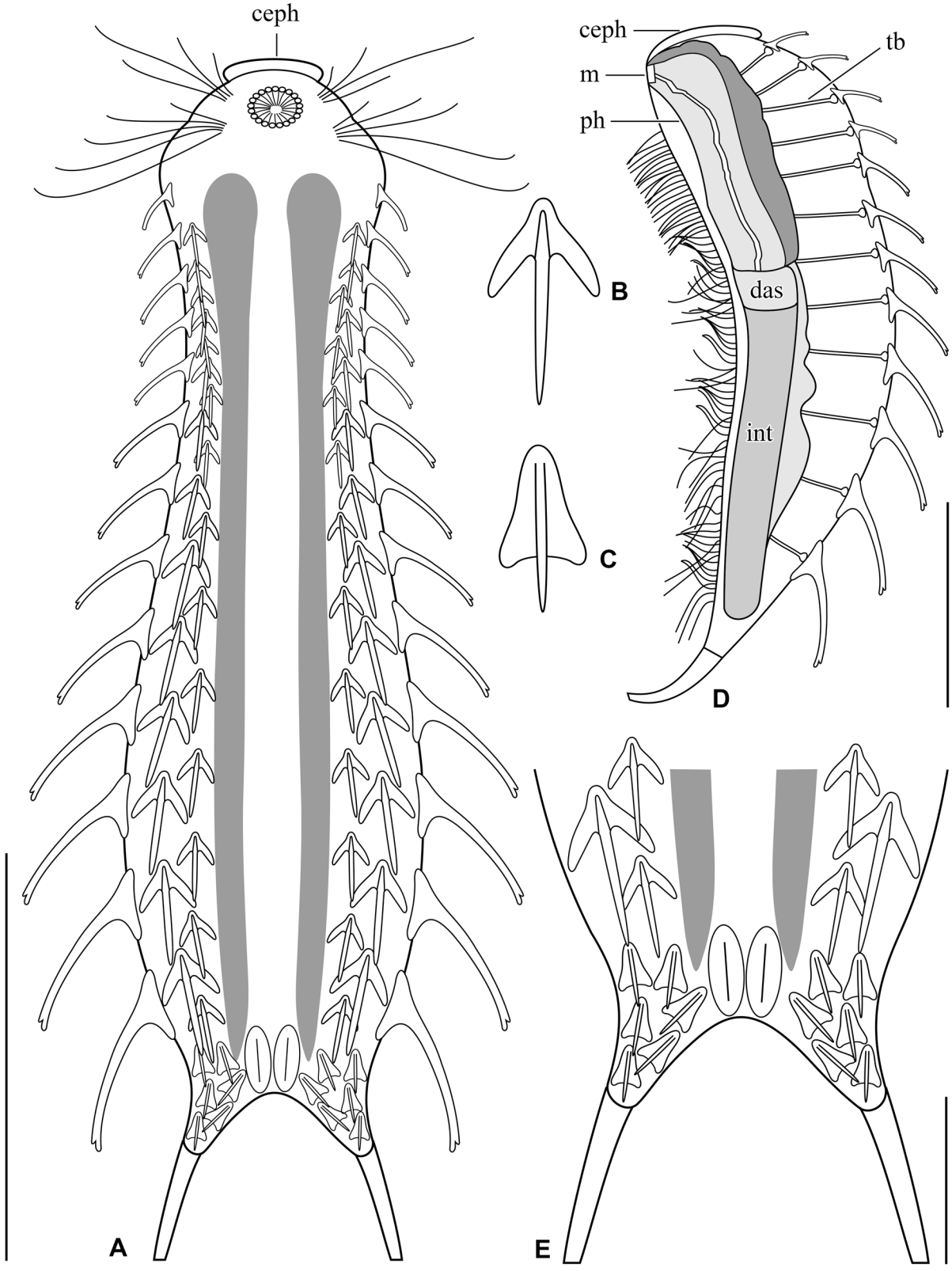

Fig. 29. *Chaetonotus* (*Hystricochaetonotus*) *luxus* sp. nov. **A**. Ventral overview showing the scale and ciliary pattern. **B**. Ventrolateral scale. **C**. Ventral furcal scale. **D**. Internal morphology. **E**. Detail of the ventral terminal body region. Scale bars: A = 30 µm; D = 20 µm; E = 10 µm.

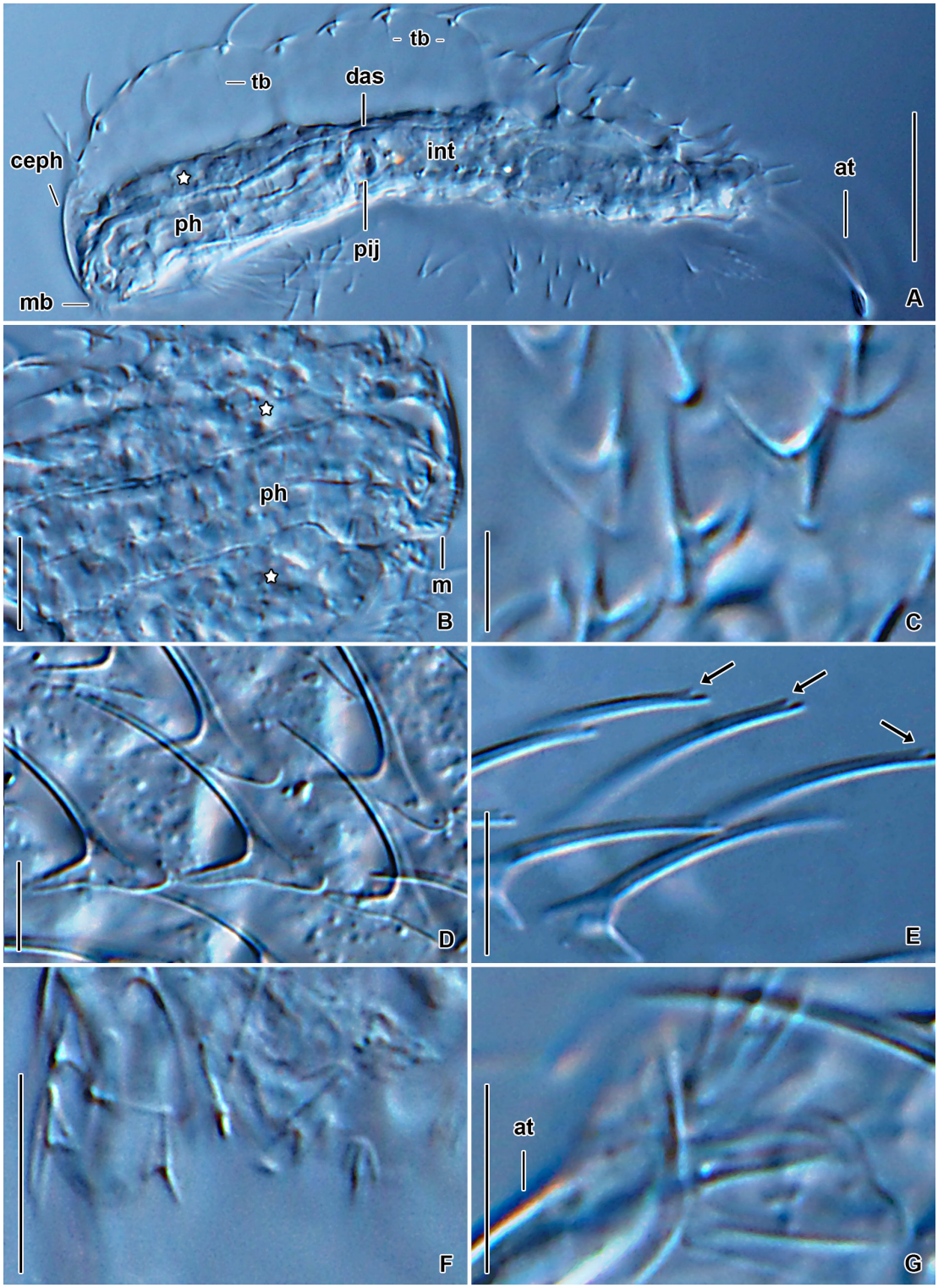

Fig. 30. *Chaetonotus* (*Hystricochaetonotus*) *luxus* sp. nov., differential interference contrast. **A, E**. Paratype (CU-FNS-17-02-20/PA-1). **B–D, F–G**. Paratype (CU-FNS-17-02-20/PA-2). **A**. Lateral overview showing the internal morphology. **B**. Anterior body region. **C**. Head scales. **D**. Dorsolateral trunk scales. **E**. Lateral view of dorsal trunk spined scales carrying a minute lateral denticle (arrows). **F**. Ventral furcal scales. **G**. Dorsolateral oblong scales lining the furca sides. White stars in (A) and (B) mark the cerebral ganglion. Scale bars: A = 15 µm; B, E = 10 µm; C–D, F–G = 5 µm.

delicate structures directed towards the center of the mouth ring (Figs 29A, 30A–B). Inner cuticular teeth are not present.

Internal morphology. The pharynx extends from ca U5 to U34, is 28–32 µm long and 5.9–8.3 µm wide, sinuous, and has no dilatations (Figs 29D, 30A–B). The intestine runs from U35 to U82 and has a separate, well-differentiated anterior section (U35–U38). A pair of protonephridia runs from ca U45 to U60. Transversal bands connected to the base of dorsal scales are well recognizable (Figs 29D, 30A). The adhesive gland (ca U80–U91) is placed right behind the terminal part of the intestine, forming a short dichotomy at the subtle furca base.

Scales. Almost the entire body is covered by not overlapping three-lobed scales that adhere to the basal cuticle layer along their whole perimeter. Scales are distributed in a minimum of 10 longitudinal rows, with 15 scales in the central row. Their size increases gradually in a posterior direction. Central dorsal and dorsolateral longitudinal rows of scales begin at the level of the anterior edge of the epipleurae (ca U5), while lateral rows start at the posterior end of the hypopleurae (ca U13). Ventral rows are hardly visible due to the thick, elongated dorsal spines (for further explanation, see below) and long locomotory cilia. Five main types of scales could be recognized with respect to the shape of the anterior lobe. (i) The head and upper-neck scales (U5–U25) are 3.2–5.4 × 2.1–5.2 µm in size and have a small, narrowly rounded anterior lobe and elongated posterior lobes, α = 153–162°, and β = 75–89° (Figs 28B, 30C). (ii) The lower-neck and anterior trunk scales (U29–42) are 2.6–3.5 × 3.7–5.8 µm in size and exhibit a slightly larger anterior lobe and elongated posterior lobes, α = 167–179°, and β = 72–83° (Fig. 28C). Both types share an indistinct and continuous transition between anterior and posterior lobes. (iii) Posterior trunk scales (U45–80) are 3.8–7.4 × 2.4–4.2 µm in size and display an elongated anterior lobe, posterior lobes about as long as the anterior lobe and distinctly set off from it, α = 153–170°, β = 75–96° (Figs 28D, 30D). (iv) Posteriormost trunk scales are 4.3–5.8 × 2.4–3.0 µm in size and have a tongue-shaped anterior lobe and short dilating posterior lobes, α = 144–164°, β = 83–85°. The transition between anterior and posterior lobes is marked (Fig. 28F). (v) The dorsal and lateral sides of the furca branches bear three pairs of narrowly trapezoid scales with rounded edges. These scales are keeled and have a size of 4.5–5.6 × 1.9–2.7 µm (Figs 28G–H, 30G).

Spines. Spines do not differentiate into various types, only their length increases from 3.4 µm to 13.5 µm in a posterior direction (Supp. file 1: Table S6). However, the width of individual spines decreases from 0.7 µm at the base to 0.2 µm at the tip and, hence, spines do not become hair-like terminally. The spine base is situated near the anterior margin of scales. All spines are distinctly curved and bear an inconspicuous lateral denticle (Figs 28A, E, H, 29A, D, 30D–E). The lateral denticle emerges comparatively near the spine apex, i.e., the *d*-value ranges only from 0.9–1.5 µm, which corresponds to a *d* ratio of 5.8–7.4%.

Ventral ciliary bands and ventral interciliary field. Unfortunately, the ventral side could not be observed in detail due to the thickness and stiffness of dorsal spines, which precluded turning over and squeezing the worms. Moreover, the ventral locomotory cilia also hampered detailed observations of the ventral side. Despite these difficulties, the following observations were conducted. The longitudinal ciliary bands begin at ca U10 and run backward to ca U84. The ciliary bands are accompanied from U13 to U75 by two ventrolateral rows of small (1.4–4.4 × 1.4–2.8 µm in size), three-lobed scales (α = 160–167°, β = 79–85°) equipped with relatively long spines (6.6–9.6 µm) (Fig. 29A–B). The furcal region (U81–U91) carries two types of scales (Figs 29A, C, E, 30F): (i) a pair of oblong, keeled scales being 6.8–7.0 × 2.8–3.0 µm in size and (ii) three-lobed, spined scales (1.9–3.8 × 1.5–2.3 µm), with an elongated anterior lobe and comparatively short, narrowly rounded posterior lobes, the transition between the anterior and posterior lobes is continuous and indistinct, α = 158–172°, and β = 73–84°.

Chaetonotus* (*Hystricochaetonotus*) *iratus sp. nov.
urn:lsid:zoobank.org:act:1A749F30-3FDF-4A02-8923-1DAE313BAB8E
Figs 31–32; Supp. file 1: Table S7

Morphological diagnosis

Body elongated and about 124 µm long. Head slightly wider than neck, separated from trunk by an inconspicuous neck constriction. Cephalion, epipleurae, and hypopleurae clearly demarcated. Trunk widest at ca U61, gradually tapers towards furca base (U82). Mouth ventral, one central cuticular tooth. Hypostomium bears two parallel, horizontally arranged lamellae accompanied by tear-shaped protuberances. Pharynx without dilatations. Intestine straight, with a marked anterior section. Scales spined, three-lobed, slightly overlapping, distributed in about 12 columns, 22 scales per column. Scales and spines increase gradually in size in a posterior direction. Dorsal surface covered by scales from posterior end of cephalion (ca U4) to furca branches (ca U83). Furca branches slightly shorter than adhesive tubes, lateral margins more or less straight, furcal indentation V-shaped, adhesive tubes comparatively short.

Molecular diagnosis

18S rRNA gene: 1716 C. ITS2: 38 C, 61 T, 67 C, 68 A, 85 T, 86 G, 91 C, 103 C, 113 T, 114 A, 124 A, 129 G, 155 C. 28S rRNA gene: 465 C, 656 T, 674 G. Cytochrome *c* oxidase subunit I (codon ordinal numbers are followed by the corresponding span of nucleotide positions in parentheses): 123 (367–369) GTG, 159 (475–477) CGG, 186 (556–558) CTA, 216 (646–648) ATC.

Reference molecules are shown in Supp. file 1: Figs S5, S11A, S17. All diagnostic molecular autapomorphies are marked by arrows. Reference alignments with corresponding nucleotide positions are in Supp. file 1: Alignments 1–4.

The *p*-distance from species described in the present study is 0.05–4.33% in 18S, 14.44–37.76% in ITS2, 0.25–9.79% in 28S, and 5.62–12.74% in COI. There are 1–16 CBCs (except for *Ch.* (*H*). *arcanus* sp. nov., *Ch.* (*H*). *luxus* sp. nov., and *Ch.* (*H*). *slavicus* sp. nov., where there are no CBCs) in the 18S rRNA molecule, 1–3 CBCs in the ITS2 molecule, and 1–18 CBCs in the first two domains of the 28S rRNA molecule (except for *Ch.* (*H*). *luxus* sp. nov. and *Ch.* (*H*). *slavicus* sp. nov., where there are no CBCs).

Etymology

The Latin adjective '*iratu·us*, *-a*, *-um*' [m, f, n] ('angry, irate') refers to the spiny appearance of the new species.

Material examined

Holotype

SLOVAKIA • adult (photomicrographs, hologenophore); Shallow section of the River Váh, Stankovany, Veľká Fatra Mts; 49°08′26.3″ N, 19°10′14.6″ E; CU-FNS-21-09-20/HO.

Photomicrographs of the holotype are available at the Department of Zoology, Comenius University in Bratislava at https://fns.uniba.sk/en/gastrotricha/. The holotype is shown in Fig. 32.

Type material

A DNA sample of the holotype specimen STV 65 has been deposited in the Natural History Museum, Vajanského nábrežie 2, 810 06 Bratislava, Slovakia (ID Collection Code 01427609).

Type locality

Shallow section of the River Váh near the village of Stankovany, Veľká Fatra Mts, Slovakia, 49°08′26.3″ N, 19°10′14.6″ E.

Gene sequences

The nuclear 18S and ITS1-5.8S-ITS2-28S rDNA sequences as well as the mitochondrial COI sequence of the holotype specimen STV 65 have been deposited in GenBank under the following accession numbers: OM421720, OM421696, and OM424075, respectively.

Description

Habitus. *Chaetonotus* (*Hystricochaetonotus*) *iratus* sp. nov. is about 124 μm long and has a slender elongated body, with a head region slightly broader than the neck and trunk (Figs 31A, J, 32A). Body width is about 21.5 μm at U10, 20.0 μm at U50, and 22.5 μm at U60. The head is relatively wide (20.2 μm at U6), with a plate-like cephalion. Epi- and hypopleurae are clearly demarcated in the head outline (Figs 31A, J, 32A). The neck (ca U13–U34) is only inconspicuously marked and smoothly continues to the trunk. In comparison with the head, the trunk is comparatively slender, gradually dilatating from about U35 to U61, where it reaches the maximum width. Then, the trunk gradually narrows towards U82, where more or less straight margins of the furca branches start to form. Dorsal sensory bristles were not observed. The furcal indentation is deeply V-shaped and approximately 19.4 μm long. Well-developed adhesive tubes are straight and approximately 10.7 μm long (Fig. 31A, J).

Head. The cephalion (U1) is clearly demarcated in the body outline, distinctly flattened, and surrounds the mouth ventrally like a bib. The epipleurae are formed approximately at U3–U7 while the hypopleurae at U8–U14. The latter structures are well recognizable in the head outline (Figs 31A, J, 32A). Two pairs of cephalic ciliary tufts (6.9–18.8 μm) emerge laterally between the cephalion and the epipleurae edge (ca U3) as well as between the epi- and the hypopleurae edge (U7). The mouth ring is oval, approximately 6.9 μm in the largest diameter, and located subapically at U2–U5. There are strong but short, rod-like reinforcements lining the walls of the mouth ring and inner delicate structures directed towards the center of the mouth ring (Figs 31I–J, 32C, F). One cuticular tooth is clearly visible in the center of the mouth ring (Figs 31I, 32F). The hypostomium (ca U5–U9) is composed of two more or less parallel, horizontally arranged lamellae whose lateral sides are accompanied by tear-shaped protuberances. Moreover, the lateral sides of the hypostomium are lined from U3 to U8 by relatively wide patches of irregularly arranged basal bodies (Figs 31I, 32F).

Internal morphology. The pharynx extends from ca U5 to U31, is 28 μm long and 6.2–8.8 μm wide, sinuous, and without dilatations (Figs 31J, 32A–B). The intestine runs from U22 to U87 and has a separate, well-differentiated anterior section (U32–U35). Transversal bands connected to the base of dorsal scales are well recognizable. The adhesive gland is placed right behind the terminal part of the intestine (ca U85–U87), forming a short dichotomy at the subtle furca base.

Scales and spines. Almost the entire body is covered by slightly overlapping, mostly three-lobed scales that adhere to the basal cuticle layer along either all or most of their perimeter. Scales are very densely packed, forming a minimum of 12 longitudinal rows on the dorsal side, with 22 scales in the central row. They have a rounded anterior lobe and elongated posterior lobes narrowly rounded distally. The transition between the anterior and posterior lobes is marked except for the ventro- and dorsolateral scales in which the transition is indistinct (Fig. 31D–G). The size of scales increases from 2.3 × 2.1 μm to 7.4 × 3.1 μm in a posterior direction. Dorsal furca branches scales are 4.3 × 3.4 μm in size, three-lobed and spined but their anterior lobe is more elongated, their posterior lobes are slightly shorter and narrower, the transition between the anterior and posterior lobes is continuous and indistinct (Fig. 31H).

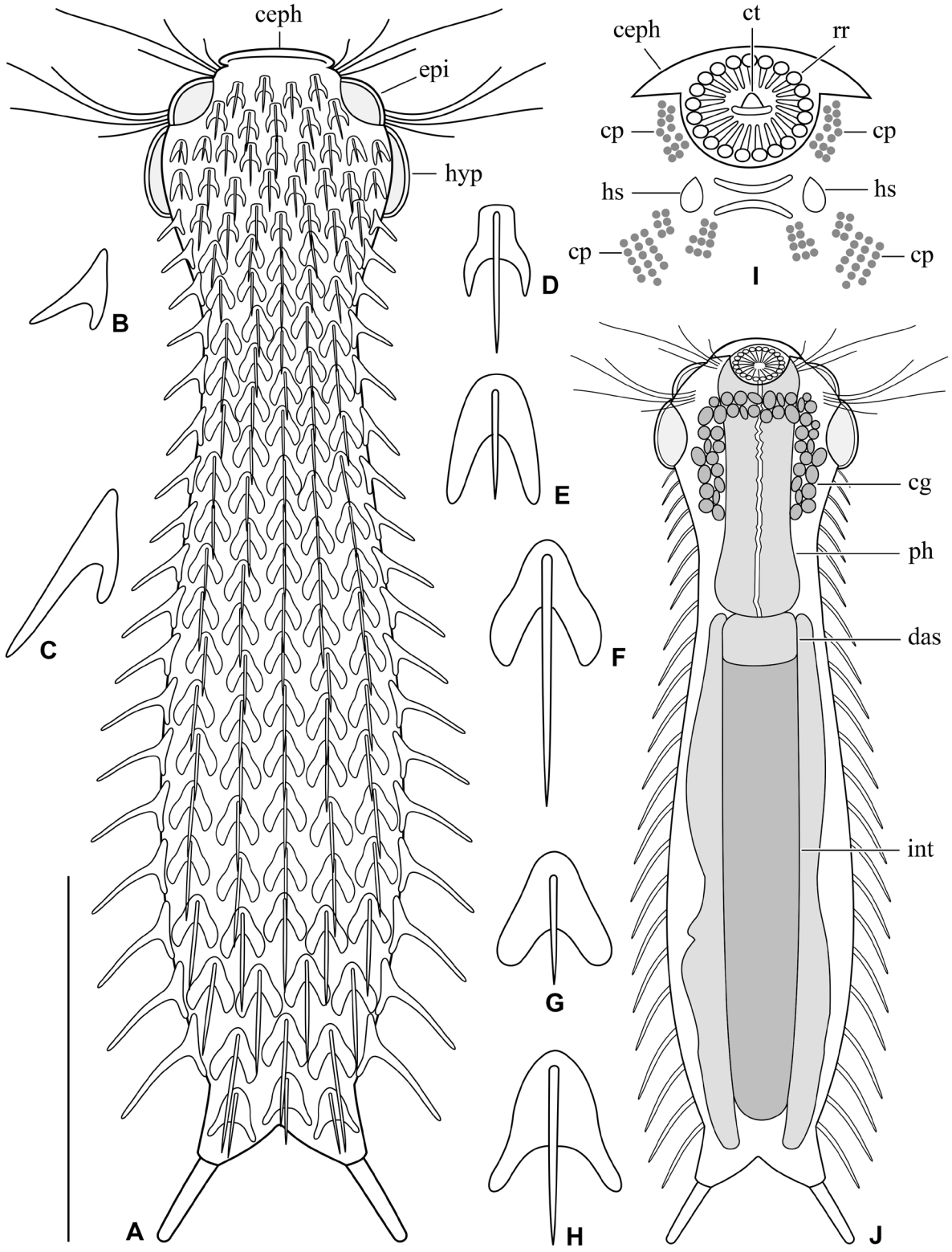

Fig. 31. *Chaetonotus* (*Hystricochaetonotus*) *iratus* sp. nov. **A**. Dorsal overview showing the scale and spine pattern. **B**, **D**. Lateral and dorsal views of a head scale. **C**, **F**. Lateral and dorsal views of a trunk scale. **E**. Dorsolateral head scale. **G**. Ventrolateral trunk scale. **H**. Furca branches scale. **I**. Detail showing the mouth region. **J**. Internal morphology. The structure of the cerebral ganglion was observed only in a single specimen. Scale bar = 30 µm.

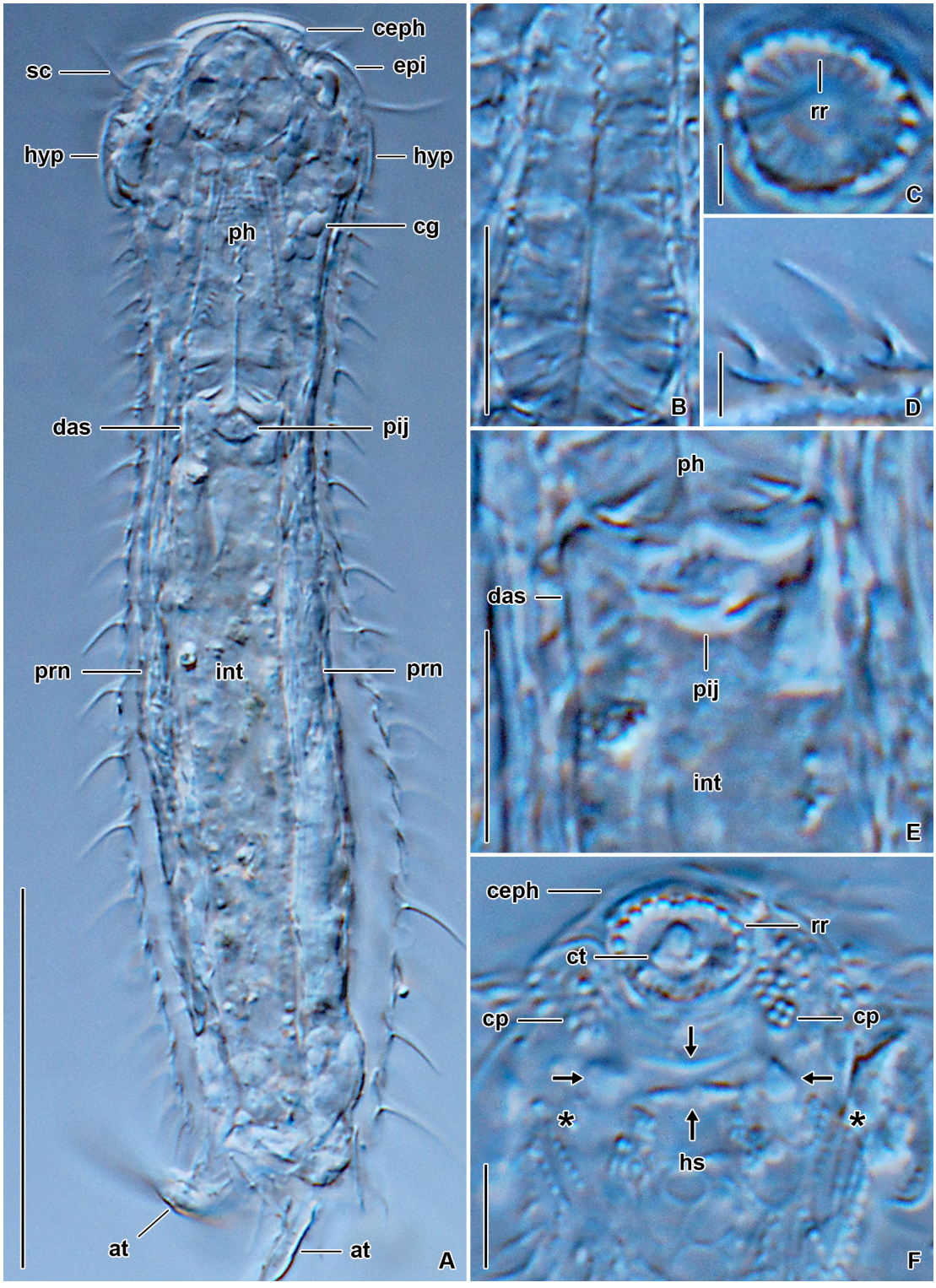

Fig. 32. *Chaetonotus* (*Hystricochaetonotus*) *iratus* sp. nov., holotype (CU-FNS-21-09-20/HO), differential interference contrast. **A**. Overview showing the internal morphology. **B**. Pharynx. **C**. Mouth. **D**. Head scales. **E**. Detail showing the posterior section of the pharynx, the pharyngeal-intestinal junction, and the differentiated anterior section of the intestine. **F**. Detail of the mouth region. Arrows mark the hypostomial structures, asterisks mark the beginning of ciliary bands. Scale bars: A = 30 µm; B = 10 µm; C–D = 2 µm; E–F = 5 µm.

Spines do not differentiate into various types, only their length slightly increases from 2.3 µm to 6.5 µm in a posterior direction (Figs 31A–H, J, 32A, D, Supp. file 1: Table S7). Spines are slightly narrower posteriorly but do not become hair-like terminally. A lateral denticle is not developed (Figs 31B–C, 32A, D).

Ventral ciliary bands and ventral interciliary field. Ventral ciliary bands commence almost right behind the hypostomium (U10) and terminate at ca U87. Their anterior region is broadened as typical of most species described herein. The ciliary bands are accompanied by two ventrolateral rows of three-lobed scales that start at U13. They are 3.6–5.3 × 2.5–3.1 µm in size and have a similar morphology as the dorsal and dorsolateral scales but the transition between the anterior and posterior lobes is continuous and hence indistinct (Fig. 31G). Unfortunately, no further features of the ventral side were observed.

Chaetonotus* (*Hystricochaetonotus*) *gulosus sp. nov.
urn:lsid:zoobank.org:act:5B6AE48A-9F1F-4F7A-8054-A01F7AB19E9B
Figs 33–36; Supp. file 1: Table S8

Morphological diagnosis

Body stocky and around 107 µm long. Head wider than neck, separated from trunk by a distinct neck constriction. Cephalion and epipleurae clearly demarcated, hypopleurae only inconspicuously marked. Trunk widest at ca U50, gradually tapers towards furca base (U80). Mouth ventral, no cuticular teeth. Hypostomium bears two parallel cuticular lamellae. Pharynx without dilatations. Intestine straight, with a marked anterior section. Scales spined, three-lobed, not overlapping, distributed in 14 columns, 12 scales per column. Scales and spines increase gradually in size in a posterior direction. Dorsal surface covered with: (i) small head and anterior neck scales with a small, broadly rounded anterior lobe, equally long posterior lobes, and marked transition between anterior and posterior lobes; (ii) small posterior neck scales with a slightly elongated anterior lobe and an indistinct transition between anterior and posterior lobes; and (iii) comparatively big and triangular trunk scales. Interciliary field covered by (i) small, oval to oblong scales without keels; (ii) a pair of small, oval scales with a keel; (iii) a single distinctly bigger, oblong, and keeled scale; and (iv) a pair of big, very narrowly ovate, and spined scales. Furca branches about as long as adhesive tubes, with lateral margins more or less straight, furcal indentation shallowly U-shaped, adhesive tubes well-developed. Ventral side of furca branches covered with minute, oval to oblong, and keeled scales.

Molecular diagnosis

18S rRNA gene: 1378 A. ITS2: 78 T, 128 T, 155 –, 172 A, 174 C, 186 –. 28S rRNA gene: 503 C. Cytochrome *c* oxidase subunit I (codon ordinal numbers are followed by the corresponding span of nucleotide positions in parentheses): 20 (58–60) TTA, 45 (133–135) GTG, 71 (211–213) CCG, 74 (220–222) ATC, 94 (280–282) CCA, 143 (427–429) TCA, 151 (451–453) TTC, 157 (469–471) AAT, 168 (502–504) CTC, 178 (532–534) ACT, 180 (538–540) GTT, 204 (610–612) ACA, 209 (625–627) CCA, 214 (640–642) GAT.

Reference molecules are shown in Supp. file 1: Figs S6, S11B, S18. All diagnostic molecular autapomorphies are marked by arrows. Reference alignments with corresponding nucleotide positions are in Supp. file 1: Alignments 1–4.

The *p*-distance from species described in the present study is 0.33–4.22% in 18S, 6.95–29.95% in ITS2, 1.46–8.84% in 28S, and 8.57–13.14% in COI. There are 1–15 CBCs in the 18S rRNA molecule, 1–4 CBCs in the ITS2 molecule (except for *Ch.* (*H.*) *arcanus* sp. nov., *Ch.* (*H.*) *luxus* sp. nov., and *Ch.* (*H.*) *slavicus* sp. nov., where there are no CBCs), and 2–17 CBCs in the first two domains of the 28S rRNA molecule.

Etymology

The Latin adjective '*gulos·us*, *-a*, *-um*' [m, f, n] ('gluttonous') refers to the stocky appearance of the new species.

Material examined

Holotype

SLOVAKIA • adult (the specimen was destroyed during DNA extraction); Vajspeterský potok creek, Rača, Bratislava, Podunajská rovina plain; 48°12′12.8″ N, 17°07′46.9″ E.

Paratype

SLOVAKIA • adult (photomicrographs); same collection data as for holotype; CU-FNS-28-10-19/PA.

Photomicrographs of the paratype specimen are available at the Department of Zoology, Comenius University in Bratislava at https://fns.uniba.sk/en/gastrotricha/. The paratype is shown in Figs 35–36.

Type material

A DNA sample of the holotype specimen VP 18 has been deposited in the Natural History Museum, Vajanského nábrežie 2, 810 06 Bratislava, Slovakia (ID Collection Code 01427574).

Type locality

Vajspeterský potok creek, Rača, Bratislava, Podunajská rovina plain, Slovakia, 48°12′12.8″ N, 17°07′46.9″ E.

Gene sequences

The nuclear 18S and ITS1-5.8S-ITS2-28S rDNA sequences as well as the mitochondrial COI sequence of the holotype specimen VP 18 have been deposited in GenBank under the following accession numbers: OM421721, OM421697, and OM424076, respectively.

Description

Habitus. *Chaetonotus* (*Hystricochaetonotus*) *gulosus* sp. nov. is about 107 µm long and has a stocky body that is tenpin-shaped, with a clearly defined head region, a narrowing neck, and a rather bulbous trunk (Fig. 33A–B). Body width is ca 18 µm at U10, ca 26 µm at U50, and ca 29 µm at U60. The head is relatively wide, with a plate-like, slightly narrower cephalion. The neck (ca U13–U27) smoothly continues to the trunk, which is distinctly wider than the head, gradually dilates from about U37 to U50 where it reaches the maximum width. Then it gradually tapers towards U80 where the curved margins of the furca branches begin to emerge. Dorsal sensory bristles arise from the cuticle in two pairs at U23 and U60 (Fig. 33A). The furcal indentation is deeply U-shaped. The furca branches are set apart and diverge posteriorly. Well-developed adhesive tubes are approximately 9 µm long and more or less straight (Figs 33A–B, 35C, 36C).

Head. The head is roughly five-lobed. The cephalion (U1–U2) is rounded, clearly demarcated in the body outline (Figs 33A–B, 34A). The epipleurae are formed approximately at U3–U6, the hypopleurae are only inconspicuously marked. Two pairs of cephalic ciliary tufts emerge laterally between the cephalion and the anterior edge of the epipleurae (ca U3) as well as close to the posterior edge of the epipleurae (U6). The mouth ring is oval, ca 4.6 µm in the largest diameter, located subterminally at U2–U4. There are strong, rod-like reinforcements lining the walls of the mouth ring and inner delicate structures directed towards the center of the mouth ring (Figs 33B, 35B). Inner cuticular teeth are not present. The hypostomium (ca U6–U9) is in a form of two parallel horizontal cuticular lamellae laterally

lined with a few ciliary patches (Fig. 33B). Each field is composed of several irregular groups of basal bodies (Figs 33B, 35B).

Internal morphology. The pharynx extends from ca U5 to U27, is about 28 µm long and 6.5–8.9 µm wide, sinuous, and has no dilatations. The cerebral ganglion appears as a mass surrounding the pharynx along its

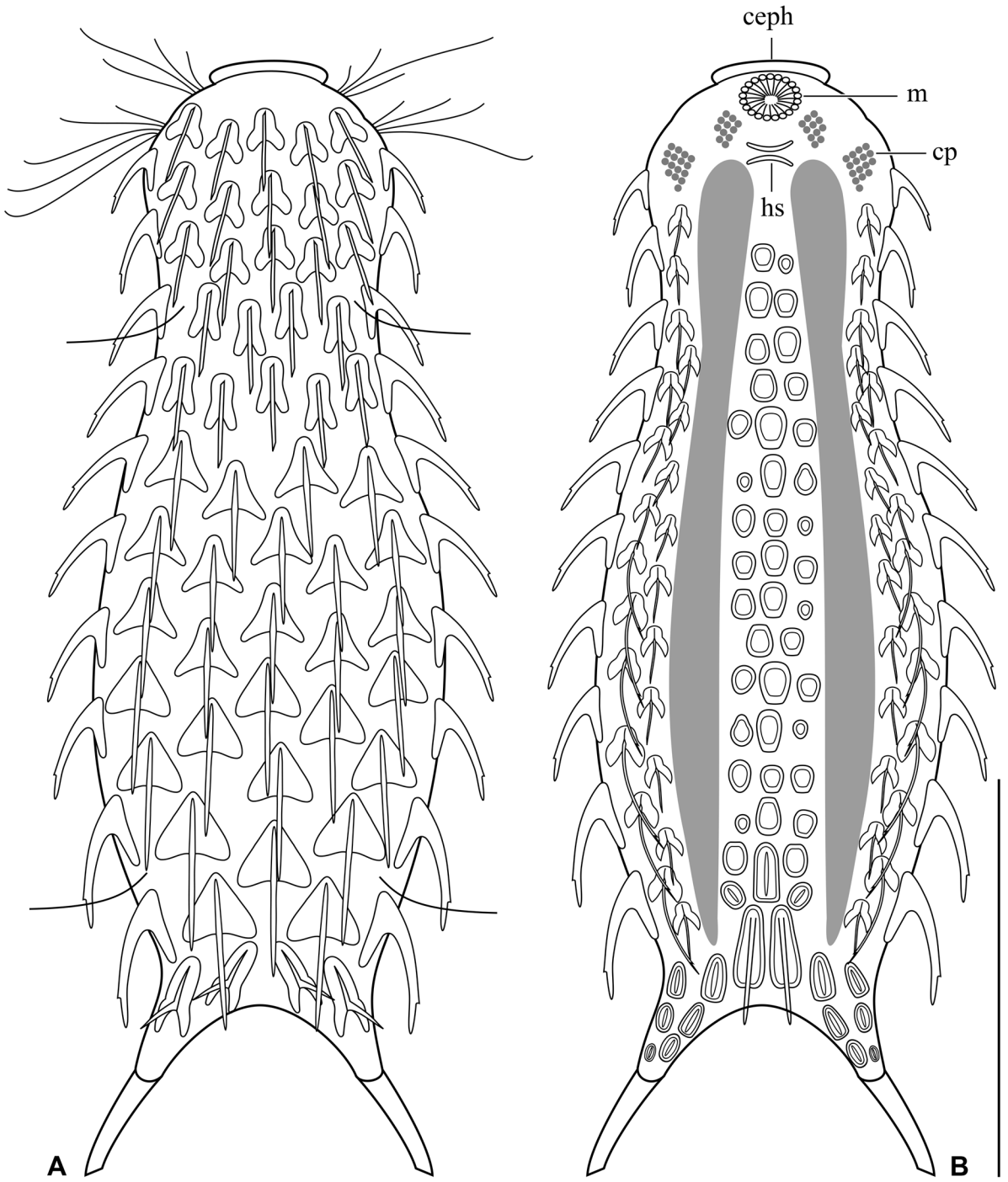

Fig. 33. *Chaetonotus* (*Hystricochaetonotus*) *gulosus* sp. nov. **A**. Dorsal overview showing the scale and spine pattern. **B**. Ventral overview showing the scale and ciliary pattern. Scale bar = 30 µm.

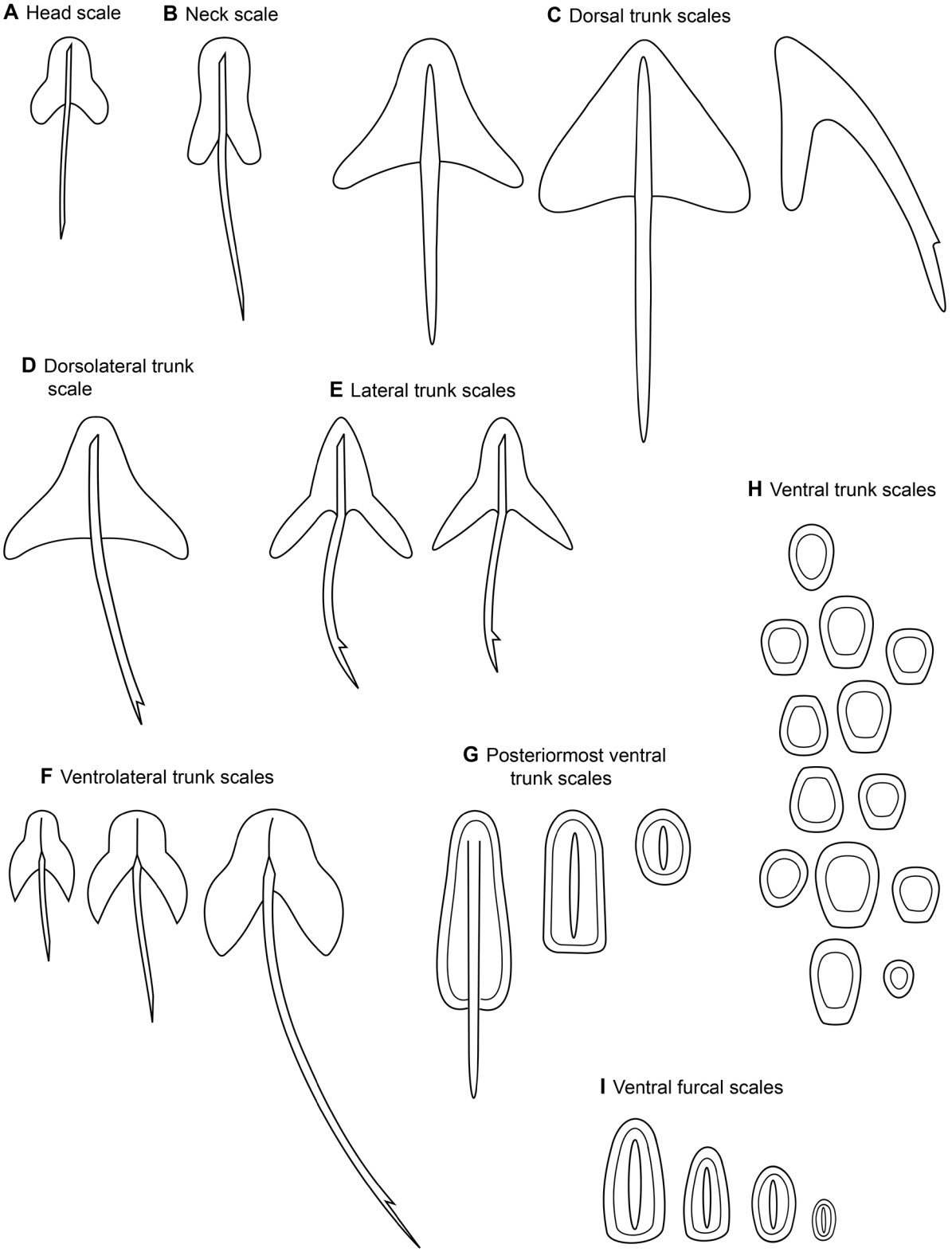

Fig. 34. *Chaetonotus* (*Hystricochaetonotus*) *gulosus* sp. nov., schematic drawings of scales. **A**. Head scale. **B**. Neck scale. **C**. Dorsal trunk scales. **D**–**E**. Dorsolateral and lateral trunk scales. **F**. Ventrolateral trunk scales. **G**. Posteriormost ventral trunk scales. **H**. Scales of the ventral interciliary field. **I**. Ventral furcal scales.

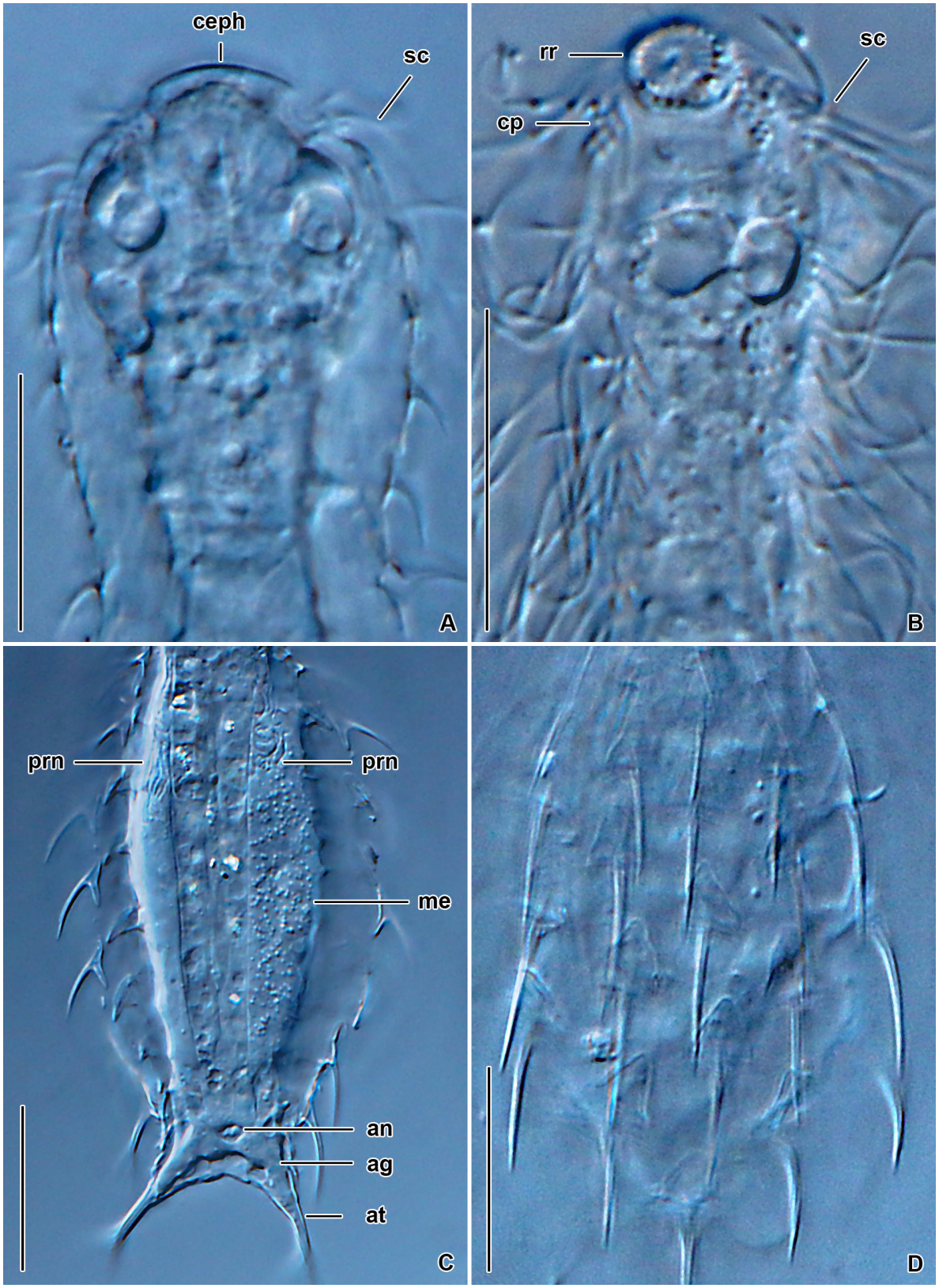

Fig. 35. *Chaetonotus* (*Hystricochaetonotus*) *gulosus* sp. nov., paratype (CU-FNS-28-10-19/PA), differential interference contrast. **A–B**. Details of the anterior body region. **C**. Optical section of the trunk and furca regions. **D**. Scale and spine pattern of the dorsal trunk region. Scale bars = 15 µm.

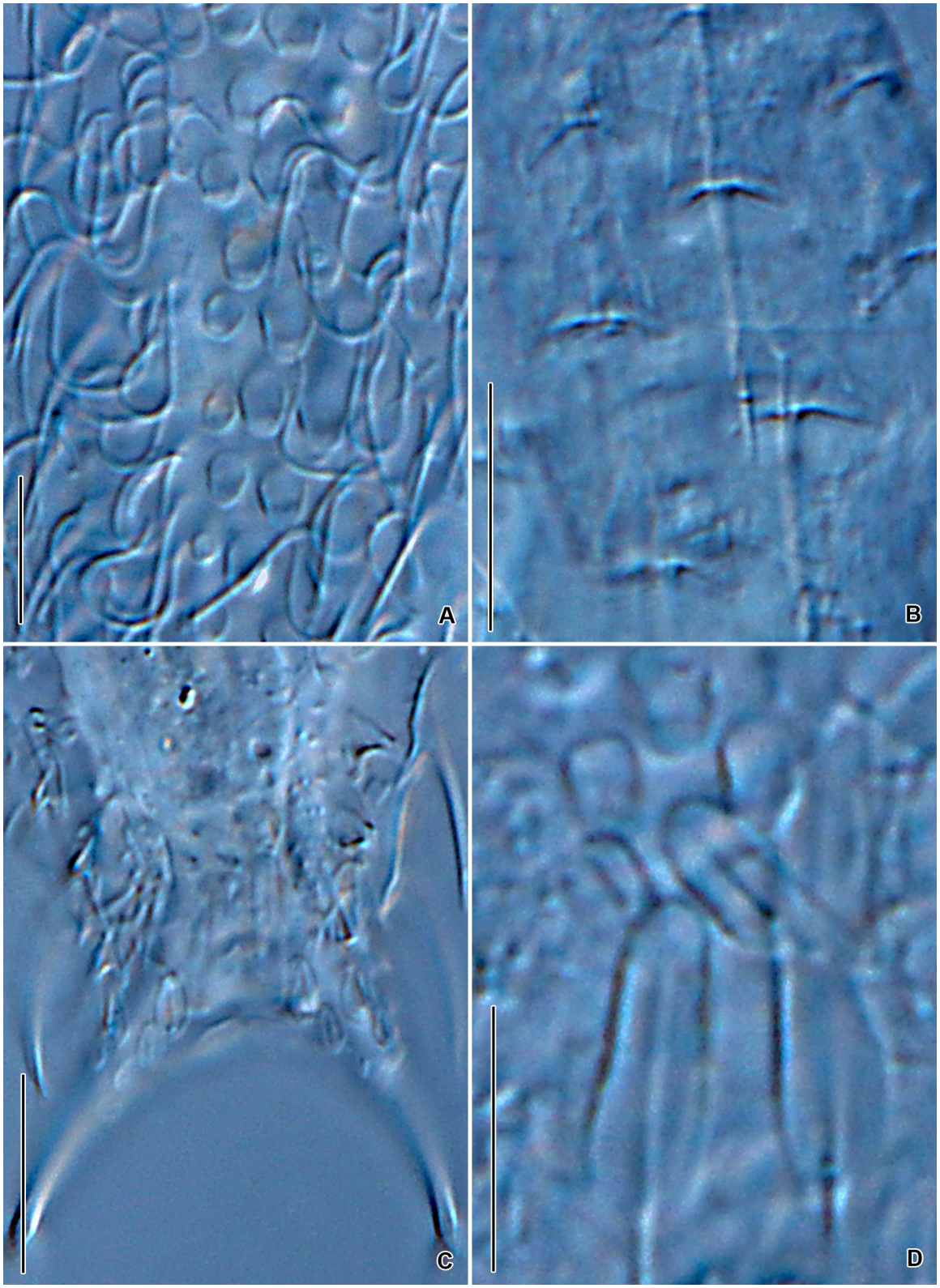

Fig. 36. *Chaetonotus* (*Hystricochaetonotus*) *gulosus* sp. nov., paratype (CU-FNS-28-10-19/PA), differential interference contrast. **A**. Scales of the ventral interciliary field. **B**. Dorsal trunk scales. **C**. Detail of the posterior body region. **D**. Posterior ventral keeled and spined scales. Scale bars: A, D = 5 µm; B–C = 10 µm.

whole length. The intestine runs from U27 to U81 and has a separate, well-differentiated anterior section (U28–U31). A pair of protonephridia runs from ca U32 to U40 (Fig. 35C). Transversal bands connected to the base of dorsal scales are well recognizable. The adhesive gland (ca U85–U91) is placed right behind the terminal part of the intestine, forming a short dichotomy at the subtle furca base (Fig. 35C).

Scales. Almost the entire body is covered by not overlapping three-lobed scales that adhere to the basal cuticle layer along their whole perimeter. Scales are distributed in 14 longitudinal rows, with 13 scales in the central dorsal row. Their size increases in a posterior direction. Central dorsal and dorsolateral longitudinal rows of scales begin at ca U5 (behind the posterior edge of the cephalion), while lateral rows start at the posterior end of the epipleurae (ca U13). Ventral rows start at U10 and exhibit a horizontal zonation pattern. Four main types of scales could be recognized with respect to the shape of the anterior lobe. (i) The head and anterior neck scales (U5–U28) are 3.1–3.5 × 2.0–2.3 µm in size, have a small, broadly rounded anterior lobe and equally long posterior lobes, the transition between the anterior and posterior lobes is marked, α = ~156°, and β = ~123° (Fig. 34A). (ii) The posterior neck scales (U29–42) are 2.7–4.3 × 2.4–3.1 µm in size, exhibit a slightly elongated anterior lobe and an indistinct and continuous transition between the anterior and posterior lobes, α = ~167°, and β = ~98° (Fig. 34B). (iii) The trunk scales (U37–80) are comparatively big (6.2–7.1 × 4.5–5.4 µm), triangular, and display a continuous and indistinct transition between the anterior and posterior lobes, α = 168–172°, and β = 96–102° (Figs 34C, 35D, 36B). Dorsolateral trunk scales are 7.4–8.4 × 4.0–4.4 µm in size and resemble anterior trunk scales (Fig. 34D). (iv) The trunk lateral scales are 5.5–5.9 × 3.7–3.8 µm in size, distinctly three-lobed, all lobes are narrowly rounded to more or less tapered, and the transition between the anterior and posterior lobes is marked (Fig. 34E).

Spines. All spines bear a distinct lateral denticle and gradually narrow towards their distal end (Figs 33A–B, 34A–F). Keels start close to the anterior margin of scales. Spines are not straight but distinctly curved (Fig. 35C–D). They do not differentiate into various types, only their length increases from 3.1 µm to 14.0 µm in a posterior direction (Supp. file 1: Table S8). The lateral denticle is comparatively distant from the spine apex, i.e., the *d*-value ranges from 1.0–3.1 µm, which corresponds to a *d* ratio of 7.5–25%.

Ventral ciliary bands and ventral interciliary field. Ciliary bands start at U10 where they are conspicuously broad. However, they begin to narrow from U25 and terminate at U80. The ciliary bands are accompanied by two ventrolateral rows of three-lobed scales that extend from U12 to U80 (Fig. 33B). They are 1.5–4.3 × 1.1–3.2 µm in size and have a marked transition between the anterior and posterior lobes, α = 149–160°, and β = 62–100° (Fig. 34F). The ventral interciliary field bears four types of horizontally distributed scales: (i) small (2.7–4.3 × 3.1–3.4 µm), oval to oblong, double-edged scales without keels (U10–U73) (Figs 33B, 34H, 36A); (ii) a pair of relatively small (4.4–5.1 × 2.6–2.7 µm), oval, double-edged, and keeled scales (U74); (iii) a single oblong (1.3–2.0 × 1.0–1.5 µm), centrally positioned, double-edged, and keeled scale (U71); and (iv) a pair of big (11.8–12.3 × 3.2–3.4 µm), very narrowly ovate, double-edged, and spined scales (U76) (Figs 34G, 36D). The furca branches (U81–U90) carry minute (1.1–3.2 × 0.5–1.4 µm), oval to oblong, and keeled scales (Figs 34I, 36C).

Chaetonotus* (*Hystricochaetonotus*) *arcanus sp. nov.
urn:lsid:zoobank.org:act:ACDC5C8E-E066-4BA7-B360-E4EC7549790B
Figs 37–38; Supp. file 1: Table S9

Morphological diagnosis

Body stocky and around 100 µm long. Head wider than neck, separated from trunk by a distinct neck constriction. Clearly demarcated cephalion, epipleurae and hypopleurae inconspicuously marked. Trunk widest at ca U37, gradually tapers towards furca base (U82). Mouth almost apical, no cuticular teeth. Hypostomium bears a single small boomerang-like cuticular structure. Pharynx with delicate dilatations.

Intestine straight, with a marked anterior section. Scales spined, three-lobed, not overlapping, distributed in about 12 columns, 14 scales per column. Spines with a short lateral denticle. Scales and spines increase gradually in size in a posterior direction. Dorsal surface covered by scales from posterior end of cephalion (ca U3) to furca branches (ca U73). Furca branches slightly longer than adhesive tubes, lateral margins more or less straight, furcal indentation deeply U-shaped, adhesive tubes well-developed.

Molecular diagnosis

ITS2: 163 G, 172 T. 28S rRNA gene: 562 A, 693 C. Cytochrome *c* oxidase subunit I (codon ordinal numbers are followed by the corresponding span of nucleotide positions in parentheses): 58 (172–174) ATA, 97 (289–291) ACG, 122 (364–366) GTA, 167 (499–501) CGG, 174 (520–522) GCG, 181 (541–543) CTG, 184 (550–552) TTA, 185 (553–555) TCA, 193 (577–579) ATC.

Reference molecules are shown in Supp. file 1: Figs S7, S12A, S19. All diagnostic molecular autapomorphies are marked by arrows. Reference alignments with corresponding nucleotide positions are in Supp. file 1: Alignments 1–4.

The *p*-distance from species described in the present study is 0.00–4.33% in 18S, 5.88–28.88% in ITS2, 0.51–7.12% in 28S, and 8.44–12.59% in COI. There are 1–16 CBCs (except for *Ch.* (*H*). *iratus* sp. nov., *Ch.* (*H*). *luxus* sp. nov., and *Ch.* (*H*). *slavicus* sp. nov., where there are no CBCs) in the 18S rRNA molecule, 1–3 CBCs in the ITS2 molecule (except for *Ch.* (*H*). *gulosus* sp. nov., *Ch.* (*H*). *luxus* sp. nov., and *Ch.* (*H*). *slavicus* sp. nov., where there are no CBCs), and 1–18 CBCs in the first two domains of the 28S rRNA molecule (except for *Ch.* (*H*). *luxus* sp. nov. and *Ch.* (*H*). *slavicus* sp. nov., where there are no CBCs).

Etymology

The Latin adjective '*arcan·us*, *-a*, *-um*' [m, f, n] ('hidden') refers to the morphological similarity of the new species with *C.* (*H.*) *superbus* sp. nov.

Material examined

Holotype

SLOVAKIA • adult (photomicrographs, hologenophore); shallow section of the River Váh, Stankovany, Veľká Fatra Mts; 49°08′26.3″ N, 19°10′14.6″ E; CU-FNS-29-09-20/HO.

Photomicrographs of the holotype are available at the Department of Zoology, Comenius University in Bratislava at https://fns.uniba.sk/en/gastrotricha/. The holotype is shown in Fig. 38.

Type material

A DNA sample of the holotype specimen STV 67 has been deposited in the Natural History Museum, Vajanského nábrežie 2, 810 06 Bratislava, Slovakia (ID Collection Code 01427571).

Type locality

Shallow section of the River Váh near the village of Stankovany, Veľká Fatra Mts, Slovakia 49°08′26.3″ N, 19°10′14.6″ E.

Gene sequences

The nuclear 18S and ITS1-5.8S-ITS2-28S rDNA sequences as well as the mitochondrial COI sequence of the holotype specimen STV 67 have been deposited in GenBank under the following accession numbers: OM421723, OM421699, and OM424078, respectively.

Description

Habitus. *Chaetonotus* (*Hystricochaetonotus*) *arcanus* sp. nov. is about 100 µm long and has a stocky, tenpin-shaped body, with a clearly defined head region, a narrowing neck, and a rather bulbous trunk

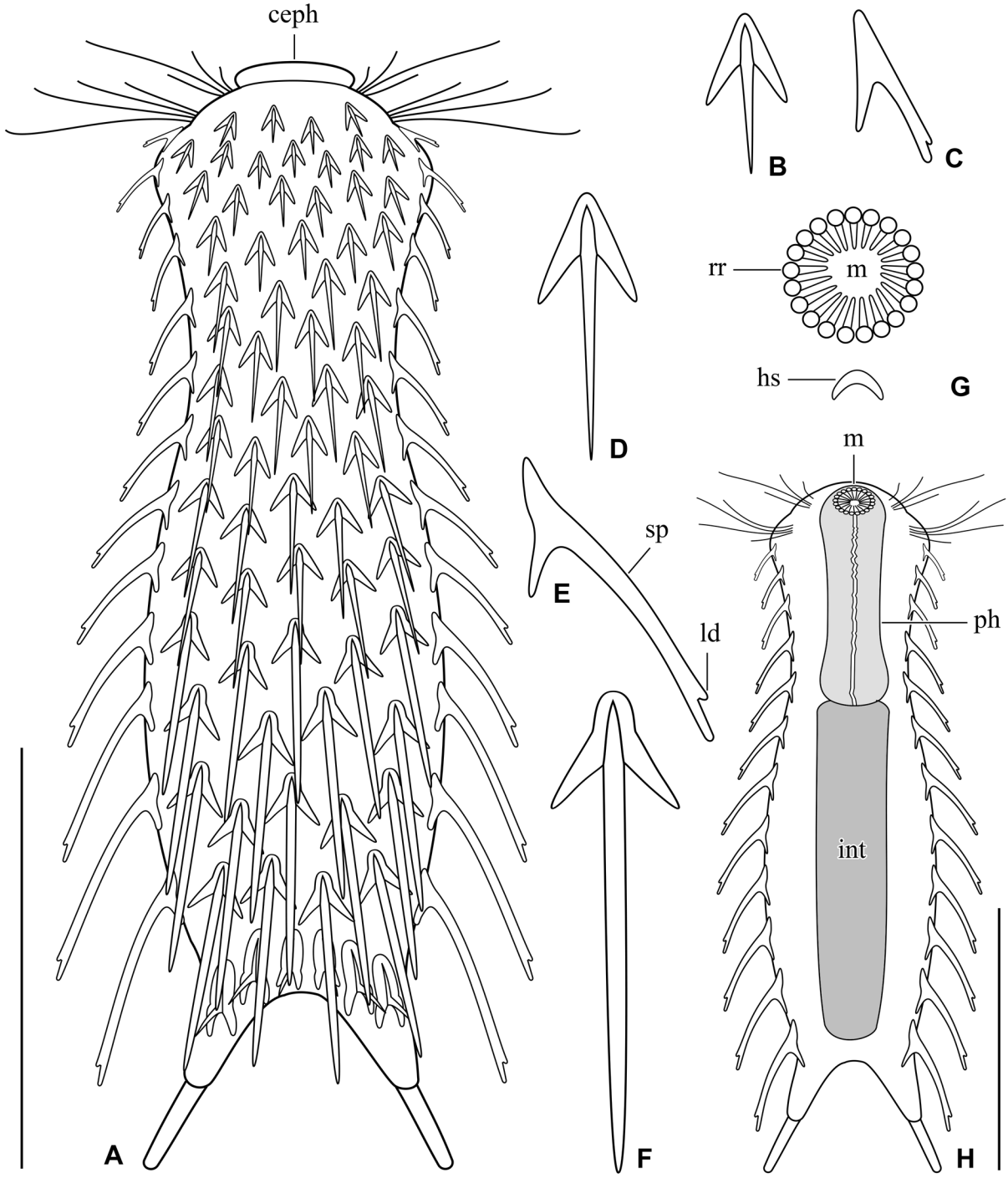

Fig. 37. *Chaetonotus* (*Hystricochaetonotus*) *arcanus* sp. nov. **A**. Dorsal overview showing the scale and spine pattern. **B**–**C**. Dorsal and lateral views of a head scale. **D**. Dorsal view of a neck scale. **E**–**F**. Lateral and dorsal views of a trunk scale. **G**. Detail showing the mouth region. **H**. Internal morphology. Scale bars = 30 µm.

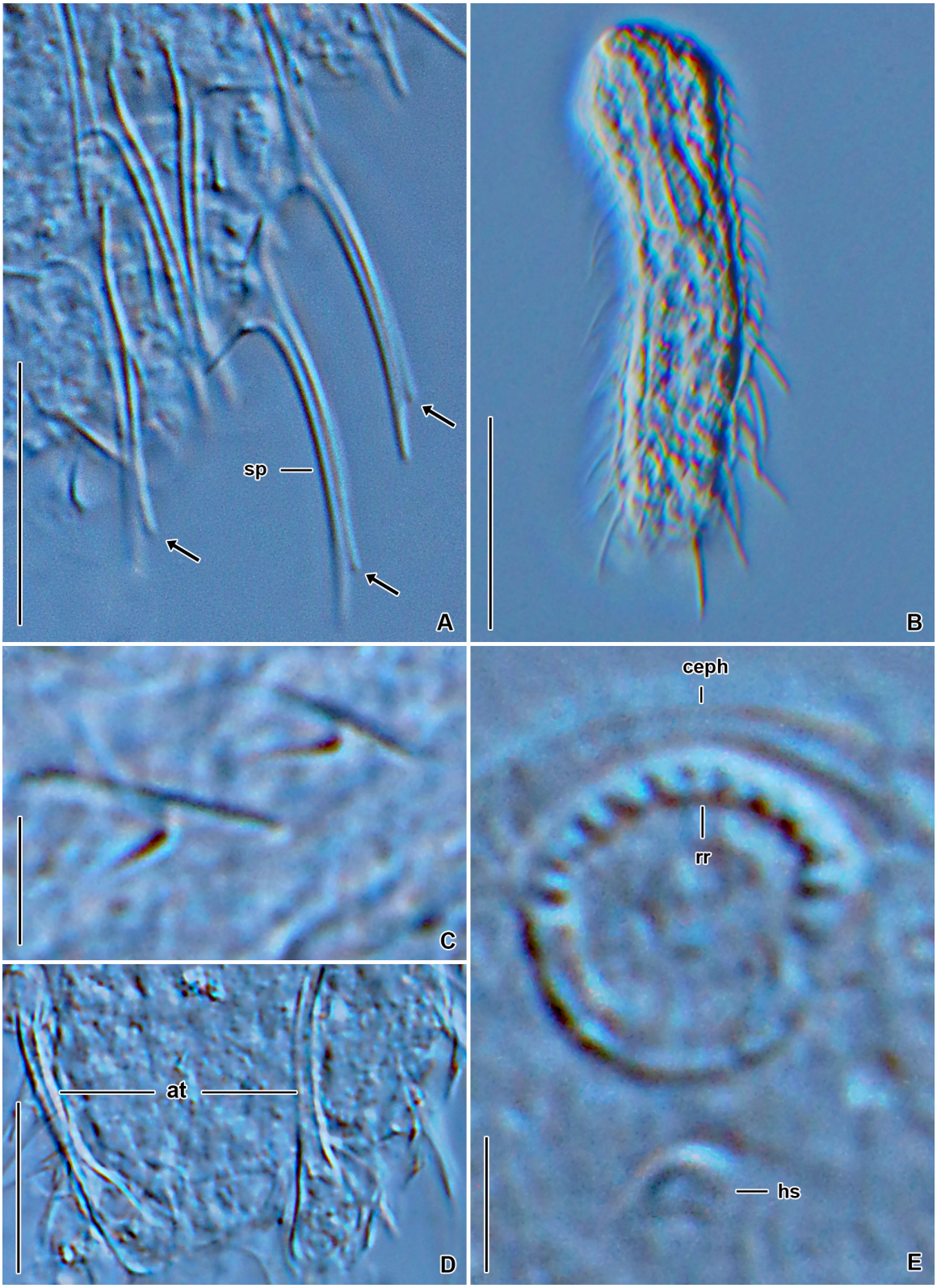

Fig. 38. *Chaetonotus* (*Hystricochaetonotus*) *arcanus* sp. nov., holotype (CU-FNS-29-09-20/HO), differential interference contrast. **A**. Dorsal trunk scales and spines. Arrows mark lateral denticles. **B**. Body overview. **C**. Head scales. **D**. Adhesive tubes curved underneath trunk. **E**. Mouth and boomerang-like hypostomial plate. Scale bars: A, D = 10 µm; B = 30 µm; C, E = 2 µm.

(Figs 37A, H, 38B). Body width is ca 19.8 µm at U10, ca 15.6 µm at U50, and ca 17.8 µm at U60. The head is relatively wide (19.8 µm at U10), with a plate-like, rounded cephalion. The neck (ca U17–U27) is rather inconspicuously marked and smoothly continues to the trunk. The trunk gradually dilatates from about U35 to U61, where it reaches the maximum width that is only slightly narrower than the maximum width of the head. Then, the trunk gradually narrows towards U82, where curved margins of the furca branches begin to emerge. Dorsal sensory bristles were not observed. The furcal indentation is deeply U-shaped. The furca branches are set apart and diverge posteriorly. Well-developed adhesive tubes are approximately 9.4 µm long and straight (Figs 37A, H, 38D).

Head. The cephalion (U1) is rounded, clearly demarcated in the body outline (Fig. 37A). The epipleurae (U3–U6) and hypopleurae (U6–U10) are only inconspicuously marked. Pairs of cephalic ciliary tufts emerge laterally at U3 and U5. The mouth ring is oval, ca 5.2 µm in the largest diameter, and located subterminally at U2–U5. There are strong but short, rod-like reinforcements lining the walls of the mouth ring and inner delicate structures directed towards the center of the mouth ring. Inner cuticular teeth are not present. The hypostomium (ca U5–U9) carries a small cuticular boomerang-like structure. The lateral sides of the hypostomium are lined by a relatively wide pair of basal body patches (from U3 to U8) (Figs 37G, 38E).

Internal morphology. The pharynx extends from ca U5 to U34, is 28–29 µm long and 4.6–7.2 µm wide, sinuous, with inconspicuously marked anterior and posterior dilatations (Figs 37H, 38B). The cerebral ganglion appears as a mass surrounding the pharynx along its whole length. The intestine runs from U35 to U82. The adhesive gland (ca U82–U91) is placed right behind the terminal part of the intestine, forming a short dichotomy at the subtle furca base.

Scales. Almost the entire body is covered by not overlapping three-lobed scales (U3–U73) that adhere to the basal cuticle layer along their whole perimeter. Scales are distributed in about 12 longitudinal rows, with 14 scales in the central row. Their size increases gradually from 3.0–4.5 × 1.9–2.2 µm to 4.9–5.6 × 4.1–4.3 µm in a posterior direction (Supp. file 1: Table S9). Central dorsal and dorsolateral longitudinal rows of scales begin at ca U3, while lateral rows start at ca U13. Two main types of scales could be recognized concerning the shape of the anterior lobe. (i) The head, neck, and upper-trunk scales (U3–U37) have a narrowly rounded anterior lobe and elongated posterior lobes, α = 156–163°, and β = 54–85°. The transition between the anterior and posterior lobes is indistinct and continuous, providing the scales with an A-shaped appearance (Figs 37B, D, 38C). (ii) The posterior trunk scales (U50–73) exhibit a broadly rounded anterior lobe and elongated posterior lobes, α = 153–167°, and β = 75–96°. The transition between the anterior and posterior lobes is marked unlike in the first scale type (Fig. 37F).

Spines. All spines bear a distinct lateral denticle and gradually narrow towards their distal end. Keels start comparatively close to the anterior margin of scales. Spines are not straight but slightly curved. They do not differentiate into various types, only their length increases in a posterior direction (Figs 37A, C, E, H, 38A–B, Supp. file 1: Table S9). More specifically, the length increase is rather inconspicuous and gradual from the head (3.1 µm) to the posterior neck region (5.8 µm). The most pronounced length change occurs at the beginning of the trunk (ca U50), where dorsal spines increase significantly from 5.8 µm to 15.2 µm (Figs 37A, H, 38B). The lateral denticle is comparatively distant from the spine apex, i.e., *d*-value ranges from 1.2–3.0 µm, which corresponds to a *d* ratio of 16.7–23.3%.

Ventral ciliary bands and ventral interciliary field. Unfortunately, the ventral side was not observed in detail.

Chaetonotus* (*Hystricochaetonotus*) *slavicus sp. nov.
urn:lsid:zoobank.org:act:9826403E-1298-4889-8E0B-3A19A9EFB3AE
Fig. 9

Molecular diagnosis

18S rRNA gene: 1548 A. ITS2: 52 G, 107 C, 115 A, 156 C, 171 A. Cytochrome *c* oxidase subunit I (codon ordinal numbers are followed by the corresponding span of nucleotide positions in parentheses): 9 (25–27) TTC, 65 (193–195) TTC, 96 (286–288) CTG, 100 (298–300) CTG, 143 (427–429) TCC, 161 (481–483) GCC.

Reference molecules are shown in Supp. file 1: Figs S8, S12B, S20. All diagnostic molecular autapomorphies are marked by arrows. Reference alignments with corresponding nucleotide positions are in Supp. file 1: Alignments 1–4.

The *p*-distance from species described in the present study is 0.05–4.38% in 18S, 5.88–31.02% in ITS2, 0.52–9.78% in 28S, and 7.85–13.59% in COI. There are 1–16 CBCs (except for *Ch.* (*H*). *arcanus* sp. nov., *Ch.* (*H*). *iratus* sp. nov., and *Ch.* (*H*). *luxus* sp. nov., where there are no CBCs) in the 18S rRNA molecule, 1–3 CBCs in the ITS2 molecule (except for *Ch.* (*H*). *arcanus* sp. nov., *Ch.* (*H*). *gulosus* sp. nov., and *Ch.* (*H*). *luxus* sp. nov., where there are no CBCs), and 2–18 CBCs in the first two domains of the 28S rRNA gene (except for *Ch.* (*H*). *arcanus* sp. nov., *Ch.* (*H*). *iratus* sp. nov., and *Ch.* (*H*). *luxus* sp. nov., where there are no CBCs).

Etymology

The Latin adjective '*slavic·us*, *-a*, *-um*' [m, f, n] ('Slavic') refers to the type locality (Devín castle) of the new species, which is an important place in Slovak history.

Material examined

Holotype

SLOVAKIA • adult (the specimen was destroyed during DNA extraction); temporary pond in the floodplain area of the River Morava, Devín, Bratislava, Podunajská rovina plain; 48°10′29.4″ N, 16°58′35.8″ E.

Paratypes

SLOVAKIA • 3 adults (the specimens were destroyed during DNA extraction); same collection data as for holotype.

Photomicrographs of the holotype are available at the Department of Zoology, Comenius University in Bratislava at https://fns.uniba.sk/en/gastrotricha/.

Type material

A DNA sample of the holotype specimen DB 40 has been deposited in the Natural History Museum, Vajanského nábrežie 2, 810 06 Bratislava, Slovakia (ID Collection Code 01427570).

Type locality

Ephemeral pond in the floodplain area of the River Morava near the foothill of the Devín castle, Bratislava, Podunajská rovina plain, Slovakia, 48°10′29.4″N 16°58′35.8″E.

Gene sequences

The nuclear 18S and ITS1-5.8S-ITS2-28S rDNA sequences as well as the mitochondrial COI sequence of the holotype specimen DB 40 have been deposited in GenBank under the following accession numbers: OM421724, OM421700, and OM424079, respectively.

Remarks

Unfortunately, all our attempts for thorough morphological investigations of this species failed. Without a name, *Ch.* (*H.*) *slavicus* sp. nov. would be nothing but a label and nucleotide sequences in the GenBank database. However, this entity can be clearly separated from other species by the combination of 18S, ITS region, 28S, and COI sequences. Moreover, it represents a distinct lineage in multi-gene phylogenies (Fig. 9). As ICZN (1999) allows that any part of an animal is eligible to be a name-bearing type (Article 72.5.1), we interpret the isolated DNA as a part of an animal and use it as type material. This strategy is also used in protists whose names are governed by the Zoological Code (e.g., Lynn *et al.* 2018; Pecina & Vďačný 2022). It is important to mention that the principle of priority applies even if any part of an animal is named before the whole animal (Article 23.3.2.1).

Key to species of the subgenus Hystricochaetonotus Schwank, 1990

The following key contains all species originally assigned to the subgenus *Hystricochaetonotus* by Schwank (1990) and, later on, by Balsamo (1990), Balsamo & Todaro (1995), Kisielewski (1997a), Kolicka (2016, 2019a), Kolicka *et al.* (2018), and Todaro (2022). The key uses body shape and size as well as the scale and spine patterns as the main species discriminators following Schwank (1990). The subgeneric assignment of species without associated molecular information needs to be tested (i.e., confirmed or rejected) with phylogenetic analyses in the future. Identification of species within the subgenus *Hystricochaetonotus* will be most reliable for specimens from which COI and/or ITS2 barcode data are available for comparison of nucleotide sequences with those from type specimens. To avoid any doubts in species identifications, the original descriptions and authoritative redescriptions need to be considered.

1. Dorsal trunk spines gradually or abruptly elongated in a posterior direction 2
– A rather small group of very abruptly elongated dorsal trunk spines 31

2. Main dorsal trunk scales rounded and posteriorly incised 3
– Main dorsal trunk scales three-lobed or triangular 4

3. Eight elongated dorsal spines arranged in an arch-like pattern; two elongated lateral spines emerging distinctly above furca base and projecting far behind adhesive tubes; head scales spineless, remaining spines gradually elongated and without lateral denticle ..... ***Ch.* (*H.*) *heterochaetus*** Daday, 1905
– Four elongated dorsal spines form a comparatively small group; two elongated lateral spines emerging at furca base and not projecting behind adhesive tubes; all other spines short and with lateral denticle ..... ***Ch.* (*H.*) *spinifer*** Stokes, 1887

4. Dorsal body side covered with evenly and rather densely arranged scales 5
– Scales absent or reduced in posterior trunk region 29

5. Dorsal spines gradually elongate posteriorly 6
– A distinct group of abruptly elongated and thick dorsal spines 20

6. Elongated dorsal spines with lateral denticle 7
– Elongated dorsal spines without lateral denticle 16

7. Lateral denticle emerges near distal end of spine 8
– Lateral denticle emerges in mid-portion of spine ..... ***Ch.* (*H.*) *polychaetus*** Daday, 1905

8. Posterior lateral spines not elongated 9
– Posterior lateral spines elongated and/or thickened 11

9. Scale base of elongated dorsal spines three-lobed 10
– Scale base of elongated dorsal spines triangular ..... ***Ch.* (*H.*) *gulosus*** sp. nov.

10. Body larger (ca 160 μm); furca branches run almost in parallel; 10–11 longitudinal rows of scales; 19–21 scales per dorsal central row ..... ***Ch.* (*H.*) *murrayi*** Remane, 1929
– Body smaller (95–124 μm); furca branches distinctly diverge posteriorly; 7 longitudinal rows of scales; 15 scales per dorsal central row ..... ***Ch.* (*H.*) *machikanensis*** Suzuki & Furuya, 2011

11. Posterior elongated lateral spines extend to at least mid-portion of adhesive tubes 12
– Posterior elongated lateral spines extend only to posterior end of furca branches ..... ***Ch.* (*H.*) *hornsundi*** Kolicka *et al.*, 2018

12. Posterior elongated lateral spines do not extend behind adhesive tubes 13
– Posterior elongated lateral spines extend far behind posterior end of adhesive tubes 15

13. Interciliary field scales with keels 14
– Interciliary field scales without keels ..... ***Ch.* (*H.*) *persimilis*** Kolicka *et al.*, 2018

14. Furca branches double-keeled scales oval and posteriorly distinctly truncated; ventral central furca base scales oblong with anterior end curved outwards ..... ***Ch.* (*H.*) *borealis*** Kolicka *et al.*, 2018
– Furca branches double-keeled scales circular; ventral central furca base scales oblong ..... ***Ch.* (*H.*) *hystrix*** Mečnikow, 1865

15. Two pairs of strongly elongated posterior lateral spines extending behind rear end of adhesive tubes ..... ***Ch.* (*H.*) *paraguayensis*** Schwank, 1990
– One pair of strongly elongated posterior lateral spines extending behind rear end of adhesive tubes ..... ***Ch.* (*H.*) *furcatus*** Kisielewski, 1991

16. Body shape slender, elongated 17
– Body tenpin-shaped, stocky 19

17. Cephalic pleurae clearly demarcated 18
– Cephalic pleurae only indistinctly marked ..... ***Ch.* (*H.*) *optabilis*** sp. nov.

18. About 30–32 scales per dorsal central row; 3 teeth in mouth ring; hypostomium in a form of pentagonal plate with two protuberances ..... ***Ch.* (*H.*) *avarus*** sp. nov.
– About 22 scales per dorsal central row; 1 tooth in mouth ring; hypostomium in a form of two horizontal lamellae accompanied by tear-shaped protuberances ..... ***Ch.* (*H.*) *iratus*** sp. nov.

19. About 13 longitudinal rows of scales; 13 scales per dorsal central row ..... ***Ch.* (*H.*) *italicus*** Balsamo & Todaro, 1995
– About 29–31 longitudinal rows of scales; 21–25 scales per dorsal central row ..... ***Ch.* (*Ch.*) *bombardus*** Kolicka *et al.*, 2018

20. Elongated dorsal spines not clubbed-like thickened 21
– Some elongated dorsal spines clubbed-like thickened ..... ***Ch.* (*H.*) *lucksi*** Voigt, 1958

21. Head and neck spines short 22
– Head and neck spines comparatively long but distinctly thinner than elongated dorsal spines 28

22. Posterior lateral spines elongated and thickened 23
– Posterior lateral spines not elongated 26

23. Two pairs of elongated posterior lateral spines 24
– One pair of elongated posterior lateral spines ..... ***Ch.* (*H.*) *mirabilis*** sp. nov.

24. Lateral denticle of elongated dorsal spines without membrane, elongated posterior lateral spines do not reach posterior end of adhesive tubes 25
– Lateral denticle of elongated dorsal spines with membrane, elongated posterior lateral spines reach posterior end of adhesive tubes ..... ***Ch.* (*H.*) *horridus*** Kolicka, 2019

25. Dorsal side of furca branches naked ..... ***Ch.* (*H.*) *persetosus*** Zelinka, 1889
– Dorsal side of furca branches carries three pairs of oblong keeled scales and one pair of rounded double-keeled scales ..... ***Ch.* (*H.*) *inaequabilis*** Kolicka, 2019

26. Lateral denticle distinct and comparatively distant from spine apex (*d*-ratio > 15%) 27
– Lateral denticle indistinct and very close to spine apex (*d*-ratio < 10%) ..... ***Ch.* (*H.*) *luxus*** sp. nov.

27. Body stocky ..... ***Ch.* (*H.*) *arcanus*** sp. nov.
– Body more or less tenpin-shaped ..... ***Ch.* (*H.*) *superbus*** sp. nov.

28. Body small (90–120 μm); 25–27 elongated dorsal spines, ca 15–25 μm long, not projecting behind adhesive tubes; 2 pairs of posterior lateral elongated spines ..... ***Ch.* (*H.*) *macrochaetus*** Zelinka, 1889
– Body larger (140–190 μm); 16–18 elongated dorsal spines, ca 60–70 μm long, projecting far behind adhesive tubes; 5–6 pairs of posterior lateral elongated spines ... ***Ch.* (*H.*) *euhystrix*** Schwank, 1990

29. Base of scales present; at most 7–9 dorsal scale rows on head; 13 elongated dorsal spines; one pair of posterior lateral elongated spines ..... ***Ch.* (*H.*) *fujisanensis*** Sudzuki, 1971
– Base of scales reduced or absent 30

30. Dorsal group comprises ca 20 elongated spines; one pair of posterior lateral elongated spines ..... ***Ch.* (*H.*) *acanthophorus*** Stokes, 1888
– Dorsal group comprises ca 13 elongated spines; two pairs of posterior lateral elongated spines ..... ***Ch.* (*H.*) *enormis*** Stokes, 1887

31. Elongated dorsal spines without lateral denticle; scales absent or not described 32
– Elongated dorsal spines with lateral denticle; scales three-lobed, keeled, and with short spine 34

32. Elongated dorsal spines emerge from reduced and rounded scales; distinctly more than 3 elongated dorsal spines 33
– Elongated dorsal spines emerge from well-developed and three-lobed scales; 3 elongated dorsal spines ..... ***Ch.* (*H.*) *trispinosus*** Balsamo, 1990

33. Ten elongated dorsal spines, up to 40 μm long, arranged in two interrupted longitudinal rows, last spine pair projects far behind adhesive tubes ..... ***Ch.* (*H.*) *decemsetosus*** Marcolongo, 1910
– Six elongated dorsal spines, up to 23 μm long, arranged in two horizontal rows, last spine pair does not reach furca base ..... ***Ch.* (*H.*) *vargai*** Rudescu, 1967

34. Scale base of elongated dorsal spines ± hemispherical 35
– Scale base of elongated dorsal spines ± three-lobed, triangular, plow-like, or reduced (highly variable in shape) 38

35. Only posterior dorsal body half bears some scales, eight elongated dorsal spines ..... ***Ch.* (*H.*) *octonarius*** Stokes, 1887
– Whole dorsal body side covered with scales 36

36. Eight elongated dorsal spines; last pair of elongated dorsal spines does not reach adhesive tubes; lateral denticle comparatively short and emerging near distal end of spine 37
– Less than 8 elongated dorsal spines; last pair of elongated dorsal spines reaches adhesive tubes; lateral denticle rather long and emerging distinctly ahead of distal end of spine ..... ***Ch.* (*H.*) *paucisetosus*** Marcolongo, 1910

37. Five elongated dorsal spines ..... ***Ch.* (*H.*) *pungens*** Balsamo, 1990
– Seven elongated dorsal spines ..... ***Ch.* (*H.*) *schlitzensis*** Schwank, 1990

38. Dorsal and lateral scales well-developed 39
– Scales reduced except for dorsal scales carrying elongated spines 43

39. Body larger (180–190 μm); elongated dorsal spines curved, long and reaching at least furcal indentation; head spined 40
– Body smaller (80–120 μm); elongated dorsal spines straight, comparatively short (15–25 μm) and not reaching furca base; head spineless 42

40. Scale base of elongated dorsal spines reduced; posteriormost elongated spines almost reach rear end of adhesive tubes; first two anterior horizontal rows of head spines distinctly elongated and thicker 41
– Scale base of elongated dorsal spines well-developed; posteriormost elongated spines reach furcal indentation; head spines of same width ..... ***Ch.* (*H.*) *anomalus*** Brunson, 1950

41. One lateral denticle on each of nine elongated dorsal spines ..... ***Ch.* (*H.*) *novenarius*** Greuter, 1917
– Two subsequent lateral denticles on each of nine elongated dorsal spines ..... ***Ch.* (*H.*) *balsamoae*** Kisielewski, 1997

42. Seven to nine elongated dorsal spines ..... ***Ch.* (*H.*) *aemilianus*** Balsamo, 1978
– Five elongated dorsal spines ..... ***Ch.* (*H.*) *ferrarius*** Schwank, 1990

43. Elongated dorsal spines long and curved, often extend behind adhesive tubes 44
– Elongated dorsal spines comparatively short and straight, do not reach furca base 46

44. Body slender and bigger (150 μm) ..... ***Ch.* (*H.*) *trilineatus*** Valkanov, 1937
– Body stocky and smaller (70–120 μm) 45

45. Eight elongated dorsal spines arranged in 3–4 horizontal rows and projecting behind adhesive tubes ..... ***Ch.* (*H.*) *trichodrymodes*** Brunson, 1950
– Seven or eight elongated dorsal spines arranged in 2 horizontal rows and not projecting behind adhesive tubes ..... ***Ch.* (*H.*) *longispinosus*** Stokes, 1887

46. Five to seven elongated dorsal spines, lateral body spines present ..... ***Ch.* (*H.*) *spinulosus*** Stokes, 1887
– Five elongated dorsal spines, lateral body spines absent ..... ***Ch.* (*H.*) *quintospinosus*** Greuter, 1917

Discussion

Differential diagnoses of new species

The new species could be well separated from each other by (i) body shape, (ii) the organization of the cephalic pleurae and hypostomium, (iii) the presence/absence of cuticular teeth and pharyngeal dilatations, (iv) the number of longitudinal rows of scales, scales in a central dorsal row and scale types as well as by (v) the spine morphology. Their differential diagnoses are summarized in Table 5.

Following Kolicka (2016, 2019a) and Kolicka *et al.* (2018) and to avoid any doubts in comparisons, only the original descriptions, authoritative redescriptions and most detailed studies were considered (Balsamo 1983; Schwank 1990; Kisielewski 1991; Suzuki & Furuya 2011). Within congeners, *Ch.* (*H.*) *mirabilis* sp. nov. most resembles the following species: *Ch.* (*H.*) *acanthophorus* Stokes, 1888, *Ch.* (*H.*) *balsamoae* Kisielewski, 1997, *Ch.* (*H.*) *euhystrix* Schwank, 1990, *Ch.* (*H.*) *horridus* Kolicka, 2019 and *C.* (*H.*) *novenarius* Greuter, 1917. These species share very conspicuous and long spines on the dorsal body side. The most important features enabling their unambiguous identification are provided in Table 6.

Chaetonotus (*H.*) *arcanus* sp. nov., *Ch.* (*H.*) *luxus* sp. nov. and *Ch.* (*H.*) *superbus* sp. nov. are morphologically most similar to the following species: *Ch.* (*H.*) *borealis* Kolicka *et al.*, 2018, *Ch.* (*H.*) *furcatus* Kisielewski, 1991, *Ch.* (*H.*) *hornsundi* Kolicka *et al.*, 2018, *Ch.* (*H.*) *hystrix* Mečnikow, 1865, *Ch.* (*H.*) *macrochaetus* Zelinka, 1889, *Ch.* (*H.*) *machikanensis* Suzuki & Furuya, 2011, *Ch.* (*H.*) *persetosus* Zelinka, 1889 and *Ch.* (*H.*) *persimilis* Kolicka *et al.*, 2018. Dorsal spines of these species are also elongated in the trunk region, but they are not so striking as in the *Ch.* (*H.*) *euhystrix* group mentioned above. All these species, however, exhibit a lateral denticle on the dorsal spines, as typical of the subgenus *Hystricochaetonotus* (Schwank 1990; Kisielewski 1997a). Differential diagnoses of *Ch.* (*H.*) *arcanus* sp. nov., *Ch.* (*H.*) *luxus* sp. nov., *Ch.* (*H.*) *superbus* sp. nov. and their most similar congeners are collated in Table 7.

Chaetonotus (*H.*) *gulosus* sp. nov. is outstanding among members of the subgenus *Hystricochaetonotus* in having comparatively big, triangular trunk scales. In this aspect, it most resembles *Ch.* (*H.*) *aemilianus* Balsamo, 1978. However, *Ch.* (*H.*) *gulosus* sp. nov. can be differentiated from it by (i) the body size (107 μm vs 80–100 μm), (ii) the arrangement of triangular scales (close to each other but not overlapping and forming about 7 horizontal rows vs loosely spaced and restricted to the central dorsal trunk region forming 3–4 horizontal rows), (iii) the length of spines emerging from the triangular scales (up to 14 μm vs 18–26 μm), and (iv) the minimum length of lateral spines (3.1 μm vs 1.8 μm).

Although *Ch.* (*H.*) *avarus* sp. nov., *Ch.* (*H.*) *optabilis* sp. nov. and *Ch.* (*H.*) *iratus* sp. nov. do not display a lateral denticle on spines, they fall within the maximally supported *Hystricochaetonotus* clade (Figs 8–9) similarly as does *Ch.* (*Ch.*) *bombardus* (Kolicka *et al.* 2018). This indicates that the presence/absence of a lateral denticle is a homoplastic feature. Indeed, a lateral denticle is present on the spines of *Lepidochaetus* Kisielewski, 1991 (Križanova & Vďačný 2021 and references cited therein) and some members of the subgenus *Chaetonotus* (for a review, see Schwank 1990). However, as other members of the subgenus *Hystricochaetonotus*, these four species also display distinctly three-lobed scales and well-developed, gradually elongating spines towards the trunk rear.

Chaetonotus (*H.*) *avarus* sp. nov. matches well *Ch.* (*Ch.*) *bombardus* in having a five-lobed head with clearly demarcated pleurae and a pharynx without anterior and posterior dilatations. However, both species could be distinguished by (i) the body shape (slender vs stocky), (ii) the number of scale rows (12 vs 29–31), (iii) the number of scales per central dorsal row (30–32 vs 21–25), (iv) the morphology of posterior lobes of dorsal scales (comparatively broadly rounded vs narrow and tapering), (v) the presence vs absence of cuticular teeth in the mouth, (vi) the morphology of the hypostomium (a pentagonal plate with two protuberances vs ship-shaped with a deep, semicircular anterior notch), (vii) the anterior

Table 5 (continued on next page). Comparison of new species of the subgenus *Hystricochaetonotus* Schwank, 1990. Abbreviation: n.a. = data not available.

Character	*Ch.* (*H.*) *arcanus* sp. nov.	*Ch.* (*H.*) *avarus* sp. nov.	*Ch.* (*H.*) *gulosus* sp. nov.	*Ch.* (*H.*) *iratus* sp. nov.	*Ch.* (*H.*) *luxus* sp. nov.	*Ch.* (*H.*) *mirabilis* sp. nov.	*Ch.* (*H.*) *optabilis* sp. nov.	*Ch.* (*H.*) *superbus* sp. nov.
Body length	100 µm	130 µm	107 µm	124 µm	87–112 µm	83–107 µm	108–143 µm	107 µm
Body shape	Stocky with a deeply U-shaped furcal indentation	Slender, elongated with a deeply V-shaped furcal indentation	Stocky with a shallowly U-shaped furcal indentation	Slender, elongated with a deeply V-shaped furcal indentation	More or less tenpin-shaped with a U-shaped furcal indentation	Tenpin-shaped with a broadly U-shaped furcal indentation	Slender, elongated with a deeply V-shaped furcal indentation	More or less tenpin-shaped with a deeply U-shaped furcal indentation
Cephalic pleurae	Only indistinctly marked	Clearly demarcated	Epipleurae clearly demarcated, hypopleurae only indistinctly marked	Clearly demarcated	Clearly demarcated	Only indistinctly marked	Only indistinctly marked	Clearly demarcated
Hypostomium	Boomerang-like plate	Pentagonal plate with two protuberances	Two horizontal lamellae	Two horizontal lamellae accompanied by tear-shaped protuberances	Absent	n.a.	Rectangular plate with small central protuberance and two lamellae	n.a.
Mouth cuticular teeth	Absent	3	Absent	1	Absent	2	Absent	Absent
Pharynx	Without dilatations	Without dilatations	Without dilatations	Without dilatations	Without dilatations	With anterior and posterior dilatations	With anterior and posterior dilatations	Without dilatations
No. of scale rows	12	14	14	12	10	10–12	16–18	10–12
No. of scales per dorsal central row	14	30–32	12	22	15	17	40–45	15
Dorsal spines	Abruptly elongated in posterior trunk region	Gradually elongated	Gradually elongated	Gradually elongated	Abruptly elongated in posterior trunk region	Abruptly elongated in posterior trunk region	Gradually elongated	Abruptly elongated in trunk region

Table 5 (continued). Comparison of new species of the subgenus *Hystricochaetonotus* Schwank, 1990. Abbreviation: n.a. = data not available.

Character	*Ch.* (*H.*) *arcanus* sp. nov.	*Ch.* (*H.*) *avarus* sp. nov.	*Ch.* (*H.*) *gulosus* sp. nov.	*Ch.* (*H.*) *iratus* sp. nov.	*Ch.* (*H.*) *luxus* sp. nov.	*Ch.* (*H.*) *mirabilis* sp. nov.	*Ch.* (*H.*) *optabilis* sp. nov.	*Ch.* (*H.*) *superbus* sp. nov.
Elongated posteriormost trunk lateral spines	Absent	Absent	Absent	Absent	Absent	Present	Absent	Absent
Lateral denticle	Present	Absent	Present	Absent	Present	Present	Absent	Present
Lateral denticle membrane	Absent	Absent	Absent	Absent	Absent	Present	Absent	Absent
Ventral ciliary bands merged anteriorly	No	Yes	No	No	No	No	No	No

Table 6. Comparison of *Chaetonotus* (*Hystricochaetonotus*) *mirabilis* sp. nov. with most similar congeners. Abbreviation: n.a. = data not available.

Character	*Ch.* (*H.*) *mirabilis* sp. nov.	*Ch.* (*H.*) *acanthophorus* Stokes, 1888	*Ch.* (*H.*) *balsamoae* Kisielewski, 1997	*Ch.* (*H.*) *euhystrix* Schwank, 1990	*Ch.* (*H.*) *horridus* Kolicka, 2019	*Ch.* (*H.*) *novenarius* Greuter, 1917
Body length	83–107 µm	80–110 µm	106–138 µm	150–160 µm	107–134 µm	111–193 µm
Body shape	Tenpin-shaped	Stocky	Tenpin-shaped	Stocky	Stocky, slightly botle-shaped	Narrowly tenpin-shaped
Cephalic pleurae	Indistinctly marked	Indistinctly marked	Clearly demarcated	Indistinctly marked	Clearly demarcated	Indistinctly marked
Mouth cuticular teeth	Present (2)	Absent	Absent	Absent	Absent	Absent
Pharyngeal dilatations	Present	Absent	Absent	Absent	Present	Absent
Furcal indentation	Broadly U-shaped	Deeply V-shaped	Narrowly U-shaped	Deeply V-shaped	Broadly V-shaped	U-shaped
Size of dorsal scales	Head: 3.25–4.13 × 1.90–3.85 µm Neck: 3.20–5.06 × 1.98–2.70 µm Trunk: 7.48–8.44 × 4.58–5.17 µm	n.a.	3.6–6.0 µm	Head: 4–5 µm Trunk: 7–12 µm	Head: 2.17–5.30 × 2.05–6.20 µm Neck: 2.77–6.37 × 2.35–5.91 µm Trunk: 3.03–13.43 × 2.12–13.37 µm	n.a.
Increase in length of dorsal spines	Abrupt	Abrupt	Abrupt	Gradual	Abrupt	Abrupt
Length of dorsal spines	Head: 2.7–3.7 µm Neck: 4.5–7.1 µm Trunk: 17–36 µm	Head and neck: 4–7 µm Trunk: 16–24 µm	Head: 9–11 µm Neck: 9–19 µm Trunk: 60–70 µm	Head and neck: 5–7 µm Trunk: 50–70 µm	Head: 0.44–13.78 µm Neck: 2.45–16.49 µm Trunk: 4.97–34.14 µm	Head: 10 µm Neck: 2.5–12.0 µm Trunk: 58–85 µm
Lateral denticle membrane	Present	Present	Absent	Present	Present	Absent
Number of lateral denticles per spine	1	1	2	1	1	1
Elongated posteriormost lateral trunk spines	Thick	Narrow	Narrow	Absent	Thick	Narrow
References	Present study	Schwank (1990)	Balsamo (1983)	Schwank (1990)	Kolicka (2019a)	Greuter (1917), Schwank (1990)

Table 7 (continued on next page). Comparison of *Chaetonotus* (*Hystricochaetonotus*) *superbus* sp. nov., *Chaetonotus* (*Hystricochaetonotus*) *arcanus* sp. nov., and *Chaetonotus* (*Hystricochaetonotus*) *luxus* sp. nov. with most similar congeners. Abbreviation: n.a. = data not available.

Character	*Ch.* (*H.*) *superbus* sp. nov.	*Ch.* (*H.*) *arcanus* sp. nov.	*Ch.* (*H.*) *luxus* sp. nov.	*Ch.* (*H.*) *borealis* Kolicka *et al.* (2018)	*Ch.* (*H.*) *furcatus* Kisielewski, 1991	*Ch.* (*H.*) *hornsundi* Kolicka *et al.* (2018)
Body length	107 µm	100 µm	87–112 µm	115–127 µm	110–148 µm	117–138 µm
Body shape	Tenpin-shaped	Stocky	Tenpin-shaped	Stocky	Stocky	More or less tenpin-shaped
Cephalic pleurae	Clearly demarcated	Indistinctly marked	Clearly demarcated	Clearly demarcated	Clearly demarcated	Clearly demarcated
Mouth cuticular teeth	Absent	Absent	Absent	Present (2)	Absent	Present (2)
Pharyngeal dilatations	Absent	Absent	Absent	Absent	Absent	Absent
Anterior section of intestine	Differentiated	Not differentiated	Differentiated	Differentiated	Not differentiated	Differentiated
Furcal indentation	U-shaped	U-shaped	U-shaped	V-shaped	U-shaped	V-shaped
Size of dorsal scales	Head: 3.17–3.84 × 1.4–2.3 µm Neck: 3.9–4.75 × 5.14–5.6 µm Trunk: 5.21–6.36 × 3.35–4.6 µm	Head: 3.0–4.5 × 1.9–2.2 µm Neck: 2.7 × 4.3 µm Trunk: 4.9–5.6 × 4.1–4.3 µm	Head: 3.2–5.4 × 2.1-5.2 µm Neck: 2.6–3.5 × 4.3–5.8 µm Trunk: 3.8–7.4 × 2.4–4.2 µm	Head: 1.9–7.1 × 1.8–6.9 µm Neck: 2.8–8.6 × 2.7–8.3 µm Trunk: 3.5–13.1 × 3.7–11.8 µm	Head: n.a. Neck: 4.3–7.0 × 4.6–6.8 µm Trunk: 6.0–10.0 × 5.3–9.8 µm	Head: 1.5–7.0 × 1.7–8.1 µm Neck: 2.1–8.7 × 2.3–9.1 µm Trunk: 3.2–13.3 × 3.2–14.4 µm
Length of dorsal spines	Head: 4.56–7.32 µm Neck: 6.7– 10.7 µm Trunk: 10.8-12.94 µm	Head: 3.1–4.9 µm Neck: 5.8 µm Trunk: 11.3–15.2 µm	Head: 3.4–6.6 µm Neck: 6.3–9 µm Trunk: 3.8–10.6 µm	Head: 2.86–11.20 µm Neck: 5.95–13.99 µm Trunk: 7.87–20.21 µm	Head: n.a. Neck: 7.9–13.8 µm Trunk: 2.0–8.2 µm	Head: n.a. Neck: 7.9–13.8 µm Trunk: 2.0–8.2 µm
Increase in length of dorsal spines	Abrupt	Abrupt	Abrupt	Gradual	Gradual	Gradual
Lateral denticle	Conspicuous	Conspicuous	Indistinct	Indistinct	Indistinct	Indistinct
References	Present study	Present study	Present study	Kolicka *et al.* (2018)	Kisielewski (1991), Kolicka (2016)	Kolicka *et al.* (2018)

Table 7 (continued). Comparison of *Chaetonotus* (*Hystricochaetonotus*) *superbus* sp. nov., *Chaetonotus* (*Hystricochaetonotus*) *arcanus* sp. nov., and *Chaetonotus* (*Hystricochaetonotus*) *luxus* sp. nov. with most similar congeners. Abbreviation: n.a. = data not available.

Character	*Ch.* (*H.*) *hystrix* Mečnikow, 1865	*Ch.* (*H.*) *macrochaetus* Zelinka, 1889	*Ch.* (*H.*) *persimilis* Kolicka *et al.*, 2018	*Ch.* (*H.*) *persetotus* Zelinka, 1889	*Ch.* (*H.*) *machikanensis* Suzuki & Furuya, 2011
Body length	87–130 µm	65–153 µm	115–136 µm	75–100 µm	95–125 µm
Body shape	Tenpin-shaped	Stocky	Stocky	Stocky	Tenpin-shaped
Cephalic pleurae	Indistinctly marked	Indistinctly marked	Clearly demarcated	Indistinctly marked	Indistinctly marked
Mouth cuticular teeth	Absent	n.a.	Present (2)	Absent	Absent
Pharyngeal swellings	Absent	Absent	Absent	Absent	Absent
Anterior section of intestine	n.a.	n.a.	Differentiated	n.a.	Not differentiated
Furcal indentation	V-shaped	V-shaped	V-shaped	V-shaped	Broadly V-shaped
Size of dorsal scales	Head and neck: 1–3 µm Trunk: 5 × 7µm	Head and neck: 2–5 µm Trunk: 8 × 9 µm	Head: 1.4–6.4 × 1.2–6.2 µm Neck: 2.3–6.1 × 2.1–7.7 µm Trunk: 3.0–11.8 × 2.6–9.9 µm	Head and neck: 5 × 6 µm Trunk: 7–8 µm	Head: n.a. Neck: 3.5 × 5.0 µm Trunk: 8 × 9 µm
Length of dorsal spines	Head and neck: 2–5 µm Trunk: 10–21 µm	Head: 4–5 µm Neck: 7–10 µm Trunk: 17–25 µm	Head: n.a. Neck: 7.9–13.8 µm Trunk: 2.0–8.2 µm	Head and neck: 2–5 µm Trunk: 15–19 µm	Head: n.a. Neck: 6 µm Trunk: 19.5 µm
Increase in length of dorsal spines	Gradual	Abrupt	Gradual	Abrupt	Gradual
Lateral denticle	Conspicuous	Conspicuous	Indistinct	Conspicuous	Conspicuous
References	Schwank (1990)	Schwank (1990)	Kolicka *et al.* (2018)	Schwank (1990)	Suzuki & Furuya (2011)

region of ventral ciliary bands (merged vs distinctly broadened but not merged), and (viii) the shape and arrangement of scales in the interciliary field (slightly overlapping, tongue-like and roughly rectangular scales vs non-overlapping and tear-shaped scales).

Chaetonotus (*H.*) *optabilis* sp. nov. resembles *Ch.* (*Ch.*) *bombardus* in having (i) rather short spines, (ii) unmerged anterior regions of the ventral ciliary bands, (iii) non-overlapping scales in the ventral interciliary field, and in lacking (iv) cuticular teeth in the mouth center. However, they can be separated by (i) the body shape (slender vs stocky), (ii) the cephalic pleurae (not recognizable vs clearly demarcated), (iii) the presence vs absence of pharyngeal dilatations, (iv) the number of scale rows (16–18 vs 29–31), (v) the number of scales per central dorsal row (40–45 vs 21–25), (vi) the morphology of posterior lobes of dorsal scales (comparatively broadly rounded vs narrow and tapering), (vii) the presence vs absence of rounded scales scattered throughout the dorsal side, (viii) the morphology of the hypostomium (a rectangular plate with small central protuberance and accompanied by two lamellae vs ship-shaped with a deep, semicircular anterior notch), (ix) the shape of scales in the interciliary field (bowl-shaped and obtriangular vs tear-shaped), and (x) the morphology of ventral furcal scales (oval to broadly fusiform and keeled vs leaf-like and spined).

Chaetonotus (*H.*) *iratus* sp. nov. and *Ch.* (*Ch.*) *bombardus* share (i) a similar body shape, (ii) clearly demarcated pleurae, (iii) a pharynx without anterior and posterior dilatations, and (iv) a similar number of scales per central dorsal row (22 vs 21–25). However, both species could be distinguished by (i) the morphology of posterior lobes of dorsal scales (comparatively broadly rounded vs narrow and tapering), (ii) the presence vs absence of a cuticular tooth in the mouth center, and (iii) the structure of the hypostomium (bears two horizontal lamellae accompanied by tear-shaped protuberances vs ship-shaped with a deep, semicircular anterior notch).

Subgeneric affiliation of the new species

As mentioned above, the genus *Chaetonotus* and its subgenera *Chaetonotus* and *Hystricochaetonotus*, as defined by characters of the external morphology by Schwank (1990) and Kisielewski (1997a), are non-monophyletic (e.g., Kånneby *et al.* 2013; Kolicka *et al.* 2018, 2020; present study). Due to the great intraspecific morphological variability and the existence of species with intermediate features, Balsamo *et al.* (2009) synonymized the subgenus *Hystricochaetonotus* with the subgenus *Chaetonotus*. They also stated that there is a continuum of morphological characters between both subgenera, which might thus form a single natural group. However, the synonymization of both subgenera did not erase the non-monophyly problem of the genus *Chaetonotus*, which embraces even members of other chaetonotid genera in molecular phylogenies (Fig. 8). Kånneby & Hochberg (2015: 214), therefore, suggested that the re-classification of the suborder Paucitubulatina needs to be based on other characters than cuticular structures. We agree and propose that molecular diagnostic characters, further splitting of the genus *Chaetonotus*, and elevation of its subgenera to the generic level might help to reduce polyphyly of *Chaetonotus*. Phylogenetic positions of type species (i.e., name-bearing types) of chaetonotid genera and subgenera will be crucial to solving the non-monophyly problem, as name-bearing types define nominal taxa and are objective standards of reference for the application of their scientific names (Article 61.1 of the ICZN 1999).

The type species of the subgenus *Hystricochaetonotus* is *Ch.* (*H.*) *hystrix*. The present phylogenetic analyses very robustly showed that *Ch.* (*H.*) *hystrix* clusters with further already described species of the subgenus *Hystricochaetonotus* (viz., *Ch.* (*H.*) *aemilianus*, *Ch.* (*H.*) *borealis*, *Ch.* (*H.*) *hornsundi*, *Ch.* (*H.*) *euhystrix* and *Ch.* (*H.*) *persimilis*), the nine newly discovered species, as well as with *Ch.* (*Ch.*) *bombardus* (Fig. 9). According to the present multi-gene phylogenetic analyses, the lineage leading to the last common ancestor of this clade is the longest internal branch within the family Chaetonotidae (Fig. 8). We, therefore, argue that the subgenus *Hystricochaetonotus* is valid and molecularly well-delimited. In the

future, only species that will statistically robustly cluster with the type species *Ch.* (*H.*) *hystrix* should be assigned to the subgenus *Hystricochaetonotus*. Indeed, the existence of this clade is corroborated by both nuclear and mitochondrial markers independently. However, only some members of this clade display all the morphological features (i.e., a cuticular covering made of three-lobed scales, spines thick and with a lateral denticle, and a varying number of spines considerably elongated to form a dorsal group) used to diagnose the subgenus *Hystrichochaetonotus* by Schwank (1990) and Kisielewski (1997a). Already Kolicka *et al.* (2018) encountered this problem, as *Ch.* (*Ch.*) *bombardus*, which conforms to the morphological diagnosis of the subgenus *Chaetonotus*, was placed in a sister position to a clade containing the following members of the subgenus *Hystricochaetonotus*: *Ch.* (*H.*) *borealis*, *Ch.* (*H.*) *hornsundi*, *Ch.* (*H.*) *persimilis*, and *Ch.* (*H.*) *hystrix*. This clade was fully statistically supported in their phylogenetic analyses. Kolicka *et al.* (2018) proposed that adding further species to the phylogenetic trees might either resolve or revise the subgeneric affiliation of *Ch.* (*Ch.*) *bombardus*. However, after the inclusion of nine further species, the situation has become even much more intricate (Fig. 9). We, therefore, decided to assign all the nine new species to the subgenus *Hystricochaetonotus*. Our decision is based on the core principle of phylogenetic systematics—the grouping of taxa based on common ancestry (e.g., Wägele 2005; Wiley & Lieberman 2011). Since members of the subgenus *Hystricochaetonotus* are morphologically highly heterogeneous, parallel evolution of *Chaetonotus*-like and/or *Hystricochaetonotus*-like characters of scales and spines very likely occurred during its radiation. Possibly, with the growing number of species and detailed morphological data, the '*Hystricochaetonotus*' clade could be split into multiple subgenera or its diagnosis could be broadened to better reconcile morphology and molecules.

Morphology and molecules in systematics and taxonomy

The phenetic approach determines taxonomic relationships based on similarity. On the other hand, morphology-based phylogeny is based on assumed homologies. These might be, however, sometimes very difficult to recognize not only in micro- but also in macroorganisms. Erroneous assumptions about homologies and not recognized homoplasies could lead to improper taxonomic frameworks (e.g., Wägele 2005; Wiley & Lieberman 2011). Moreover, there is no law in nature that would require that the diversity and evolutionary relationships be also reflected in the morphological disparity or similarity. A textbook example of how morphology can disguise true evolutionary relationships and classification is that of aquatic cetaceans (whales and dolphins), which evolved from even-toed ungulates, with hippopotami as their closest living relatives. Despite their huge size, detailed anatomical data, and a body of fossil record, this fact was recognized only after the application of molecular methods and resulted in paraphyly of the traditional order Artiodactyla Owen, 1848 (Geisler & Theodor 2009). Such sort of non-monophyly problems becomes even more true in the microscopic world. For instance, characters of cuticular structures, which are traditionally used in the chaetonotid taxonomy (Kisielewski 1997a), are distributed homoplastic along phylogenetic trees inferred from several thousands of nucleotide characters (Kieneke & Schmidt-Rhaese 2015: 89), causing polyphyly/paraphyly of *Chaetonotus* and its subgenera *Chaetonotus*, *Hystricochaetonotus*, and *Primochaetus* Kisielewski, 1997 (e.g., Kånneby *et al.* 2013; Kolicka *et al.* 2020; Križanová & Vďačný 2021; Figs 12–13). To reconcile these problems, which became apparent already in the first morphology-based cladistic analyses (Kieneke *et al.* 2008), molecular data need to be called and fully integrated into the gastrotrich systematics. It is also important to mention that molecular data are necessary to avoid tautology that might affect morphology-based frameworks since chaetonotid genera and subgenera have been defined only morphologically and rather broadly. Besides the circular reasoning, limitations of cladistic analyses include also the lack of explicit assumptions about character evolution and phylogenetic informativeness of the characters selected as well as the non-detection of multiple changes in the course of evolution. Although molecular markers provide much more independent and neutrally evolving characters than morphology, the reliability of molecular phylogenetic analyses significantly depends on the sequence quality, data curation (e.g., alignment and masking strategies), taxon sampling, and accuracy of species identification (for a review,

see, for instance, Lücking *et al.* 2021). Electropherograms need to be, therefore, always very carefully inspected during sequence assembly and sequences containing PCR or sequencing errors should be excluded from analyses. It is also recommended to test various alignment strategies and tree-building methods to ensure the robustness of phylogenetic trees. Hologenophores (i.e., specimens that first served for morphological and then for molecular analyses) constitute an essential link between sequence data and their taxonomic origin, providing a means to verify the taxonomic identity of the specimens sequenced (Pleijel *et al.* 2008; Degma 2018). Finally, the taxon sampling should be comprehensive and balanced, which applies also to morphological analyses.

Already in the late 70's of the past century, Woese & Fox (1977) noted that an organism's genome seems to be the ultimate record of its evolutionary history and molecules can be used to estimate the branching order of speciation events. Essential components of ribosomes were among the first molecules utilized in the reconstruction of the evolutionary history of all cellular domains of life. Ribosomal RNA genes have hypervariable regions separated by highly conserved stretches of DNA, which is transcribed into structurally constrained RNAs (Petrov *et al.* 2014). Hypervariable regions diverge with increasing evolutionary distance while conserved regions essential for the secondary and tertiary structure remain unchanged, causing rRNA genes to be subject to both neutral and purifying selection (Chakravorty *et al.* 2007). Similar rules hold also for the internal transcribed spacers (ITS1 and ITS2) of rRNA genes, though their molecular evolution is much faster and more neutral as they represent non-coding DNA (Coleman 2003, 2007, 2009). At the turn of the millennium, the mitochondrial gene encoding for cytochrome *c* oxidase subunit I was added to rRNA genes to improve the delimitation of very closely related species. The taxonomic power of COI comes from its accelerated molecular evolution, which stems from the absence of an excision repair system in animal mitochondria (e.g., Hebert *et al.* 2003a, 2003b and references cited therein).

Ribosomal RNA genes were considered to be also a reliable molecular clock, though in its relaxed form that accounts for the rate variation across species, different genes, and different sites along a single gene. The conventional estimate for evolutionary rates of prokaryotic 16S rDNA is 1.8×10^{-10} substitutions per site per year, i.e., 1.8% sequence divergence per 100 Ma (Ochman & Wilson 1987). In microbial eukaryotes, the homologous 18S rDNA evolves at a rate of $1.24–3.96 \times 10^{-10}$ substitutions per site per year, i.e., about 2.6% sequence divergence per 100 Ma (Wright & Lynn 1997; Vďačný 2015; Vďačný *et al.* 2019). In multicellular organisms, about 0.8% sequence divergence per 100 Ma is considered to reflect the rate of the whole 18S rDNA whereas the 2% difference might reflect the rapid evolution of hypervariable regions of the 18S rRNA molecule. ITS2 molecules evolve about 23–55 times faster than 18S rDNA (Bargues *et al.* 2000 and references cited therein). Nevertheless, the coding part of the rDNA cistron evolves comparatively slowly and is subject to concerted evolution, a process that converts copies of a gene in a multigene family into the same copy. Every single mutation fixed in the rDNA cistron, therefore, matters. To reflect this very important fact, we included molecular autapomorphies and 2D structures of molecules into species diagnoses in the present study.

We have recently assessed the utility of molecules in the identification of chaetonotid species (Križanová & Vďačný 2021). The present barcoding analyses (Fig. 4A–D) corroborate very well our previous findings. More specifically, intra- and interspecies *p*-distances of 18S sequences might overlap, i.e., two distinct species might share identical 18S rDNA sequences. This phenomenon is associated with the high conservativeness of the 18S rRNA gene (see above) and/or a rather recent divergence of species. However, a few nucleotide positions might be rarely polymorphic, leading to intraspecies distances of up to 0.11% (present study). Due to the combination of high conservativeness and rare polymorphism, 18S is not suitable to become a DNA barcode or even a pre-barcode in the chaetonotid molecular taxonomy. On the other hand, 28S can be used as a DNA pre-barcode, whereby helices 25es7–25es7c are taxonomically most important since species-specific mutations tend to accumulate

therein. And, eventually, COI is an ideal mitochondrial DNA barcode enabling unambiguous identification of chaetonotids. In the present study, we have added ITS2 as a further reliable nuclear DNA barcode (Fig. 4B). Each studied species of the subgenus *Hystricochaetonotus* has a unique primary and secondary structure of the ITS2 molecule (Supp. file 1: Figs S9–S12). Furthermore, the interspecies *p*-distances range from 5.88% to as much as 34.76% and there are up to four CBCs between species (Table 3). It is important to note that no intraspecies variability has been detected in ITS2, which might be associated with its shortness. According to Müller *et al.* (2007), a single CBC in a helix can differentiate two species with a probability of 0.93. Interestingly, we have detected at least a single CBC within the rDNA cistron between almost all species pairs (Table 3). If there are no CBCs, species could be well separated by the primary structure of 18S, ITS2, and/or 28S and by the primary structure of COI. These findings document that rDNA cistron along with COI are powerful tools for the delimitation and identification of gastrotrich species.

Conclusions

Extant gastrotrich species are the outcome of millions of years of evolution that has been written not only in their morphology but also in their molecules. Hitherto, this fact has not been reflected in species diagnoses that traditionally contain only morphological features. We, therefore, argue here for the full integration of molecules in gastrotrich taxonomic and classification frameworks and for their place in species recognition, identification, and diagnosis. Molecules should also become reliable diagnostic features of cryptic or near-cryptic species, as they contain the key characters that distinguish among them. Using the integrative morpho-molecular taxonomic approach, we have discovered and characterized nine new gastrotrich species collected from the continental waters of Central Europe.

Acknowledgments

We are very grateful to Ivan Rurik for his help with bioinformatics tools. We also thank Dr Małgorzata Kolicka and Dr Martin Vinther Sørensen for their valuable suggestions and insights that helped improve the quality of the manuscript in many ways. This work was supported by the Slovak Research and Development Agency under contract No. APVV-19-0076 and by the Comenius University in Bratislava under the Grant No. UK/210/2022.

References

Appeltans W., Ahyong S.T., Anderson G., Angel M.V., Artois T., Bailly N., Bamber R., Barber A., Bartsch I., Berta A., Błażewicz-Paszkowycz M., Bock P., Boxshall G., Boyko C.B., Brandão S.N., Bray R.A., Bruce N.L., Cairns S.D., Chan T.Y., Cheng L., Collins A.G., Cribb T., Curini-Galletti M., Dahdouh-Guebas F., Davie P.J., Dawson M.N., De Clerck O., Decock W., De Grave S., de Voogd N.J., Domning D.P., Emig C.C., Erséus C., Eschmeyer W., Fauchald K., Fautin D.G., Feist S.W., Fransen C.H., Furuya H., Garcia-Alvarez O., Gerken S., Gibson D., Gittenberger A., Gofas S., Gómez-Daglio L., Gordon D.P., Guiry M.D., Hernandez F., Hoeksema B.W., Hopcroft R.R., Jaume D., Kirk P., Koedam N., Koenemann S., Kolb J.B., Kristensen R.M., Kroh A., Lambert G., Lazarus D.B., Lemaitre R., Longshaw M., Lowry J., Macpherson E., Madin L.P., Mah C., Mapstone G., McLaughlin P.A., Mees J., Meland K., Messing C.G., Mills C.E., Molodtsova T.N., Mooi R., Neuhaus B., Ng P.K., Nielsen C., Norenburg J., Opresko D.M., Osawa M., Paulay G., Perrin W., Pilger J.F., Poore G.C., Pugh P., Read G.B., Reimer J.D., Rius M., Rocha R.M., Saiz-Salinas J.I., Scarabino V., Schierwater B., Schmidt-Rhaesa A., Schnabel K.E., Schotte M., Schuchert P., Schwabe E., Segers H., Self-Sullivan C., Shenkar N., Siegel V., Sterrer W., Stöhr S., Swalla B., Tasker M.L., Thuesen E.V., Timm T., Todaro M.A., Turon X., Tyler S., Uetz P., van der Land J., Vanhoorne B., van Ofwegen L.P., van Soest R.W., Vanaverbeke J., Walker-Smith G., Walter T.C., Warren A., Williams G.C., Wilson S.P. & Costello M.J. 2012. The magnitude of global marine species diversity. *Current Biology* 22 (23): 2189–2202. https://doi.org/10.1016/j.cub.2012.09.036

Astaloš B., Fenďa P., Gajdoš P., Krumpál M., Krumpálová Z., Mašán P., Mihál I., Pčola Š., Svatoň J. & Thomka V. 2003. *Pavúkovce Národného parku Poloniny* (*Arachnida: Araneae, Pseudoscorpiones, Opiliones, Acari – Parasitiformes)* [*Arachnids of the Poloniny National Park* (*Arachnida: Araneae, Pseudoscorpiones, Opiliones, Acari – Parasitiformis)*]. Štátna ochrana prírody SR & Správa Národného parku Poloniny, Banská Bystrica, Snina. [In Slovak.]

Balsamo M. 1983. Gastrotrichi. *In*: Consiglio Nazionale delle Ricerche (ed.) *Guide per il Riconoscimento delle Specie animali delle Acque interne italiane* 20: 1–92.

Balsamo M. 1990. Gastrotrichs from Lakes Bolsena, Chiusi and Montepulciano (central Italy), with the description of four new species. *Bolletino di zoologia* 57 (2): 165–178. https://doi.org/10.1080/11250009009355693

Balsamo M. & Todaro M.A. 1995. Gastrotricha from Trentino: the Viotte of Monte Bondone (Trento, Italy). *Studi trentini di scienze naturali. Acta biologica* 70: 9–22.

Balsamo M., d'Hondt J.-L., Kisielewski J. & Pierboni L. 2008. Global diversity of gastrotrichs (Gastrotricha) in freshwaters. *Hydrobiologia* 595 (1): 85–91. https://doi.org/10.1007/s10750-007-9006-4

Balsamo M., Pierboni L., Grilli P. & Plazi P. 2009. Taxonomic and nomenclatural notes on freshwater Gastrotricha. *Zootaxa* 2158 (1): 1–19. https://doi.org/10.11646/zootaxa.2158.1.1

Balsamo M., Grilli P., Guidi L. & d'Hondt J.-L. 2014. Gastrotricha. Biology, ecology and systematics. Families Dasydytidae, Dichaeturidae, Neogosseidae, Proichthydiidae. *In*: Dumont H.J.F. (ed.) *Identification Guides to the Plankton and Benthos of Inland Waters, Volume 24*: 1–187. Backhuys Publishers & Margraf Publishers, Weikersheim.

Balsamo M., d'Hondt J.-L., Kisielewski J., Todaro M., Tongiorgi P., Guidi L., Grilli P. & de Jong Y. 2015. Fauna Europaea: Gastrotricha. *Biodiversity Data Journal* 3: e5800. https://doi.org/10.3897/BDJ.3.e5800

Balsamo M., Artois T., Smith J.P., Todaro M.A., Guidi L., Leander B.S. & van Steenkiste N.W. 2020. The curious and neglected soft-bodied meiofauna: Rouphozoa (Gastrotricha and Platyhelminthes). *Hydrobiologia* 847: 2613–2644. https://doi.org/10.1007/s10750-020-04287-x

Bargues M.D., Marcilla A., Ramsey J.M., Dujardin J.P., Schofield C.J. & Mas-Coma C. 2000. Nuclear rDNA-based molecular clock of the evolution of Triatominae (Hemiptera: Reduviidae), vectors of Chagas disease. *Memórias do Instituto Oswaldo Cruz (Rio de Janeiro)* 95 (4): 567–573. https://doi.org/10.1590/s0074-02762000000400020

Bosco I., Lourenço A.P., Guidi L., Balsamo M., Hochberg R. & Garraffoni A.R.S. 2020. Integrative description of a new species of *Acanthodasys* Remane, 1927 (Gastrotricha, Macrodasyida, Thaumastodermatidae) based on four distinct morphological techniques and molecular data. *Zoologischer Anzeiger* 286: 31–42. https://doi.org/10.1016/j.jcz.2020.03.003

Buchar J. 1983. *Zoogeografie* [*Zoogeography*]. Státní pedagogické nakladatelství, Praha. [In Czech.]

Cartopy 2014. Cartopy: a cartographic Python library with Matplotlib support. Met Office, Exeter, UK.

Cerca J., Purschke G. & Struck T.H. 2018. Marine connectivity dynamics: clarifying cosmopolitan distributions of marine interstitial invertebrates and the meiofauna paradox. *Marine Biology* 165 (8): e123. https://doi.org/10.1007/s00227-018-3383-2

Chakravorty S., Helb D., Burday M., Connell N. & Alland D. 2007. A detailed analysis of 16S ribosomal RNA gene segments for the diagnosis of pathogenic bacteria. *Journal of Microbiological Methods* 69 (2): 330–339. https://doi.org/10.1016/j.mimet.2007.02.005

Coleman A.W. 2003. ITS2 is a double-edged tool for eukaryote evolutionary comparisons. *Trends in Genetics* 19 (7): 370–375. https://doi.org/10.1016/S0168-9525(03)00118-5

Coleman A.W. 2007. Pan-eukaryote ITS2 homologies revealed by RNA secondary structure. *Nucleic Acids Research* 35 (10): 3322–3329. https://doi.org/10.1093/nar/gkm233

Coleman A.W. 2009. Is there a molecular key to the level of "biological species" in eukaryotes? A DNA guide. *Molecular Phylogenetics and Evolution* 50 (1): 197–203. https://doi.org/10.1016/ j.ympev.2008.10.008

Crooks G.E., Hon G., Chandonia J.-M. & Brenner S.E. 2004. WebLogo: a sequence logo generator. *Genome Research* 14 (6): 1188–1190. https://doi.org/10.1101/gr.849004

Darty K., Denise A. & Ponty Y. 2009. VARNA: interactive drawing and editing of the RNA secondary structure. *Bioinformatics* 25 (15): 1974–1975. https://doi.org/10.1093/ bioinformatics/btp250

Degma P. 2018. Field and laboratory methods. *In*: Schill R.O. (ed.) Water Bears: The Biology of Tardigrades. *Zoological Monographs* 2: 349–369. https://doi.org/10.1007/978-3-319-95702-9

Elias R. & Hoksza D. 2017. TRAVeLer: a tool for template-based RNA secondary structure visualization. *BMC Bioinformatics* 18 (1): e487. https://doi.org/10.1186/s12859-017-1885-4

Garraffoni A.R.S. & Melchior M.P. 2015. New species and new records of freshwater *Heterolepidoderma* (Gastrotricha: Chaetonotidae) from Brazil with an identification key to the genus. *Zootaxa* 4057 (4): 551–568. https://doi.org/10.11646/zootaxa.4057.4.5

Garraffoni A.R.S., Araújo T.Q., Lourenço A.P., Guidi L. & Balsamo M. 2017. A new genus and new species of freshwater Chaetonotidae (Gastrotricha: Chaetonotida) from Brazil with phylogenetic position inferred from nuclear and mitochondrial DNA sequences. *Systematics and Biodiversity* 15 (1): 49–62. https://doi.org/10.1111/j.1463-6409.2012.00558.x

Garraffoni A.R.S., Araújo T.Q., Lourenço A.P., Guidi L. & Balsamo M. 2019a. Integrative taxonomy of a new *Redudasys* species (Gastrotricha: Macrodasyida) sheds light on the invasion of fresh water habitats by macrodasyids. *Scientific Reports* 9: e2067. https://doi.org/10.1038/s41598-018-38033-0

Garraffoni A.R.S., Kieneke A., Kolicka M., Corgosinho P.H.C., Prado J., Nihei S.S. & Freitas A.V.L. 2019b. ICZN Declaration 45: a remedy for the nomenclatural and typification dilemma regarding soft-bodied meiofaunal organisms? *Marine Biodiversity* 49: 2199–2207. https://doi.org/10.1007/s12526-019-00983-7

Geisler J.H. & Theodor J.M. 2009. Hippopotamus and whale phylogeny. *Nature* 458 (7236): E1–E4. https://doi.org/10.11646/10.1038/nature07776

Giere O. 2009. *Meiobenthology. The Microscopic Motile Fauna of Aquatic Sediments*. Springer, Berlin, Heidelberg. https://doi.org/10.1007/978-3-540-68661-3

Greuter A. 1917. Beiträge zur Systematik der Gastrotrichen in der Schweiz. *Revue suisse de Zoologie* 25: 35–76. Available from https://biodiversitylibrary.org/page/10710334 [accessed 1 Apr. 2022].

Hall T.A. 1999. BioEdit: a user-friendly biological sequence alignment editor and analysis program for Windows 95/98/NT. *Nucleic Acids Symposium Series* 41: 95–98.

Hebert P.D.N., Cywinska A., Ball S.L. & deWaard J.R. 2003a. Biological identifications through DNA barcodes. *Proceedings of the Royal Society B* 270 (1512): 313–321. https://doi.org/10.1098/rspb.2002.2218

Hebert P.D.N., Ratnasingham S. & deWaard J.R. 2003b. Barcoding animal life: cytochrome *c* oxidase subunit 1 divergences among closely related species. *Proceedings of the Royal Society B* 270 (Supplement): S96–S99. https://doi.org/10.1098/rsbl.2003.0025

Hoang D.T., Chernomor O., von Haeseler A., Minh B.Q. & Vinh L.S. 2018. UFBoot2: improving the ultrafast bootstrap approximation. *Molecular Biology and Evolution* 35 (2): 518–522. https://doi.org/10.1093/molbev/msx281

Holecová M. & Franc V. 2001. Červený (ekosozologický) zoznam chrobákov (Coleoptera) Slovenska [Red (ecosozological) list of beetles (Coleoptera) of Slovakia]. *In*: Baláž D., Maglocký Š. & Marhold K. (eds) Červený zoznam rastlín a živočíchov Slovenska [Red list of plants and animals of Slovakia]. *Ochrana prírody* 20 (Supplement): 111–128. [In Slovak with English title translation and summary.]

Hummon W.D., Balsamo M. & Todaro M.A. 1992. Italian marine Gastrotricha: I. Six new and one redescribed species of Chaetonotida. *Bollettino di Zoologia* 59 (4): 499–516. https://doi.org/10.1080/11250009209386711

Hunter J.D. 2007. Matplotlib: a 2D graphics environment. *Computing in Science and Engineering* 9: 90–95. https://doi.org/10.1109/MCSE.2007.55

ICZN 1999. *International Code of Zoological Nomenclature*. *Fourth Edition*. International Trust for Zoological Nomenclature, London. Available from https://www.iczn.org/the-code/the-code-online/ [accessed 1 Apr. 2022].

ICZN 2017. Declaration 45—Addition of Recommendations to Article 73 and of the term "specimen, preserved" to the Glossary. *Bulletin of Zoological Nomenclature* 73 (2–4): 96–97. https://doi.org/10.21805/bzn.v73i2.a2

Kånneby T. 2011. New species and new records of freshwater Chaetonotida (Gastrotricha) from Sweden. *Zootaxa* 3115 (1): 29–55. https://doi.org/10.11646/zootaxa.3115.1.3

Kånneby T. & Hochberg R. 2015. Phylum Gastrotricha. *In*: Thorp J.H. & Rogers D.C. (eds) *Key to Nearctic Fauna: Thorp and Covich's Freshwater Invertebrates*: 211–223. Elsevier, London.

Kånneby T., Todaro M.A. & Jondelius U. 2012. A phylogenetic approach to species delimitation in freshwater Gastrotricha from Sweden. *Hydrobiologia* 683 (1): 185–202. https://doi.org/10.1007/s10750-011-0956-1

Kånneby T., Todaro M.A. & Jondelius U. 2013. Phylogeny of Chaetonotidae and other Paucitubulatina (Gastrotricha: Chaetonotida) and the colonization of aquatic ecosystems. *Zoologica Scripta* 42 (1): 88–105. https://doi.org/10.1111/j.1463-6409.2012.00558.x

Katoh K., Rozewicki J. & Yamada K.D. 2019. MAFFT online service: multiple sequence alignment, interactive sequence choice and visualization. *Briefings in Bioinformatics* 20 (4): 1160–1166. https://doi.org/10.1093/bib/bbx108

Kieneke A. & Nikoukar H. 2017. Integrative morphological and molecular investigation of *Turbanella hyalina* Schultze, 1853 (Gastrotricha: Macrodasyida), including a redescription of the species. *Zoologischer Anzeiger* 267: 168–186. https://doi.org/10.1016/j.jcz.2017.03.005

Kieneke A. & Schmidt-Rhaesa A. 2015. Gastrotricha. *In*: Schmidt-Rhaesa A. (ed.) *Handbook of Zoology 3. Gastrotricha and Gnathifera*: 1–134. De Gruyter, Berlin, Boston. https://doi.org/10.1515/9783110274271

Kieneke A., Riemann O. & Ahlrichs W.H. 2008. Novel implications for the basal internal relationships of Gastrotricha revealed by an analysis of morphological characters. *Zoologica Scripta* 37 (4): 429–460. https://doi.org/10.1111/j.1463-6409.2008.00334.x

Kisielewski J. 1981. Gastrotricha from raised and transitional peat bogs in Poland. *Monografie Fauny Polski* 11: 1–143.

Kisielewski J. 1991. Inland-water Gastrotricha from Brazil. *Annales Zoologici (Warszawa)* 43 (Supplement 2): 1–168.

Kisielewski J. 1997a. On the subgeneric division of the genus *Chaetonotus* Ehrenberg (Gastrotricha). *Annales Zoologici (Warszawa)* 46: 145–151.

Kisielewski J. 1997b. *Brzuchorzęski (Gastrotricha)*. *Fauna Słodkowodna Polski*. Zeszyt 31, Wydawnictwo Uniwersytetu Łódzkiego, Łódź.

Kolicka M. 2016. Gastrotrichs in bromeliads – newly recorded *Chaetonotus* (*Hystricochaetonotus*) *furcatus* Kisielewski, 1991 (Chaetonotida) from the Łódź Palm House. *Zoosystema* 38 (1): 141–155. https://doi.org/10.5252/z2016n1a5

Kolicka M. 2019a. Gastrotricha – not only in sediments: new epiphytic species of Chaetonotida from the Jubilee Greenhouse of the Botanical Garden in Kraków. *European Journal of Taxonomy* 511: 1–100. https://doi.org/10.5852/ejt.2019.511

Kolicka M. 2019b. New *Chaetonotus* (*Wolterecka*) *semovitus* sp. nov. (Gastrotricha: Chaetonotida: Chaetonotidae) from a palm house in Vienna (Austria). *Annales Zoologici (Warszawa)* 69 (2): 447–475. https://doi.org/10.3161/00034541ANZ2019.69.2.011

Kolicka M. 2020. *Systematics of the Gastrotrichs from the family Chaetonotidae (Gastrotricha, Chaetonotida) Based on the Integrative Taxonomy Approach*. PhD thesis, Adam Mickiewicz University, Poznań, Poland.

Kolicka M., Dabert M., Dabert J., Kånneby T. & Kisielewski J. 2016. *Bifidochaetus*, a new Arctic genus of freshwater Chaetonotida (Gastrotricha) from Spitsbergen revealed by an integrative taxonomic approach. *Invertebrate Systematics* 30 (4): 398–419. https://doi.org/ 10.1071/ IS16001

Kolicka M., Kotwicki L. & Dabert M. 2018. Diversity of Gastrotricha on Spitsbergen (Svalbard Archipelago, Arctic) with a description of seven new species. *Annales Zoologici (Warszawa)* 68 (4): 609–739. https://doi.org10.3161/00034541ANZ2018 .68.4.001

Kolicka M., Dabert M., Olszanowski Z. & Dabert J. 2020. Sweet or salty? The origin of freshwater gastrotrichs (Gastrotricha, Chaetonotida) revealed by molecular phylogenetic analysis. *Cladistics* 36 (5): 458–480. https://doi.org/10.1111/cla.12424

Križanová F. & Vďačný P. 2021. Description of *Lepidochaetus tirjakovae* sp. nov. (Gastrotricha: Paucitubulatina: Chaetonotidae), using morphology and DNA barcoding. *Zoologischer Anzeiger* 292: 207–224. https://doi.org/10.1016/j.jcz.2021.04.003

Kumar S., Stecher G., Li M., Knyaz C. & Tamura K. 2018. MEGA X: molecular evolutionary genetics analysis across computing platforms. *Molecular Biology and Evolution* 35 (6): 1547–1549. https://doi.org/10.1093/molbev/msy096

Lorenz R., Bernhart S.H., Höner zu Siederdissen C., Tafer H., Flamm C., Stadler P.F. & Hofacker I.L. 2011. ViennaRNA Package 2.0. *Algorithms for Molecular Biology* 6: e26. https://doi.org/10.1186/1748-7188-6-26

Lorenz R., Hofacker I.L. & Stadler P.F. 2016. RNA folding with hard and soft constraints. *Algorithms for Molecular Biology* 11: e8. https://doi.org/10.1186/s13015-016-0070-z

Lücking R., Leavitt S.D. & Hawksworth D.L. 2021. Species in lichen-forming fungi: balancing between conceptual and practical considerations, and between phenotype and phylogenomics. *Fungal Diversity* 109 (1): 99–154. https://doi.org/10.1007/s13225-021-00477-7

Lynn D.H., Doerder F.P., Gillis P.L. & Prosser R.S. 2018. *Tetrahymena glochidiophila* n. sp., a new species of *Tetrahymena* (Ciliophora) that causes mortality to glochidia larvae of freshwater mussels (Bivalvia). *Diseases of Aquatic Organisms* 127: 125–136. https://doi.org/10.3354/dao03188

Magpali L., Machado D.R.P., Araújo T.Q. & Garraffoni A.R.S. 2021. Long distance dispersal and pseudo-cryptic species in Gastrotricha: first description of a new species (Chaetonotida, Chaetonotidae, *Polymerurus*) from an oceanic island with volcanic rocks. *European Journal of Taxonomy* 746: 62–93. https://doi.org/10.5852/ejt.2021.746.1319

Mathews D.H. 2004. Using an RNA secondary structure partition function to determine confidence in base pairs predicted by free energy minimization. *RNA* 10 (8): 1178–1190. https://doi.org/10.1261/rna.7650904

Müller T., Philippi N., Dandekar T., Schultz J. & Wolf M. 2007. Distinguishing species. *RNA* 13 (9): 1469–1472. https://doi.org/10.1261/rna.617107

Nguyen L.T., Schmidt H.A., von Haeseler A. & Minh B.Q. 2015. IQ-TREE: a fast and effective stochastic algorithm for estimating maximum-likelihood phylogenies. *Molecular Biology and Evolution* 32 (1): 268–274. https://doi.org/10.1093/molbev/msu300

Ochman H. & Wilson A.C. 1987. Evolution of bacteria: evidence for a universal substitution rate in cellular genomes. *Journal of Molecular Evolution* 26 (1–2): 74–86. https://doi.org/10.1007/BF02111283

Pecina L. & Vďačný P. 2022. DNA barcoding and coalescent-based delimitation of endosymbiotic clevelandellid ciliates (Ciliophora: Clevelandellida): a shift to molecular taxonomy in the inventory of ciliate diversity in panesthiine cockroaches. *Zoological Journal of the Linnean Society* 194 (4): 1072–1102. https://doi.org/10.1093/zoolinnean/zlab063

Petrov A.S., Bernier C.R., Gulen B., Waterbury C.C., Hershkovits E., Hsiao C., Harvey S.C., Hud N.V., Fox G.E, Wartell R.M. & Williams L.D. 2014. Secondary structures of rRNAs from all three domains of life. *PLoS One* 9 (2): e88222. https://doi.org/10.1371/ journal.pone.0088222

Pleijel F., Jondelius U., Norlinder E., Nygren A., Oxelman B., Schander C., Sundberg P. & Thollesson M. 2008. Phylogenies without roots? A plea for the use of vouchers in molecular phylogenetic studies. *Molecular Phylogenetics and Evolution* 48 (1): 369–371. https://doi.org/10.1016/j.ympev.2008.03.024

Popenda M., Szachniuk M., Antczak M., Purzycka K.J., Lukasiak P., Bartol N., Blazewicz J. & Adamiak R.W. 2012. Automated 3D structure composition for large RNAs. *Nucleic Acids Research* 40 (14): e112. https://doi.org/10.1093/nar/gks339

Rao G.C. & Clausen C. 1970. *Planodasys marginalis* gen. et. sp. nov. and Planodasyidae fam. nov. (Gastrotricha, Macrodasyoidea). *Sarsia* 42 (1): 73–82. https://doi.org/10.1080/00364827.1970.10411164

Ronquist F., Teslenko M., van der Mark P., Ayres D.L., Darling A., Höhna S., Larget B., Liu L., Suchard M.A. & Huelsenbeck J.P. 2012. MrBayes 3.2: efficient Bayesian phylogenetic inference and model choice across a large model space. *Systematic Biology* 61 (3): 539–542. https://doi.org/10.1093/sysbio/sys029

Schwank P. 1990. Gastrotricha. *In*: Schwoerbel J. & Zwick P. (eds) *Süsswasserfauna von Mitteleuropa. Band 3. Gastrotricha und Nemertini*: 1–252. Gustav Fischer Verlag, Stuttgart, Jena, New York.

Seibel P.N., Müller T., Dandekar T., Schultz J. & Wolf M. 2006. 4SALE – a tool for synchronous RNA sequence and secondary structure alignment and editing. *BMC Bioinformatics* 7: e498. https://doi.org/10.1186/1471-2105-7-498

Suzuki T.G. & Furuya H. 2011. Two new species of *Chaetonotus* (Gastrotricha, Chaetonotida, Chaetonotidae) from Japan. *Zootaxa* 3011 (1): 27–37. https://doi.org/10.11646/zootaxa.3011.1.3

Sweeney B.A., Hoksza D., Nawrocki E.P., Ribas C.E., Madeira F., Cannone J.J., Gutell R, Maddala A., Meade C.D., Williams L.D., Petrov A.S., Chan P.P., Lowe T.M., Finn R.D. & Petrov A.I. 2021. R2DT is a framework for predicting and visualising RNA secondary structure using templates. *Nature Communication* 12 (1): e3494. https://doi.org/10.1038/s41467-021-23555-5

Todaro M.A. 2022. Freshwater. *In*: Todaro M.A. (ed.) *Gastrotricha World Portal*. Available from http://www.gastrotricha.unimore.it/freshwater.htm [accessed 1 Apr. 2022].

Todaro M.A., Dal Zotto M., Jondelius U., Hochberg R., Hummon W.D., Kånneby T. & Rocha C.E. 2012. Gastrotricha: a marine sister for a freshwater puzzle. *PLoS One* 7 (2): e31740. https://doi.org/10.1371/journal.pone.0031740

Todaro M.A., Sibaja-Cordero J.A., Segura-Bermúdez O.A., Coto-Delgado G., Goebel-Otárola N., Barquero J.D., Cullell-Delgado M. & Dal Zotto M. 2019. An introduction to the study of Gastrotricha, with a taxonomic key to families and genera of the group. *Diversity* 11 (7): e117. https://doi.org/10.3390/d11070117

Trifinopoulos J., Nguyen L. T., von Haeseler A. & Minh B.Q. 2016. W-IQ-TREE: a fast online phylogenetic tool for maximum likelihood analysis. *Nucleic Acids Research* 44 (W1): W232–W235. https://doi.org/10.1093/nar/gkw256

Vďačný P. 2015. Estimation of divergence times in litostomatean ciliates (Ciliophora: Intramacronucleata), using Bayesian relaxed clock and 18S rRNA gene. *European Journal of Protistology* 51 (4): 321–334. https:// doi.org/10.1016/j.ejop.2015.06.008

Vďačný P., Rajter Ľ., Stoeck T. & Foissner W. 2019. A proposed timescale for the evolution of armophorean ciliates: clevelandellids diversify more rapidly than metopids. *Journal of Eukaryotic Microbiology* 66 (1): 167–181. https://doi.org/10.1111/jeu.12641

Wägele J.-W. 2005. *Foundations of Phylogenetic Systematics*. *Second Edition*. Verlag Dr Friedrich Pfeil, München.

Wiley E.O. & Lieberman B.S. 2011. *Phylogenetics: Theory and Practice of Phylogenetic Systematics*. *Second Edition*. Wiley-Blackwell, Hoboken, New Jersey.

Woese C.R. & Fox G.E. 1977. Phylogenetic structure of the prokaryotic domain: the primary kingdoms. *Proceedings of the National Academy of Sciences of the United States of America* 74 (11): 5088–5090. https://doi.org/10.1073/pnas.74.11.5088

Wolf M., Friedrich J., Dandekar T. & Müller T. 2005. CBCAnalyzer: inferring phylogenies based on compensatory base changes in RNA secondary structures. *In Silico Biology* 5 (3): 291–294.

Wolf M., Chen S., Song J., Ankenbrand M. & Müller T. 2013. Compensatory base changes in ITS2 secondary structures correlate with the biological species concept despite intragenomic variability in ITS2 sequences – a proof of concept. *PloS One* 8 (6): e66726. https://doi.org/10.1371/journal.pone.0066726

Wright A.-D.G. & Lynn D.H. 1997. Maximum ages of ciliate lineages estimated using a small subunit rRNA molecular clock: crown eukaryotes date back to the Paleoproterozoic. *Archiv für Protistenkunde* 148 (4): 329–341. https://doi.org/10.1016/S0003-9365(97)80013-9

Zuker M. 2003. Mfold web server for nucleic acid folding and hybridization prediction. *Nucleic Acids Research* 31 (13): 3406–3415. https://doi.org/10.1093/nar/gkg595

Manuscript received: 8 April 2022
Manuscript accepted: 19 July 2022
Published on: 11 October 2022
Topic editor: Tony Robillard
Section editor: Martin Vinter Sørensen
Desk editor: Pepe Fernández

Printed versions of all papers are also deposited in the libraries of the institutes that are members of the *EJT* consortium: Muséum national d'histoire naturelle, Paris, France; Meise Botanic Garden, Belgium; Royal Museum for Central Africa, Tervuren, Belgium; Royal Belgian Institute of Natural Sciences, Brussels, Belgium; Natural History Museum of Denmark, Copenhagen, Denmark; Naturalis Biodiversity Center, Leiden, the Netherlands; Museo Nacional de Ciencias Naturales-CSIC, Madrid, Spain; Leibniz Institute for the Analysis of Biodiversity Change, Bonn – Hamburg, Germany; National Museum, Prague, Czech Republic.

Supplementary file

Supp. file 1. Additional data. https://doi.org/10.5852/ejt.2022.840.1941.7825

Table S1. List of taxa with GenBank accession numbers of 18S, 28S and COI sequences included in phylogenetic analyses.

Table S2. Morphometric characterization of *Chaetonotus* (*Hystricochaetonotus*) *mirabilis* sp. nov. All measurements are given in µm. Ranges include the smallest and the largest structure measurement. N = number of specimens analyzed.

Table S3. Morphometric characterization of *Chaetonotus* (*Hystricochaetonotus*) *superbus* sp. nov. All measurements are given in µm. Ranges include the smallest and the largest structure measurement. N = number of specimens analyzed.

Table S4. Morphometric characterization of *Chaetonotus* (*Hystricochaetonotus*) *optabilis* sp. nov. All measurements are given in µm. Ranges include the smallest and the largest structure measurement. N = number of specimens analyzed.

Table S5. Morphometric characterization of *Chaetonotus* (*Hystricochaetonotus*) *avarus* sp. nov. All measurements are given in µm. Ranges include the smallest and the largest structure measurement. N = number of specimens analyzed.

Table S6. Morphometric characterization of *Chaetonotus* (*Hystricochaetonotus*) *luxus* sp. nov. All measurements are given in µm. Ranges include the smallest and the largest structure measurement. N = number of specimens analyzed.

Table S7. Morphometric characterization of *Chaetonotus* (*Hystricochaetonotus*) *iratus* sp. nov. All measurements are given in µm. Ranges include the smallest and the largest structure measurement.

Table S8. Morphometric characterization of *Chaetonotus* (*Hystricochaetonotus*) *gulosus* sp. nov. All measurements are given in µm. Ranges include the smallest and the largest structure measurement.

Table S9. Morphometric characterization of *Chaetonotus* (*Hystricochaetonotus*) *arcanus* sp. nov. All measurements are given in µm. Ranges include the smallest and the largest structure measurement.

Fig. S1. Secondary structure of the 18S rRNA molecule of *Chaetonotus* (*Hystricochaetonotus*) *superbus* sp. nov. The single diagnostic molecular autapomorphy is situated in the terminal loop of helix 11 (red arrow). The reference 18S secondary structure map of *Saccharomyces cerevisiae* Meyen ex E.C.Hansen (inset) is from http://apollo.chemistry.gatech.edu/RibosomeGallery (Petrov *et al*. 2014).

Fig. S2. Secondary structure of the 18S rRNA molecule of *Chaetonotus* (*Hystricochaetonotus*) *optabilis* sp. nov. Diagnostic molecular autapomorphies are marked by red arrows. The reference 18S secondary structure map of *Saccharomyces cerevisiae* Meyen ex E.C.Hansen (inset) is from http://apollo.chemistry.gatech.edu/RibosomeGallery (Petrov *et al*. 2014).

Fig. S3. Secondary structure of the 18S rRNA molecule of *Chaetonotus* (*Hystricochaetonotus*) *avarus* sp. nov. Diagnostic molecular autapomorphies are marked by red arrows. The reference 18S secondary structure map of *Saccharomyces cerevisiae* Meyen ex E.C.Hansen (inset) is from http://apollo.chemistry.gatech.edu/RibosomeGallery (Petrov *et al*. 2014).

Fig. S4. Secondary structure of the 18S rRNA molecule of *Chaetonotus* (*Hystricochaetonotus*) *luxus* sp. nov. The reference 18S secondary structure map of *Saccharomyces cerevisiae* Meyen ex E.C.Hansen (inset) is from http://apollo.chemistry.gatech.edu/RibosomeGallery (Petrov *et al*. 2014).

Fig. S5. Secondary structure of the 18S rRNA molecule of *Chaetonotus* (*Hystricochaetonotus*) *iratus* sp. nov. The single diagnostic molecular autapomorphy is situated in helix 44 (red arrow). The reference 18S secondary structure map of *Saccharomyces cerevisiae* Meyen ex E.C.Hansen (inset) is from http://apollo.chemistry.gatech.edu/RibosomeGallery (Petrov *et al*. 2014).

Fig. S6. Secondary structure of the 18S rRNA molecule of *Chaetonotus* (*Hystricochaetonotus*) *gulosus* sp. nov. The single diagnostic molecular autapomorphy is situated in helix 39es9 (red arrow). The reference 18S secondary structure map of *Saccharomyces cerevisiae* Meyen ex E.C.Hansen (inset) is from http://apollo.chemistry.gatech.edu/RibosomeGallery (Petrov *et al*. 2014).

Fig. S7. Secondary structure of the 18S rRNA molecule of *Chaetonotus* (*Hystricochaetonotus*) *arcanus* sp. nov. The reference 18S secondary structure map of *Saccharomyces cerevisiae* Meyen ex E.C.Hansen (inset) is from http://apollo.chemistry.gatech.edu/RibosomeGallery (Petrov *et al*. 2014).

Fig. S8. Secondary structure of the 18S rRNA molecule of *Chaetonotus* (*Hystricochaetonotus*) *slavicus* sp. nov. The single diagnostic molecular autapomorphy is situated in a bulge of helix 41 (red arrow). The reference 18S secondary structure map of *Saccharomyces cerevisiae* Meyen ex E.C.Hansen (inset) is from http://apollo.chemistry.gatech.edu/RibosomeGallery (Petrov *et al*. 2014).

Fig. S9. Putative secondary structure of ITS2 molecules. **A**. *Chaetonotus* (*Hystricochaetonotus*) *mirabilis* sp. nov. **B**. *Chaetonotus* (*Hystricochaetonotus*) *superbus* sp. nov. Diagnostic molecular autapomorphies are marked by red arrows.

Fig. S10. Putative secondary structure of ITS2 molecule of *Chaetonotus* (*Hystricochaetonotus*) *luxus* sp. nov. Diagnostic molecular autapomorphies are marked by red arrows.

Fig. S11. Putative secondary structure of ITS2 molecules. **A**. *Chaetonotus* (*Hystricochaetonotus*) *iratus* sp. nov. **B**. *Chaetonotus* (*Hystricochaetonotus*) *gulosus* sp. nov. Diagnostic molecular autapomorphies are marked by red arrows.

Fig. S12. Putative secondary structure of ITS2 molecules. **A**. *Chaetonotus* (*Hystricochaetonotus*) *arcanus* sp. nov. **B**. *Chaetonotus* (*Hystricochaetonotus*) *slavicus* sp. nov. Diagnostic molecular autapomorphies are marked by red arrows.

Fig. S13. Secondary structure of the first two domains of the 28S rRNA molecule of *Chaetonotus* (*Hystricochaetonotus*) *superbus* sp. nov. Diagnostic molecular autapomorphies are marked by red arrows. The reference 28S secondary structure map of *Saccharomyces cerevisiae* Meyen ex E.C.Hansen (inset) is from http://apollo.chemistry.gatech.edu/RibosomeGallery (Petrov *et al*. 2014).

Fig. S14. Secondary structure of the first two domains of the 28S rRNA molecule of *Chaetonotus* (*Hystricochaetonotus*) *optabilis* sp. nov. Diagnostic molecular autapomorphies are marked by red arrows. The reference 28S secondary structure map of *Saccharomyces cerevisiae* Meyen ex E.C.Hansen (inset) is from http://apollo.chemistry.gatech.edu/RibosomeGallery (Petrov *et al*. 2014).

Fig. S15. Secondary structure of the first two domains of the 28S rRNA molecule of *Chaetonotus* (*Hystricochaetonotus*) *avarus* sp. nov. Diagnostic molecular autapomorphies are marked by red arrows. The reference 28S secondary structure map of *Saccharomyces cerevisiae* Meyen ex E.C.Hansen (inset) is from http://apollo.chemistry.gatech.edu/RibosomeGallery (Petrov *et al*. 2014).

Fig. S16. Secondary structure of the first two domains of the 28S rRNA molecule of *Chaetonotus* (*Hystricochaetonotus*) *luxus* sp. nov. The reference 28S secondary structure map of *Saccharomyces cerevisiae* Meyen ex E.C.Hansen (inset) is from http://apollo.chemistry.gatech.edu/RibosomeGallery (Petrov *et al*. 2014).

Fig. S17. Secondary structure of the first two domains of the 28S rRNA molecule of *Chaetonotus* (*Hystricochaetonotus*) *iratus* sp. nov. Diagnostic molecular autapomorphies are marked by red arrows. The reference 28S secondary structure map of *Saccharomyces cerevisiae* Meyen ex E.C.Hansen (inset) is from http://apollo.chemistry.gatech.edu/RibosomeGallery (Petrov *et al*. 2014).

Fig. S18. Secondary structure of the first two domains of the 28S rRNA molecule of *Chaetonotus* (*Hystricochaetonotus*) *gulosus* sp. nov. The single diagnostic molecular autapomorphy is situated in helix 25es7a (red arrow). The reference 28S secondary structure map of *Saccharomyces cerevisiae* Meyen ex E.C.Hansen (inset) is from http://apollo.chemistry.gatech.edu/RibosomeGallery (Petrov *et al*. 2014).

Fig. S19. Secondary structure of the first two domains of the 28S rRNA molecule of *Chaetonotus* (*Hystricochaetonotus*) *arcanus* sp. nov. Diagnostic molecular autapomorphies are marked by red arrows. The reference 28S secondary structure map of *Saccharomyces cerevisiae* Meyen ex E.C.Hansen (inset) is from http://apollo.chemistry.gatech.edu/RibosomeGallery (Petrov *et al*. 2014).

Fig. S20. Secondary structure of the first two domains of the 28S rRNA molecule of *Chaetonotus* (*Hystricochaetonotus*) *slavicus* sp. nov. The reference 28S secondary structure map of *Saccharomyces cerevisiae* Meyen ex E.C.Hansen (inset) is from http://apollo.chemistry.gatech.edu/RibosomeGallery (Petrov *et al*. 2014).

Alignment 1. 18S rRNA gene.

Alignment 2. ITS2 molecule.

Alignment 3. First two domains of the 28S rRNA gene.

Alignment 4. Cytochrome *c* oxidase subunit I.